

AD-A160 464

A COMPARISON OF MOISTURE VARIABLES IN THE VERTICAL
INTERPOLATIONS OF A 4-D ASSIMILATION SYSTEM(U) AIR
FORCE GEOPHYSICS LAB HANSCOM AFB MA K MITCHELL ET AL.
11 APR 85 AFGL-TR-85-0090

1/1

UNCLASSIFIED

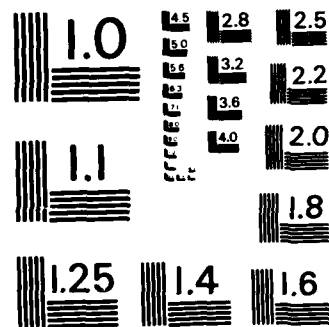
F/8 12/1

NL

END

FILMED

DTIC



MICROCOPY RESOLUTION TEST CHART
 NATIONAL BUREAU OF STANDARDS-1963-A

AFGL-TR-85-0090
ENVIRONMENTAL RESEARCH PAPERS, NO. 910

AD-A160 464

A Comparison of Moisture Variables in the Vertical Interpolations of a 4-D Assimilation System

KENNETH MITCHELL
CHIEN-HSIUNG YANG



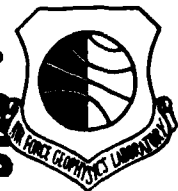
11 April 1985



Approved for public release; distribution unlimited.



DTIC FILE COPY



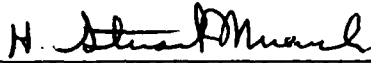
DTIC
ELECTE
OCT 22 1985
E

ATMOSPHERIC SCIENCES DIVISION PROJECT 2310
AIR FORCE GEOPHYSICS LABORATORY

HANSCOM AFB, MA 01731
85 10 22 030

"This technical report has been reviewed and is approved for publication"

FOR THE COMMANDER



H. STUART MUENCH, Acting Chief
Atmospheric Prediction Branch



KENNETH R. HARDY, Acting Director
Atmospheric Sciences Division

This document has been reviewed by the ESD Public Affairs Office (PA) and is releasable to the National Technical Information Service (NTIS).

Qualified requestors may obtain additional copies from the Defense Technical Information Center. All others should apply to the National Technical Information Service.

If your address has changed, or if you wish to be removed from the mailing list, or if the addressee is no longer employed by your organization, please notify AFGL/DAA, Hanscom AFB, MA 01731. This will assist us in maintaining a current mailing list.

UNCLASSIFIED

SECURITY CLASSIFICATION OF THIS PAGE

REPORT DOCUMENTATION PAGE				
1a. REPORT SECURITY CLASSIFICATION Unclassified		1b. RESTRICTIVE MARKINGS AD-A160464		
2a. SECURITY CLASSIFICATION AUTHORITY		3. DISTRIBUTION/AVAILABILITY OF REPORT Approved for public release; distribution unlimited.		
2b. DECLASSIFICATION/DOWNGRADING SCHEDULE				
4. PERFORMING ORGANIZATION REPORT NUMBER(S) AFGL-TR-85-0090 ERP, No. 910		5. MONITORING ORGANIZATION REPORT NUMBER(S)		
6a. NAME OF PERFORMING ORGANIZATION Air Force Geophysics Laboratory	6b. OFFICE SYMBOL (If applicable) LYP	7a. NAME OF MONITORING ORGANIZATION		
6c. ADDRESS (City, State and ZIP Code) Hanscom AFB Massachusetts 01731		7b. ADDRESS (City, State and ZIP Code)		
8a. NAME OF FUNDING/SPONSORING ORGANIZATION Air Force Office of Scientific Research	8b. OFFICE SYMBOL (If applicable) AFOSR/NC	9. PROCUREMENT INSTRUMENT IDENTIFICATION NUMBER		
8c. ADDRESS (City, State and ZIP Code) Bolling AFB DC 20332		10. SOURCE OF FUNDING NOS.		
		PROGRAM ELEMENT NO. 61102F	PROJECT NO. 2310	TASK NO. G7
				WORK UNIT NO. 05
11. TITLE (Include Security Classification) A Comparison of Moisture Variables in the Vertical Interpolations of a 4-D (over)				
12. PERSONAL AUTHOR(S) Mitchell, Kenneth, and Yang, Chien-hsiung				
13a. TYPE OF REPORT Scientific, Annual	13b. TIME COVERED FROM 10/1/83 TO 9/30/84	14. DATE OF REPORT (Yr., Mo., Day) 1985 April 11	15. PAGE COUNT 88	
16. SUPPLEMENTARY NOTATION				
17. COSATI CODES			18. SUBJECT TERMS (Continue on reverse if necessary and identify by block number)	
FIELD 04	GROUP 02	SUB. GR.	Humidity analysis Data assimilation Numerical weather prediction Moisture variables Spectral forecast model Interpolation	
19. ABSTRACT (Continue on reverse if necessary and identify by block number)				
<p>A fundamental activity of numerous numerical weather prediction centers is objective analysis of the global atmosphere. Typically, the objective analysis is a product of a four-dimensional (4-D) global data assimilation system. Such a system includes objective analysis, initialization, and global forecast model components. It is common for the objective analysis to be performed on constant pressure surfaces, while the forecast model operates on the standard sigma (σ) coordinate or a close variant. This necessitates vertical interpolations between pressure surfaces and σ-coordinate surfaces before and after the forecast.</p> <p>This study shows that the choice of moisture variable and interpolation method in the vertical interpolation can be crucial to preserving a reasonable moisture distribution in humidity assimilations. The use of relative humidity (RH), dewpoint (T_d), and specific humidity (Q) are tested in four two-point interpolation methods including linear, logarithmic, exponential, and power law. The standard use of logarithmic interpolation, (over)</p>				
20. DISTRIBUTION/AVAILABILITY OF ABSTRACT UNCLASSIFIED/UNLIMITED <input checked="" type="checkbox"/> SAME AS RPT <input type="checkbox"/> DTIC USERS <input type="checkbox"/>		21. ABSTRACT SECURITY CLASSIFICATION Unclassified		
22a. NAME OF RESPONSIBLE INDIVIDUAL Kenneth Mitchell		22b. TELEPHONE NUMBER (Include Area Code) (617) 861-2954	22c. OFFICE SYMBOL LYP	

DD FORM 1473, 83 APR

EDITION OF 1 JAN 73 IS OBSOLETE

UNCLASSIFIED
SECURITY CLASSIFICATION OF THIS PAGE

UNCLASSIFIED

SECURITY CLASSIFICATION OF THIS PAGE

11. Title (Contd)

Assimilation System

19. Abstract (Contd) ^{sub 4}

[that is, linear interpolation in $\ln(P)$] is shown to be a suitable choice when vertically interpolating RH or T_d , but a singularly poor choice when interpolating Q. Logarithmic interpolation of Q is shown to produce an overwhelming positive moisture bias in the middle troposphere in humidity assimilations. This bias is traced to a pronounced convexity in typical vertical profiles of Q as a function of $\ln(P)$. Tests of cubic spline interpolation of Q in $\ln(P)$ showed negligible improvement. Instead, power law interpolation of Q [that is, linear interpolation of $\ln(Q)$ in $\ln(P)$] proves to be sufficiently accurate, as Q is found to satisfy a power law in P of approximately P to the third power.

Keywords: Humidity analysis

UNCLASSIFIED

SECURITY CLASSIFICATION OF THIS PAGE

Accession For	
NTIS GRA&I	<input checked="" type="checkbox"/>
DTIC TAB	<input type="checkbox"/>
Unannounced	<input type="checkbox"/>
Justification	
By _____	
Distribution/ _____	
Availability Codes	
Avail and/or	
Dist	Special
A-1	



Preface

The authors wish to thank several persons who contributed to the development and preparation of this report. Dr. Stephen Brenner assisted in the executions of the AFGL spectral model in Section 4. Mr. Sam Yee provided several helpful suggestions regarding the spectral truncation tests in Section 3.3. Mr. Don Aiken was instrumental in formatting and maintaining the FGGE data sets and in generating all the computer graphics.

We also thank Mr. Don Chisholm for his thorough review of the manuscript. His helpful suggestions aided us in clarifying several sections. In addition, we extend our appreciation to Ms. Betty Blanchard for her patient typing of the manuscript.

The computer codes for the preprocessor and postprocessor of the AFGL spectral model were the central codes in this study. The original codes were provided by NMC, whose cooperation we gratefully acknowledge. We especially thank Major John Warburton, the Air Force Liaison Officer to NMC, and Drs. Joseph Gerrity and Joseph Sela of NMC for their efforts in providing AFGL with excellent documentation of these codes. Finally, we thank Mr. Karekin Agazarian and Mr. Don Aiken for assisting us in adapting these codes for use at AFGL.

Contents

1. INTRODUCTION	1
2. MOISTURE PREPROCESSING/POSTPROCESSING	4
2.1 Vertical Interpolation	7
2.2 Moisture Variables	10
2.3 The Processing Sequence	12
3. ANALYSIS OF PROCESSING ERROR	14
3.1 Extrapolation Error	15
3.2 Interpolation Error	22
3.3 Horizontal Truncation Error	48
3.4 Terrain Effects	52
4. A PSEUDO 4-D DATA ASSIMILATION	55
5. CONCLUSIONS	68
REFERENCES	71
APPENDIX A: POWER LAW INTERPOLATION	73
APPENDIX B: AN ALTERNATIVE VERIFICATION	75
LIST OF ACRONYMS	77

Illustrations

1. Schematic Diagram of a 6-Hourly Intermittent Data Assimilation System (Top) Contrasted With a Standard Forecast Execution Over the Same Time Period (Bottom) 2
2. Diagram of Components of a Complete Forecast Cycle (Solid-Line Path) and Components of a Synthesized Analysis Sequence (Dashed-Line Path) 5
3. Illustration of Vertical σ -Coordinate in NMC/AFGWC Global Spectral Model 8
4. Graphical Illustration of the Interpolation and Extrapolation of Moisture Variable f in the NMC/AFGWC Pre- and Postprocessor ($Z = \text{Ln}P$) 11
5. Vertical Profiles of Global Mean BIAS and RMSE for the (S_1, A_1) Verification of the 00Z FGGE III-A Analysis of 17 January 1978, Synthesized by Applying the Computations of Tables 4 and 5 to Six Moist σ -Layers for the Three Choices of Vertically Interpolated Moisture Variable of $F = (RH, Q, T_d)$ 16
6. Illustration of Bias Effects of Currently Operational Upper Moisture Extrapolation Sequence in NMC/AFGWC Pre- and Postprocessor for 6 or 7 Moist σ -Layers in Either the 9- or 12-Layer Resolutions in Table 2. The moisture variable f is assumed to decrease with height (see Figure 7) 17
7. Vertical Profiles of Global Mean \bar{T} , \bar{T}_d , \bar{RH} , and \bar{Q} for a Sample of Six Winter 1978 FGGE III-A Analyses for 00Z on 15, 17, 19 January and 12Z on 15, 18, 20 January. Location of lowest six σ -layers of 9- or 12-layer resolution in Table 2 is shown for $P_s = 101.3 \text{ cb}$ 18
8. Illustration of Bias Effects of Current (Left) and Proposed (Right) Lower Moisture Extrapolation Sequence in NMC/AFGWC Pre- and Postprocessor in Either the 9- or 12-Layer Resolutions in Table 2. The moisture variable f is assumed to decrease with height (Figure 7) 19
9. As in Figure 5 Except for Both Six (Dashed Curve) and Seven (Solid Curve) Moist σ -Layers and Using Linear Lower and Upper Extrapolation in Postprocessing. When not given, dashed curve is coincident with solid curve 20
10. As in Figure 9 Except for the 00Z FGGE III-A Analysis of 18 July 1978 21
11. Illustration of Relation of Convex and Concave Curvature of a General Monotonic Increasing Function $F(Z)$ to Bias in First-Order Vertical Interpolation in Pre- and Postprocessing 23

Illustrations

- | | |
|---|----|
| <p>12. Vertical Profiles of the Analyzed N. H. Mean Specific Humidity, \bar{Q}, and $\text{Ln}\bar{Q}$, Plotted Against P and $\text{Ln}P$ for an Averaged Sample of Six 1978 FGGE III-A Analyses in (a) January (Using 00Z on 15, 17, 19 January and 12Z on 15, 18, 20 January) and (b) July (Using 00Z on 16, 18, 20 July and 12Z on 17, 19, 22 July)</p> | 24 |
| <p>13. Vertical Profiles of the Observed January (a) and July (b) N. H. Mean Specific Humidity, \bar{Q}, and $\text{Ln}\bar{Q}$, Plotted Against P and $\text{Ln}P$ (From the 1963-1973 RAOB Climatology of Oort16)</p> | 25 |
| <p>14. A Sample of Interpolated Q-Profiles for n Iterations (n = 0, 8, 16, 24) of the Pair of P$\rightarrow$$\sigma$ and $\sigma\rightarrow$P Logarithmic Interpolations [Eqs. (1) and (2) With F = Q, Z = $\text{Ln}P$] Applied to the Input Q-Profile of Table 6a and Using the Seven Moist σ-Layers of the 12-Layer Column of Table 2 With $P_S = 101.3$ cb</p> | 31 |
| <p>15. Vertical Profiles of the Global Mean BIAS and RMSE for the Synthesized FGGE III-A Analysis (17 January 1978, 00Z) Obtained Using Power Law Interpolation of Q (Solid Curve) and Logarithmic Interpolation of Q (Dashed Curve, Repeated From Q-Based Solid Curve in Figure 9) in the NMC/AFGWC Pre- and Postprocessor</p> | 33 |
| <p>16. Vertical Profiles of the N. H. January Mean FGGE III-A Analyzed Relative Humidity, RH, and Dew-point, T_d, Plus Ln RH and Ln T_d, Plotted Against P and $\text{Ln}P$. From the same sample of analyses as Figure 12a</p> | 34 |
| <p>17. Vertical Profiles of the Global Mean BIAS and RMSE for the Synthesized FGGE III-A Analysis (17 January 1978, 00Z) Obtained by Executing the NMC/AFGWC Pre- and Postprocessor for the 12-Layer σ-Structures of Table 2 (Solid Curve) and Table 10 (Dashed Curve) Using Vertical Interpolations of F = (RH, $\text{Ln}Q$, T_d) in Z = $\text{Ln}P$</p> | 38 |
| <p>18. Latitude-Height Contour Analysis of the Zonal Mean of the 1978 FGGE III-A Analysis of RH for the Winter Case (a) and the Summer Case (b) Representing the Inputs for Figure 19 and Figure 20, Respectively. Contour interval is RH = 10 percent</p> | 39 |
| <p>19. Latitude-Height Contour Analysis of the Zonal Mean BIAS (Top), RMSE (Middle), and Analyzed RH (Bottom) for the Synthesized FGGE III-A Analysis (17 January 1978, 00Z) Obtained Using Logarithmic Interpolation of RH (a), T_d (c), and Q (d), and Power Law Interpolation of Q (b). Contour interval is RH = 2 percent (except RH = 10 percent in bottom plot). Dashed contours denote negative values (BIAS only)</p> | 40 |

Illustrations

- | | |
|---|----|
| 20. As in Figure 19 Except for the FGGE III-A Analysis of 18 July 1978, 00Z | 44 |
| 21. Latitude-Height Contour Analysis of the Zonal Mean RMSE for the Synthesized FGGE III-A Analysis (17 January 1978, 00Z) Obtained by Skipping All Spectral Transforms in Pre- and Postprocessing While Using Logarithmic Interpolation of RH (Top), and T_d (Bottom), and Power Law Interpolation of Q (Middle). Contour interval is RH = 2 percent | 49 |
| 22. As in Figure 21 Except Spectral Transforms Reinstated in Pre- and Postprocessing, Where Transformed Moisture Variable was RH (Top), LnQ (Middle), and T_d (Bottom) | 50 |
| 23. Vertical Profiles of the Global Mean BIAS and RMSE for the Synthesized FGGE III-A Analysis (17 January 1978, 00Z) Obtained by Executing the NMC/AFGWC Pre- and Postprocessor Using Vertical Interpolation of $F = (RH, LnQ, \text{ or } T_d)$ in LnP With the Indicated Choices of Horizontal Spectral Transforms (a) and With no Transforms for Either the Original or Zero Terrain (b) | 51 |
| 24. As in Figure 21 Except Zero Terrain Imposed Globally | 54 |
| 25. Repeat of the Dot-Dashed Curve (a) and the Solid Curve (b) of Global Mean RMSE in the RH-Based Interpolations of Figure 23(b) and (a) Respectively, Alongside the Parallel Cases (Dotted Curves) Where Postprocessed RH Values are the Adjusted Values of RH^* in Eq. (B1) | 55 |
| 26. Latitude-Height Contour Analysis of the Zonal Mean of RH^* in Eq. (B1) Corresponding to the Global Mean of RH^* in Figure 25(a) and Figure 25(b) | 56 |
| 27. Vertical Profiles of the Global Mean BIAS and RMSE for the (S_1^n, A_1) , (F_1^{nT}, A_1) , and (F_1, A_1) Verifications (Defined in Text) Associated With the 48-hr Pseudo 4-D Assimilation ($n=8, T=6$ hr) Starting From the 00Z 1978 FGGE III-A Analysis of 17 January [19 January for (S_1^n, A_1)]. Results given for the four vertical interpolations of $F = (RH, LnQ, T_d, \text{ or } Q)$ in $Z = LnP$ | 57 |
| 28. Temporal Trend at $P = 40$ cb Level for the Global Mean BIAS and RMSE of the (S_1^n, A_1) , (F_1^{nT}, A_1) , and (F_1, A_1) Verifications in Figure 27. The (S_1^n, A_1) trend is shown for a given number of cycles, n , as it is not strictly defined over time intervals | 58 |

Illustrations

- | | |
|--|----|
| <p>29. Latitude-Height Contour Analysis of the Zonal Mean BIAS Valid at 48 h ($n=8$, $T=6$ hr) and Given From Top to Bottom for the (S_1^n, A_1), (F_1^n, A_1), and (F_1, A_1) Verifications, Respectively, in Figure 27. Parts (a) through (d), respectively, represent the interpolation types depicted from left to right in Figure 27</p> | 59 |
| <p>30. As in Figure 29 but for Zonal Mean RMSE</p> | 63 |

Tables

- | | |
|---|----|
| <p>1. Summary of the Analyzed and Vertically Interpolated Moisture Variables in the 4-D Assimilation at Five NWP Facilities</p> | 6 |
| <p>2. The Vertical σ-Layer Structure for Several Resolutions of the NMC/AFGWC Global Spectral Model</p> | 8 |
| <p>3. List of Interpolation Type Provided by Eqs. (1) and (2) for Various Functional Transformations, $F = F(f)$ and $Z = Z(P)$, of the Moisture Variable f and Vertical Coordinate P</p> | 9 |
| <p>4. Summary of Vertical Interpolation and Extrapolation Procedures for the Moisture Field in the NMC/AFGWC Pre- and Postprocessor (Where $Z = \ln P$)</p> | 10 |
| <p>5. Sequence of Moisture Computations in the NMC/AFGWC Preprocessor (a) and Postprocessor (b)</p> | 13 |
| <p>6. Profiles of Interpolated Specific Humidity \tilde{Q}, After a Pair of $P \rightarrow \sigma$ and $\sigma \rightarrow P$ Interpolations Using the Functional Transformations $F(Z)$ in Table 2 Applied to the Observed N.H. Q-Profile for January in Figure 13(a) [Table 6 (a) and (b)] and for July in Figure 13(b) [Table 6 (c) and (d)]. Tables 6(a) and (c) used the first-order interpolation in Eqs. (1) and (2). Table 6 (b) and (d) used the cubic-spline interpolation after Ahlberg et al.¹⁷ Seven moist σ-layers were taken from the last column in Table 2 (with $P_s = 101.3$ cb). Errors $\tilde{Q}-Q$ are given as equivalent RH errors, derived using the corresponding temperature profile (uninterpolated)</p> | 27 |

Tables

7. As in Table 6 Except FGGE III-A Analyzed N. H. Mean Q-Profiles of Figure 12 Replace Those of Figure 13 as Inputs	29
8. Vertical Profiles of the Global Mean BIAS (a) and RMSE (b) for the Synthesized FGGE III-A Analysis (17 January 1978, 00Z) Obtained Using the Four Interpolation Types of Table 3 and the Moisture Variables $f = (RH, Q, T_d)$ in the Vertical Interpolations of the NMC/AFGWC Pre- and Postprocessor	32
9. Vertical Profiles of the Global Mean BIAS and RMSE for Three Winter and Three Summer Synthesized FGGE-III-A Analyses Obtained Using Logarithmic Interpolation of RH and T_d and Power Law Interpolation of Q in the Vertical Interpolations of the NMC/AFGWC Pre- and Postprocessor. Also given are the sample mean and sample standard deviation BIAS and RMSE	36
10. The 12-Layer σ -Structure Used in the Pre- and Postprocessor Runs for Figure 17 (Compare With Table 2)	37

A Comparison of Moisture Variables in the Vertical Interpolations of a 4-D Assimilation System

1. INTRODUCTION

Global NWP centers routinely generate objective analyses of the global atmosphere to provide an accurate depiction of its structure at a given time and on a uniform three-dimensional (3-D) grid. Characteristically, the analysis function is performed in the context of a global four-dimensional (4-D) data assimilation system. The crucial components of a 4-D assimilation system are observations, objective analysis (interpolation of observations to a uniform grid), initialization (balancing of mass and motion fields), and short-range forecast (usually of 6- or 12-hr duration).

NWP centers such as ECMWF,¹ NMC,² and AFGWC³ currently use similar 4-D data assimilation systems.* All three centers employ 6-hr update cycles, as

(Received for Publication 11 April 1985)

1. Lorenc, A., and Tibaldi, S. (1979) *The Treatment of Humidity in ECMWF's Data Assimilation Scheme*, ECMWF Research Department, Technical Memorandum No. 7, Reading, Berkshire, U.K., 103 pp.
2. Morone, L., and Dey, C. (1983) *The NMC Global Data Assimilation System*. Preprints, Sixth Conf. on Numerical Weather Prediction, 6-9 June, 1983 Amer. Meteor. Soc., Omaha, Nebr., pp. 115-119.
3. Koermer, J. (1983) *The Advanced Weather Analysis and Prediction System*. Preprints, Sixth Conf. on Numerical Weather Prediction, 6-9 June, 1983, Amer. Meteor. Soc., Omaha, Nebr., pp. 82-84.

*See list of acronyms at the end of this report.

illustrated in Figure 1. An optimal interpolation (OI) objective analysis of the observations updates a 6-hr forecast from a global spectral model (GSM). The analyzed mass and motion fields are then balanced using a normal mode initialization (NMI) procedure. Next, a 6-hr GSM forecast provides the first-guess fields for the next OI analysis. Necessarily, this process involves vertical interpolations to transfer the analysis fields on pressure surfaces to the σ -coordinate surfaces of the GSM before the forecast and vice versa after the forecast. These interpolation steps are referred to as the preprocessor and postprocessor, respectively.

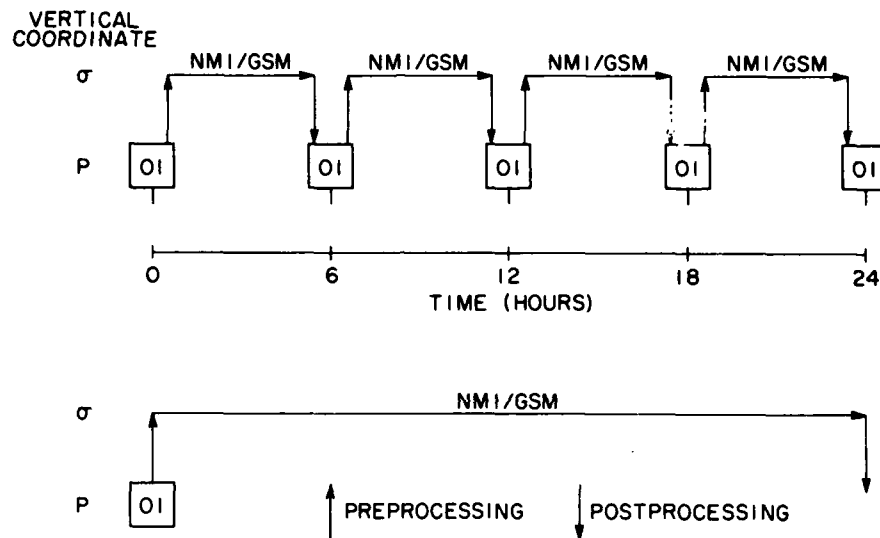


Figure 1. Schematic Diagram of a 6-Hourly Intermittent Data Assimilation System (Top) Contrasted With a Standard Forecast Execution Over the Same Time Period (Bottom)

A major difficulty of data assimilation is that because of biases and inaccuracies in the forecast, initialization, and pre- and postprocessing, continuous repetitions of the 6-hr cycle contribute an undesirable climatic drift to the assimilation. This climatic drift can occur despite the corrective effects of the objective analysis. This is particularly true in the case of humidity assimilation, since characteristically there are fewer humidity observations than wind and mass observations to support the objective analysis. Heretofore, most attention to the climate drift problem has focused on the initialization and forecast model components, with lesser attention paid to the vertical interpolation interfaces in pre- and postprocessing. Similarly, even less attention has been given to climatic drift in the humidity fields as compared to the mass and motion fields.

Historically, the lack of attention to global humidity analysis derives from studies^{4,5} that show that outside the tropics large-scale models fairly quickly generate reasonable humidity fields after one or two days, independent of the input humidity analysis. Rather, the humidity fields evolve in response to the large-scale model's developing vertical motion fields. Hence in the extratropics, the task of humidity analysis may be redundant for purposes of initializing many large-scale NWP models. In this context, FNOC chooses not to perform a humidity analysis in its global data assimilation system.⁶ Instead, the first-guess forecast field of humidity becomes the initial moisture field for the subsequent assimilation cycle.

However, objective analysis is not necessarily performed merely to initialize NWP models. Often, objective analysis is important for depicting atmospheric structure for diagnostic general circulation studies or in military applications to assess the impact of the earth's atmosphere on military systems. For these kinds of applications, humidity analyses derived in the manner of FNOC, from assimilation systems that do not assimilate humidity observations, can develop significant biases owing to model errors.^{4,7}

Even when the main use of humidity analysis is to provide initial conditions for a large-scale model, the assimilation of observed humidity data is important in the tropics. There the coupling of the mass and motion fields is weak and the time required to generate reasonable vertical motion fields (and hence humidity fields) is several days. Furthermore, improved accuracy in describing the initial moisture field in large-scale models has been shown to reduce the global spin-up time for parameterized processes like precipitation, convective heating, and surface moisture fluxes.⁴ For these reasons, in the AFGL global modeling effort, where a chief goal is the production of skillful global cloud forecasts in the one to four day range, humidity analysis and assimilation is considered a necessary and important task.

4. Tibaldi, S. (1982) The ECMWF humidity analysis and its general impact on global forecasts and on the forecast in the Mediterranean area in particular, Riv. Meteorol. Aeronaut. 42:311-328.
5. Smagorinsky, J., Miyakoda, K., and Strickler, R. (1970) The relative importance of variables in initial conditions for dynamical weather prediction, Tellus 22:141-157.
6. Rosmond, T. (1981) NOGAPS: Navy Operational Global Atmospheric Prediction System. Preprints, Fifth Conf. on Numerical Weather Prediction, 2-6 November, 1981, Amer. Meteor. Soc., Monterey, Calif., pp. 74-79.
7. Sirutis, J. Miyakoda, K., and Ploshay, J. (1979) Moisture distribution derived in mathematical models and four-dimensional analysis. Proceedings International Workshop on Atmospheric Water Vapor, 11-13 September, 1979, Vail, Colo., pp. 489-496.

In this study, it will be shown that the choice of moisture variable in the vertical interpolations of the pre- and postprocessor can be crucial to preserving a reasonable moisture distribution in humidity assimilations. Section 2 reviews the several vertical interpolation methods and moisture variable choices that are considered. Section 3 presents results of the use of relative humidity (RH), dewpoint (T_d), and specific humidity (Q) in applications of several vertical interpolations tested within the NMC pre- and postprocessor applied to a set of 1978 FGGE III-A analyses. The extent to which the vertical interpolation errors of the pre- and postprocessor might accumulate in a 4-D assimilation is examined in Section 4 by means of a "pseudo" 48-hr data assimilation. Finally, in Section 5, conclusions and recommendations are presented.

2. MOISTURE PREPROCESSING/POSTPROCESSING

The several steps in a given forecast cycle in Figure 1 are depicted in further detail in Figure 2. It shows that the preprocessing step entails first vertical interpolation (from P to σ) and then spectral transformation from physical gridpoint space to spectral coefficient space in the horizontal direction. The postprocessor reverses those steps. In this study, primary emphasis is given to the errors in the vertical interpolation of moisture fields. Some attention is also given (in Section 3.3) to horizontal truncation errors in the spectral representation of moisture. This study begins with the use of the P to σ and σ to P vertical interpolation algorithms as used in the NMC pre- and postprocessor. This choice is motivated by the inclusion of the NMC processors in the family of new NWP models, referred to as the Advanced Weather Analysis and Prediction System or AWAPS, presently being implemented at AFGWC.³ Concurrently, several research requirements have been conveyed to AFGL in the area of global forecasting and analysis of moisture and clouds. This study is one of several efforts addressing these research requirements.

The general configuration of the global 4-D assimilation system in the AWAPS is given in the top of Figure 1. Through an interagency agreement, NMC has provided AFGWC with the GSM, NMI, and pre- and postprocessor. In addition AFGWC has developed and implemented an OI objective analysis package called the High Resolution Analysis System or HIRAS.⁸ Unlike the NMC OI analysis, which

8. Wilfong, T., Stobie, J., Renninger, L., Lewis, M., Lewis, F., Carr, E., Weiner, A., and Tuell, J. (1984) The Air Force Global Weather Central's high resolution analysis system. Preprints, Sixth Conf. on Numerical Weather Prediction, 6-9 June, 1983, Amer. Meteor. Soc., Omaha, Nebr. pp. 266-268.

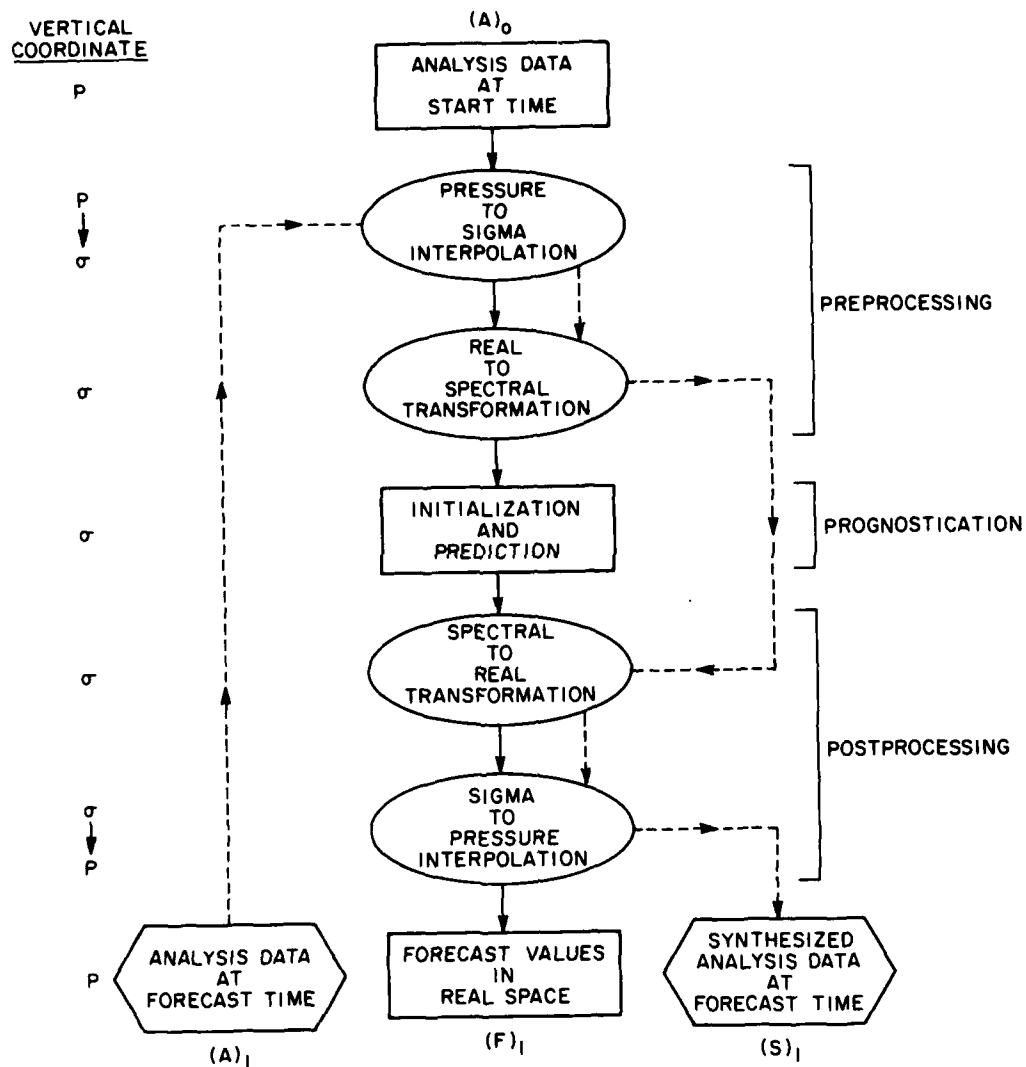


Figure 2. Diagram of Components of a Complete Forecast Cycle (Solid-Line Path) and Components of a Synthesized Analysis Sequence (Dashed-Line Path)

analyzes relative humidity, the AFGWC OI analysis model is presently designed to analyze specific humidity. Consequently, for the sake of expediency, AFGWC replaced relative humidity (RH) with specific humidity (Q) in the vertical interpolations of the NMC pre- and postprocessor.

It is fairly common in pre- and postprocessing to vertically interpolate the same moisture variable that is objectively analyzed. This is apparent in Table 1, which summarizes for five NWP facilities the moisture variable used in the objective analysis and vertical interpolations of the respective 4-D assimilation system. The expedient choice of moisture variable for vertical interpolation is not necessarily the best choice, however. Preliminary AFGL tests¹¹ of the NMC/AFGWC pre- and postprocessor indicated that the use of Q in the vertical interpolations introduced a significant positive moisture bias in the 6-hr first-guess forecast fields of Figure 1. This problem led to the present investigation into alternate choices of moisture variable and/or vertical interpolation method in the processing steps.

Table 1. Summary of the Analyzed and Vertically Interpolated Moisture Variables in the 4-D Assimilation at Five NWP Facilities

NWP Center	Analyzed Moisture Variable	Vertically Interpolated Variable	Vertical P→σ/σ→P Interpolation
AFGWC ⁸	Q	Q	Linear in LnP
NMC ²	RH	RH*	Linear in LnP
ECMWF ¹	Q†	Q	Cubic spline in LnP
GFDL ⁹	T _d	Q	Cubic spline in P
GLAS ¹⁰	RH	RH*	Linear in LnP

*Analyzed residuals of RH in preprocessor

†Layer integrated

9. Stern, W., and Ploshay, J. (1983) An assessment of GFDL's continuous data assimilation system used for processing FGGE data. Preprints, Sixth Conf. on Numerical Weather Prediction, Amer. Meteor. Soc., 6-9 June, 1983, Omaha, Nebr., pp. 90-95.
10. Baker, W. (1983) Objective analysis and assimilation of observational data from FGGE, Mon. Wea. Rev. 111:328-342.
11. Brenner, S., Yang, C., and Yee, S. (1982) The AFGL Spectral Model of the Moist Global Atmosphere: Documentation of the Baseline Version, AFGL-TR-82-0393, AD A129283.

Except for ECMWF, Table 1 is current at the time of writing. In the case of ECMWF, Table 1 shows the procedures used to perform the ECMWF 1979 FGGE III-B humidity analyses. As suggested in Lorenc and Tibaldi,¹ the latter analyses likely include nontrivial errors from vertical interpolations of Q (see their Figure 7). As documented in Lönnerberg and Shaw,¹² ECMWF has since replaced cubic spline interpolation of Q in LnP with a procedure using layer averages of RH in P. However, the present authors found no ECMWF reports in the public domain that documented tests leading to this change. The present study will show why vertical interpolation of Q in LnP is a singularly poor choice and will suggest several suitable alternatives.

2.1 Vertical Interpolation

Vertical interpolation in 4-D assimilation is necessary whenever the analysis model and forecast model utilize a different vertical coordinate. As depicted in Figure 1, the NMC and AFGWC OI analyses are performed on constant pressure surfaces while the GSM employs the standard σ -coordinate. This coordinate is defined by $\sigma = P/P_g$, where P_g denotes the surface pressure. Hence $0 \leq \sigma \leq 1$ and $P(\sigma)$, the pressure of a given σ -layer, is given by $P(\sigma) = \sigma P_g$. Table 2 presents the σ -layer structure used in the NMC/AFGWC GSM for various vertical resolutions.¹³ Figure 3 schematically illustrates the vertical σ -structure of the 6-layer GSM. In all the experiments in this study, we employ the 12-layer σ -structure of Table 2, following the NMC operational practice at the time reported by Sela.¹⁴

We next briefly review the several vertical interpolations to be tested here in the NMC/AFGWC pre- and postprocessor. To facilitate concurrent presentation of these vertical interpolation schemes, a generalized notation is adopted. One can begin by considering a general function F of an independent variable Z. To first order, given known values of F_1 and F_2 at two locations Z_1 and Z_2 , the interpolated value \tilde{F} at some location \tilde{Z} between Z_1 and Z_2 is given by the linear formula

$$\tilde{F} = F_1 + A(\tilde{Z} - Z_1) \quad , \quad (1)$$

12. Lönnerberg, P., and Shaw, D., Eds. (1983) ECMWF Data Assimilation: Scientific Documentation, ECMWF Research Dept., Research Manual 1, Reading, Berkshire, U.K., 103 pp.
13. Warburton, J., Ed. (1983) NMC/AWS Global Spectral Model Maintenance Manual, NMC Development Division, National Meteorological Center, NOAA, Washington, D.C.
14. Sela, J. (1980) Spectral modeling at the National Meteorological Center, Mon. Wea. Rev. 108:1279-1292.

Table 2. The Vertical σ -Layer Structure for Several Resolutions of the NMC/AFGWC Global Spectral Model

Index	6-Layer		9-Layer		12-Layer	
	$\Delta\sigma_k$	σ_k	$\Delta\sigma_k$	σ_k	$\Delta\sigma_k$	σ_k
1	0.100	0.950	0.075	0.962	0.075	0.962
2	0.150	0.824	0.125	0.862	0.125	0.862
3	0.170	0.664	0.150	0.724	0.150	0.724
4	0.230	0.462*	0.150	0.574	0.150	0.574
5	0.200	0.245	0.125	0.436	0.125	0.436
6	0.150	0.062	0.075	0.337*	0.075	0.337
7			0.100	0.249	0.050	0.275*
8			0.100	0.148	0.050	0.225
9			0.100	0.041	0.050	0.175
10					0.050	0.124
11					0.050	0.074
12					0.050	0.021

*Highest moist σ -layer in NMC/AFGWC GSM.

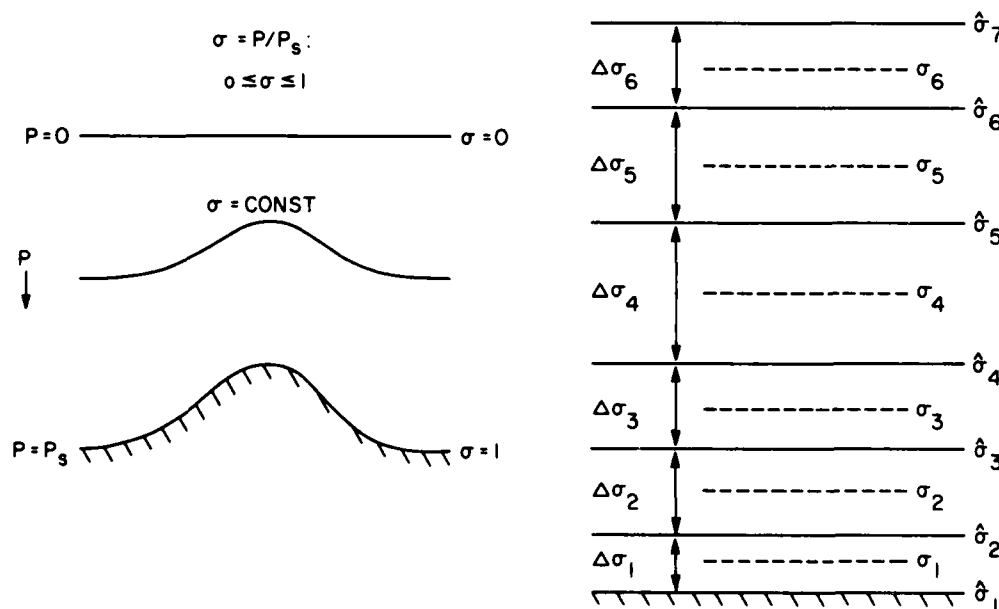


Figure 3. Illustration of Vertical σ -Coordinate in NMC/AFGWC Global Spectral Model

where

$$A = \frac{F_2 - F_1}{Z_2 - Z_1} \quad (2)$$

The error or remainder term implicit in Eq. (1) is

$$R = F''(Z^*) \frac{(\tilde{Z} - Z_1)^2}{2} \quad (3)$$

where F'' is the second derivative of F at some Z^* between \tilde{Z} and Z_1 .

For generality, consider F and Z to represent elementary transformations of more fundamental physical quantities f and z , such that $F = F(f)$ and $Z = Z(z)$. In particular, we let f generically denote the chosen moisture variable (RH , Q , or T_d) and take z to be the pressure P . In Table 3, it is seen that by taking F and Z to represent various combinations of $\text{Ln}f$ or f and $\text{Ln}P$ or P , respectively, the first-order interpolation algorithm in Eqs. (1) and (2) can represent any one of four standard interpolation types (namely linear, logarithmic, exponential, or power law). As an example, the equivalence between Eqs. (1) and (2) and the interpolation type given in Table 3, in the case of power law interpolation, is shown in Appendix A.

Table 3. List of Interpolation Type Provided by Eqs. (1) and (2) for Various Functional Transformations, $F = F(f)$ and $Z = Z(P)$, of the Moisture Variable f and Vertical Coordinate P

Case	F	Z	Interpolation Type
1	f	$\text{Ln}P$	logarithmic: $\tilde{f} = a \text{Ln}(\tilde{P}/b)$
2	f	P	linear: $\tilde{f} = a\tilde{P} + b$
3	$\text{Ln}f$	$\text{Ln}P$	power law: $\tilde{f} = a\tilde{P}^b$
4	$\text{Ln}f$	P	exponential: $\tilde{f} = a \text{Exp}(\tilde{P}/b)$

In the NMC/AFGWC pre- and postprocessor, $F = f$ and $Z = \text{Ln}P$ (case 1 in Table 3). Thus, the NMC/AFGWC processors assume the moisture variable f varies logarithmically with P . This assumption is common in Table 1. We shall find in Section 3.2 that this is a good assumption for the choice of $f = T_d$ and a fair assumption for $f = RH$. For $f = Q$ on the other hand, we shall find that Q does not vary logarithmically with P , but rather closely satisfies a power law in P .

The special case of extrapolation must also be considered. In this case levels (Z_1, Z_2) would be the two lowest or two highest levels at which F is known, and thus either $\tilde{Z} < Z_1 < Z_2$ (upper extrapolation) or $Z_1 < Z_2 < \tilde{Z}$ (lower extrapolation). Different extrapolation assumptions are applied to the moisture variable f in the NMC/AFGWC preprocessor and postprocessor. In the preprocessor, linear extrapolation following Eqs. (1) and (2) is applied, while in the postprocessor constant extrapolation is used. Both the interpolation and extrapolation procedures for the moisture variable f in the NMC/AFGWC processors are summarized in Table 4 and illustrated schematically in Figure 4.

Table 4. Summary of Vertical Interpolation and Extrapolation Procedures for the Moisture Field in the NMC/AFGWC Pre- and Postprocessor (Where $Z = \ln P$)

	Preprocessor ($P \rightarrow \sigma$)	Postprocessor ($\sigma \rightarrow P$)
Levels of Known Data	6 standard pressure levels*	GSM moist σ layers†
Levels of Interpolated Data	GSM moist σ layers†	6 standard pressure levels*
Interpolation $Z_a \leq \tilde{Z} \leq Z_b$	Linear in Z Eqs. (1) and (2)	Linear in Z Eqs. (1) and (2)
Lower Extrapolation $Z_a < Z_b < \tilde{Z}$	Linear in Z Eqs. (1) and (2)	Constant $F(\tilde{Z}) = F(Z_b)$
Upper Extrapolation $\tilde{Z} < Z_a < Z_b$	Linear in Z Eqs. (1) and (2)	Constant $F(\tilde{Z}) = F(Z_a)$

*100, 85, 70, 50, 40, 30 cb

†See Table 2.

2.2 Moisture Variables

In this study, relative humidity (RH), specific humidity (Q), and dewpoint (T_d) are tested in the vertical interpolations. It is evident in Table 1 that these moisture variables are current choices in global objective analysis models and thus likely candidates for vertical interpolation.

Fundamental expressions for RH, Q, and T_d are derived from the vapor pressure, e , and saturation vapor pressure, e_s , given with respect to water by

$$e_s(T) = C/\text{EXP}[L/(1.61 R_d T)] \quad . \quad (4)$$

$$e(T_d) = C/\text{EXP}[L/(1.61 R_d T_d)] \quad . \quad (5)$$

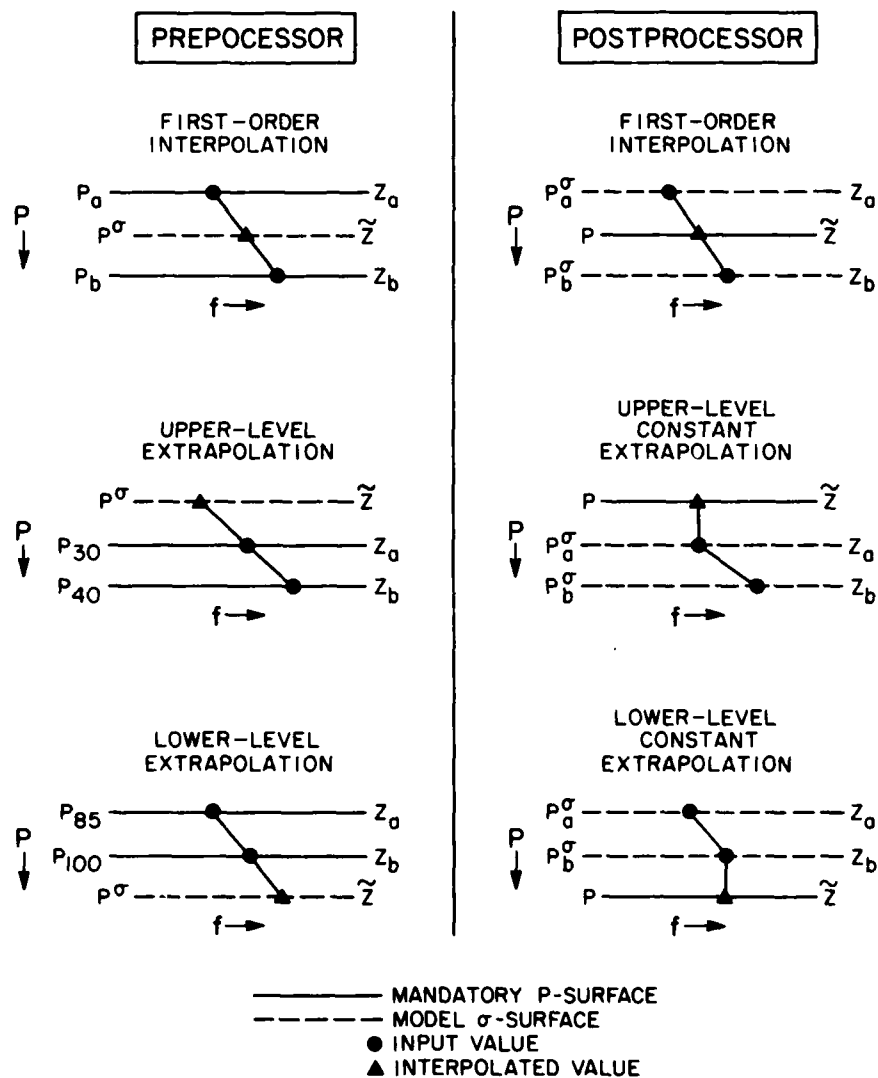


Figure 4. Graphical Illustration of the Interpolation and Extrapolation of Moisture Variable f in the NMC/AFGWC Pre- and Postprocessor ($Z = \ln P$)

Here the constant $C = 2.645 \times 10^8$ cb, the latent heat of vaporization $L = 2.51 \times 10^6 \text{ Jkg}^{-1}$ (at $T = 273.16\text{K}$), and the gas constant for dry air $R_d = 287 \text{ Jkg}^{-1}\text{K}^{-1}$. RH and Q are obtained from e and e_s through

$$\text{RH}(T_d, T) = (e/e_s) \times 100 \quad , \quad (6)$$

$$Q(T_d, P) = \frac{0.622e}{P - 0.378e} \quad . \quad (7)$$

Lastly, T_d is obtained by rewriting Eq. (5) according to

$$T_d = \frac{L/(1.61 R_d)}{\text{Ln}(C/e)} \quad . \quad (8)$$

With Eqs. (4) through (8) and given a value of T and P, any value of RH, Q, or T_d can be used to derive either of the remaining two moisture variables whenever needed. While polynomial approximations¹⁵ for e_s and e can be used in place of Eqs. (4) and (5), we chose not to pursue these approximations here. Implicit in Eqs. (4) through (8) is the computation of the humidity variables with respect to vapor pressure over water for all values of temperature, regardless of whether or not it is subfreezing. This is necessary to be consistent with the FGGE III-A objective analyses of RH, which are specified universally with respect to water. As discussed below, they are used here for both input and assessment fields.

2.3 The Processing Sequence

In a complete 4-D assimilation system such as that in Figure 1, the errors arising from the pre- and postprocessing steps can be difficult to separate from other sources of error. Therefore, to highlight moisture processing error, Section 3 examines the processing error obtained by generating and verifying a "synthesized analysis". As depicted by the dashed-line path in Figure 2, the synthesized analysis is produced by applying the NMC/AFGWC pre- and postprocessor alone to an input FGGE III-A analysis. As such, the synthesized analysis represents a static transformation of the original input analysis, since no forecast model (or initialization) is executed.

Table 5 gives the specific steps in the cycle of pre- and postprocessing used in this study to generate a synthesized analysis. We note that 30-wave rhomboidal truncation (denoted R30) is utilized in the spectral transform steps of Table 5,

15. Lowe, P. (1977) Approximating polynomial for the computation of saturation vapor pressure, J. Appl. Meteorol. 16:100-105.

Table 5. Sequence of Moisture Computations in the NMC/AFGWC Preprocessor (a) and (b) Postprocessor

(a) Preprocessor	
Step	Computation Performed
1	Input FGGE III-A analysis of RH and heights H on $2.5^\circ \times 2.5^\circ$ (144×73) latitude-longitude grid on standard pressure surfaces.
2	Horizontally interpolate the analyzed RH and H fields to the 76 GSM Gaussian latitudes on standard pressure surfaces.
3	Hydrostatically derive temperature T (and surface pressure P_g) on standard pressure surfaces from the height fields, H, and input model terrain.
4	Apply Eqs. (4) through (8) as necessary to convert the (144×76) fields of T and RH to the desired moisture field $f = (RH, Q, \text{ or } T_d)$ on standard pressure surfaces.
5	Vertically interpolate moisture field f of step 4 from standard pressure surfaces to GSM σ -layers of Table 2 using one of the linear interpolation/extrapolation types in Table 3. Hydrostatically derive T on σ -layers using T and H on standard pressure surfaces.
6	Apply Eqs. (4) through (8) as necessary to derive Q from T and moisture field $f = (RH, Q, \text{ or } T_d)$ on GSM σ -layers.
7	Spectrally transform (144×76) gridded fields of Q and T on GSM σ -layers to spherical harmonic coefficients of Q and T.
(b) Postprocessor	
Step	Computation Performed
1	Spectrally transform spherical harmonic coefficients of Q and T to (144×76) Gaussian latitude grid on GSM σ -layers.
2	Apply Eqs. (4) through (8) as necessary to convert gridded Q and T fields on GSM σ -layers to moisture field $f = (RH, Q, \text{ or } T_d)$. Choice of f here agrees with that in step 4, Table 5(a).
3	Vertically interpolate T and moisture field f from GSM σ -layers to standard pressure surfaces using the linear interpolation/extrapolation type of Table 3 used in step 5, Table 5(a).
4	Apply Eqs. (4) through (8) as necessary to convert T and moisture field f to (144×76) RH field on standard pressure surfaces. (This step unnecessary if moisture field $f = RH$.)
5	Output (144×76) RH field on Gaussian latitude grid on standard pressure surfaces for subsequent verification.

again following the NMC operational practice at the time reported by Sela.¹⁴ In some tests in Section 3.3, the spectral transforms in Table 5 are eliminated to isolate processing errors due to vertical interpolation.

3. ANALYSIS OF PROCESSING ERROR

In Figure 2, the solid-line path depicts the total forecast cycle F_1 . The total forecast error shall be denoted (F_1, A_1) representing the verification of the total forecast cycle F_1 against the analysis A_1 , both valid at time t_1 . The dashed-line path in Figure 2 depicts the synthesis or static processing cycle S_1 . The synthesis or processing error shall be denoted (S_1, A_1) representing the verification of the synthesized analysis S_1 against the original analysis A_1 . This section will examine the processing error (S_1, A_1) , while Section 4 will consider total forecast error as well.

In this study the two error quantities computed at each standard pressure level are the global mean RMSE and BIAS. They are obtained from

$$\text{RMSE}(P) = \left\{ \frac{1}{2} \sum_{j=1}^J \left[\text{RMSE}_j^2(P) \right] W_j \right\}^{1/2} \quad (9)$$

$$= \left\{ \frac{1}{2} \sum_{j=1}^J \left[\frac{1}{I} \sum_{i=1}^I (M_{ij} - V_{ij})^2 \right] W_j \right\}^{1/2}$$

$$\text{BIAS}(P) = \left\{ \frac{1}{2} \sum_{j=1}^J \left[\text{BIAS}_j(P) \right] W_j \right\} \quad (10)$$

$$= \left\{ \frac{1}{2} \sum_{j=1}^J \left[\frac{1}{I} \sum_{i=1}^I (M_{ij} - V_{ij}) \right] W_j \right\}$$

where M_{ij} are the "model-produced" RH values (either F_1 or S_1) and V_{ij} are the "verifying" RH values of the analysis A_1 at each horizontal grid point (i, j) on a given pressure surface P . The indices $i=1, 2, \dots, I$ and $J=1, 2, \dots, J$ respectively denote the longitudinal points (equally spaced) and the latitudinal points (non-equally spaced at Gaussian latitudes) of the global grid. W_j is the Gaussian quadrature weight satisfying $\sum_{j=1}^J W_j = 2$. RMSE_j and BIAS_j represent zonal mean values.

The 1978 FGGE III-A analyses, which are products of the operational NMC 4-D data assimilation system in 1978, were used as the input and assessment objective analyses for this study. These analyses provide fields of height H at the lowest 12 standard pressure levels and RH at the lowest six standard pressure

levels on a regular 144×73 latitude-longitude grid ($2.5^\circ \times 2.5^\circ$). The III-A analyses were interpolated horizontally to the 76 Gaussian latitudes of the R30 GSM, transforming the fields to 144×76 . Throughout our verifications, we use the RH analyses [step 2, Table 5(a)] and RH forecasts [step 5, Table 5(b)] on this 144×76 Gaussian grid. Thus in Eqs. (9) and (10), $I = 144$ and $J = 76$. By staying consistently on the Gaussian grid, we eliminate horizontal interpolation error from our measures of vertical interpolation error.

Note that the quantities M_{ij} and V_{ij} in Eqs. (9) and (10) shall always be taken as values of RH, regardless of the moisture variable used in the vertical interpolations. Thus, the vertical interpolations of Q and T_d , when verified in terms of RH, may suffer additionally from processing errors in the temperature field [step 4, Table 5(b)]. While doing so may risk representing the performance of RH interpolations too favorably, it is easier to judge the significance of moisture field errors when expressed in terms of RH. As will be seen later, the implicit favoritism toward RH-based interpolations in the verifications will prove to be small in most cases and never a dominant factor in the comparisons. Nevertheless, for completeness, at the end of Section 3 we try to quantify the degree of RH-favoritism in the verifications.

3.1 Extrapolation Error

This section begins the examination of verification statistics for examples of processing error (S_1, A_1). The first examples show substantial extrapolation errors at the upper and lower levels, so we initially focus on these errors and methods to eliminate them. The investigation of extrapolation errors in this section will entail only the standard logarithmic interpolation type (case 1, Table 3). The next section, which examines interpolation errors in the interior of the moist vertical domain, shall pursue the remaining interpolation types in Table 3.

It is important for this section to note in Table 2 that NMC presently does not carry a prognostic moisture field at all σ -layers. Rather, to save computation time, NMC chooses in its GSM to carry a prognostic moisture field only at σ -layers essentially in the troposphere. It is evident in Table 2 that for typical surface pressures, the highest moist σ -layer that NMC recommends is neither consistently above nor below 30 cb for all three vertical resolutions. For example, in the 9- and 12-layer resolutions (in which the first six σ -layers are identical) six and seven moist σ -layers are recommended respectively. Therefore, to further save computation time in the GSM, we first tested using just six moist σ -layers in our 12-layer experiments with the pre- and postprocessor.

For the three choices of RH, Q , or T_d as the vertically interpolated moisture variable f , Figure 5 presents the vertical profiles of the global mean BIAS and RMSE for the processing error (S_1, A_1) obtained by applying the processing steps

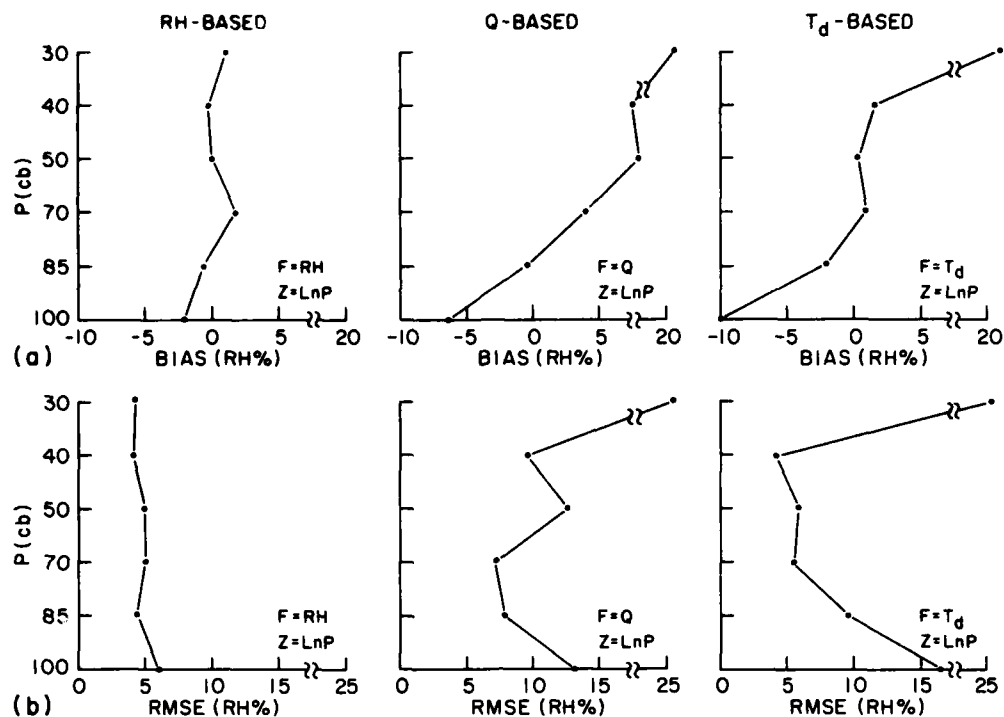


Figure 5. Vertical Profiles of Global Mean BIAS and RMSE for the (S₁, A₁) Verification of the 00Z FGGE III-A Analysis of 17 January 1978, Synthesized by Applying the Computations of Tables 4 and 5 to Six Moist σ -Layers for the Three Choices of Vertically Interpolated Moisture Variable of $F = (RH, Q, T_d)$

of Table 5 to the 00Z FGGE III-A analysis of 17 January 1978. The results in Figure 5 incorporate the operational NMC/AFGWC first-order interpolation/extrapolation algorithms of Eqs. (1) and (2) using $F = f$ and $Z = \text{Ln}P$ (case 1, Table 3), as further depicted in Table 4 and Figure 4.

In Figure 5, the strikingly large BIAS errors at 100 and 30 cb in the Q- and T_d -based profiles result from a common extrapolation problem, which we illustrate shortly. (The reader should note the break in horizontal scale at the right of each plot in Figure 5.) Though much smaller, the bias error at 100 and 30 cb in the RH-based profile stems from the same extrapolation weakness. Inspection of the latitude-height cross-sections (not shown) of the zonal mean BIAS corresponding to Figure 5 confirmed that both the 100- and 30-cb BIAS were quite uniform across all latitudes and not dominated by extreme values in some limited latitude zone.

The left side of Figure 6 schematically illustrates that, given the input of moisture values on only six standard pressure surfaces and given a moisture variable that decreases with height in the upper troposphere, then the constant upper

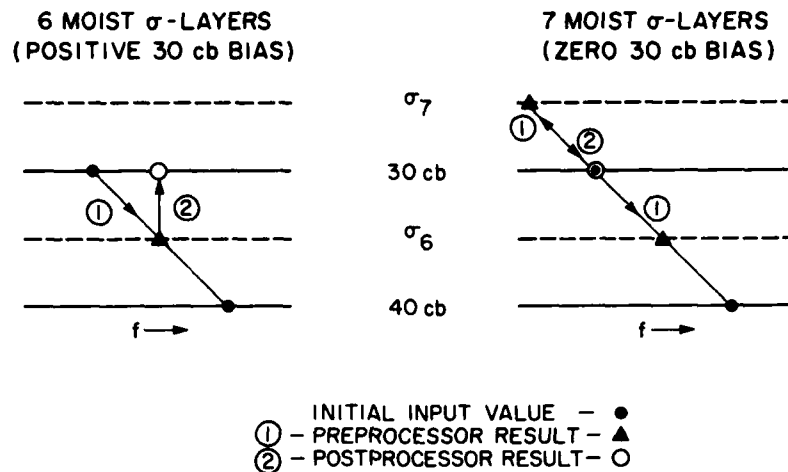
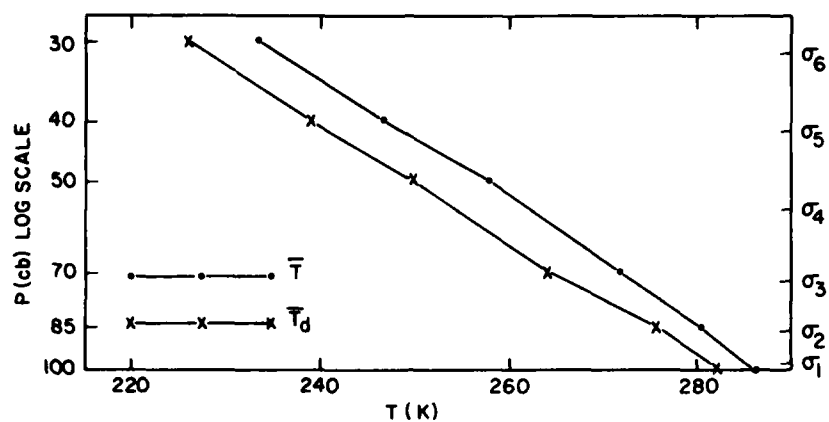
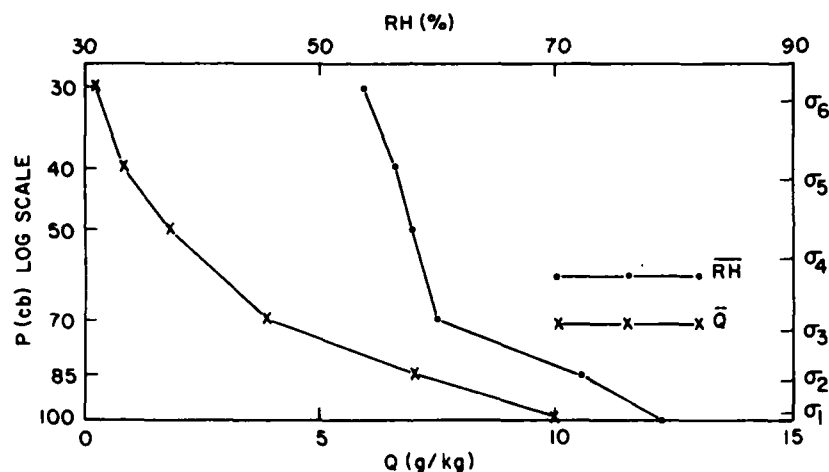


Figure 6. Illustration of Bias Effects of Currently Operational Upper Moisture Extrapolation Sequence in NMC/AFGWC Pre- and Postprocessor for 6 or 7 Moist σ -Layers in Either the 9- or 12-Layer Resolutions in Table 2. The moisture variable f is assumed to decrease with height (see Figure 7)

extrapolation in the postprocessor will always yield a positive (S_1, A_1) bias at 30 cb if the highest moist σ -layer is below 30 cb. This conclusion holds regardless of the total number of moist σ -layers in the chosen vertical resolution. The magnitude of this 30-cb bias will depend on the vertical "lapse rate" of the chosen moisture variable, the proximity of the highest moist σ -layer to 30 cb, and whether the moisture variable is a relative or absolute measure of humidity. Figure 7 presents the sample mean vertical profile of the globally averaged RH, Q , and T_d for six January 1978 FGGE III-A analyses (original, nonsynthesized). For reference purposes, Figure 7 also gives the sample mean temperature profile, as well as representative locations of the six moist σ -layers (for $P_s = 101.3$ cb). We find that all three moisture variables decrease with height at all levels. Similarly, based on the mean temperature profile, the mean profiles of saturation Q and T_d (not shown) decrease with height at all levels. Obviously, saturation values of Q become very small at the cold temperatures at 30 cb, rendering interpolation or extrapolation errors in Q (when expressed as RH errors) very sensitive to small errors. For the current σ -structure (12-layer) and the "climatology" of Figure 7, the positive (S_1, A_1) bias at 30 cb in Figure 5 is acceptably small when using RH (NMC choice), but is unacceptably large when using Q (AFGWC choice) or T_d . These large biases are shown in Figure 5 as equivalent RH biases.



A.



B.

Figure 7. Vertical Profiles of Global Mean T, T_d, RH, and Q for a Sample of Six Winter 1978 FGGE III-A Analyses for 00Z on 15, 17, 19 January and 12Z on 15, 18, 20 January. Location of lowest six σ-layers of 9- or 12-layer resolution in Table 2 is shown for P_s = 101.3 cb

To eliminate the upper extrapolation bias, the approach illustrated on the right of Figure 6 is recommended, wherein the highest moist σ-layer is chosen above 30 cb. Thereby, upper extrapolation of moisture is invoked only in pre-processing (which employs linear instead of constant extrapolation, Figure 4) while in the postprocessor the final 30-cb moisture value is now determined by interpolation. In fact, given a moist σ-layer above 30 cb and at least one between 30 through 40 cb, the processing sequence on the right of Figure 6 will exactly

reproduce the original input moisture value f at 30 cb (disregarding roundoff error and horizontal spectral truncation error).

Rather than follow the right of Figure 6, one may argue that instead one could still retain only six moist σ -layers and employ linear instead of constant upper extrapolation in the postprocessor. This is a fair alternative for RH or T_d (though not Q), as shown shortly. But this alternative does not exactly reproduce the input moisture value at 30 cb unless at least two moist σ -layers exist between 30 through 40 cb. Finally, we caution that in coarse vertical resolutions, where the first σ -layer above 30 cb may exist well above the tropopause (above which the moisture content in the stratosphere is thought to become quasi-constant with height) or in resolutions carrying several active moist σ -layers in the stratosphere, other extrapolation approaches to replace that recommended in the right of Figure 6 should be explored.

The 100-cb negative bias in all three profiles in Figure 5 arises in similar fashion from the constant lower extrapolation in postprocessing shown in Table 4 and Figure 4. The left of Figure 8 illustrates the drying effect of constant lower extrapolation of a moisture variable that decreases with height. This drying effect is especially pronounced in Figure 5 for the absolute moisture variables of $f = Q$

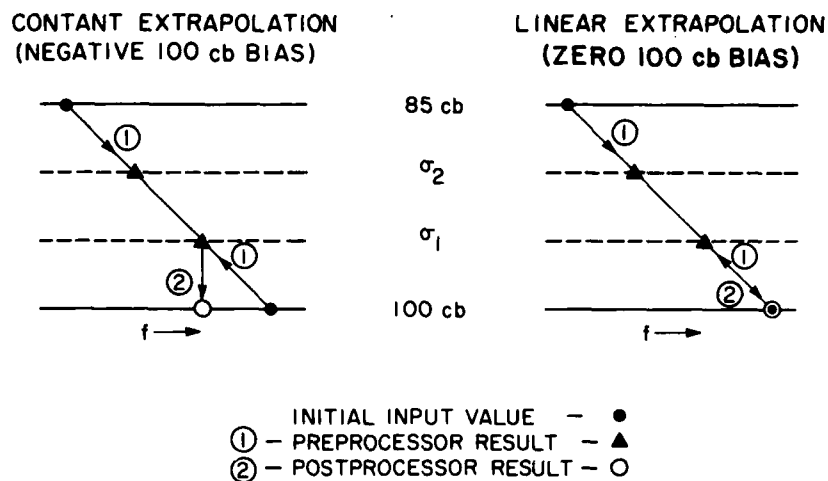


Figure 8. Illustration of Bias Effects of Current (Left) and Proposed (Right) Lower Moisture Extrapolation Sequence in NMC/AFGWC Pre- and Postprocessor in Either the 9- or 12-Layer Resolutions in Table 2. The moisture variable f is assumed to decrease with height (Figure 7)

or $f = T_d$, since the postprocessor applies linear lower extrapolation of temperature and thus the saturation values of T_d and Q will increase downward. The right of Figure 8 shows the improvement obtained by applying linear lower extrapolation for the moisture variable in postprocessing. Indeed, whenever two or more σ -layers are carried within 85 to 100 cb, linear lower extrapolation in postprocessing will give 100-cb synthesized moisture values f that agree exactly with the input values (again disregarding roundoff and spectral truncation errors).

Figure 9 shows the results of repeating the test in Figure 5 using the recommended linear lower and upper extrapolation of the moisture variable throughout the preprocessor and postprocessor. The solid curves of Figure 9 were obtained using seven moist σ -layers (following the right of Figure 6), while the dashed curves were obtained using six moist σ -layers. In the case of seven moist layers, the BIAS at 100 and 30 cb is now virtually zero for all the moisture variables. In

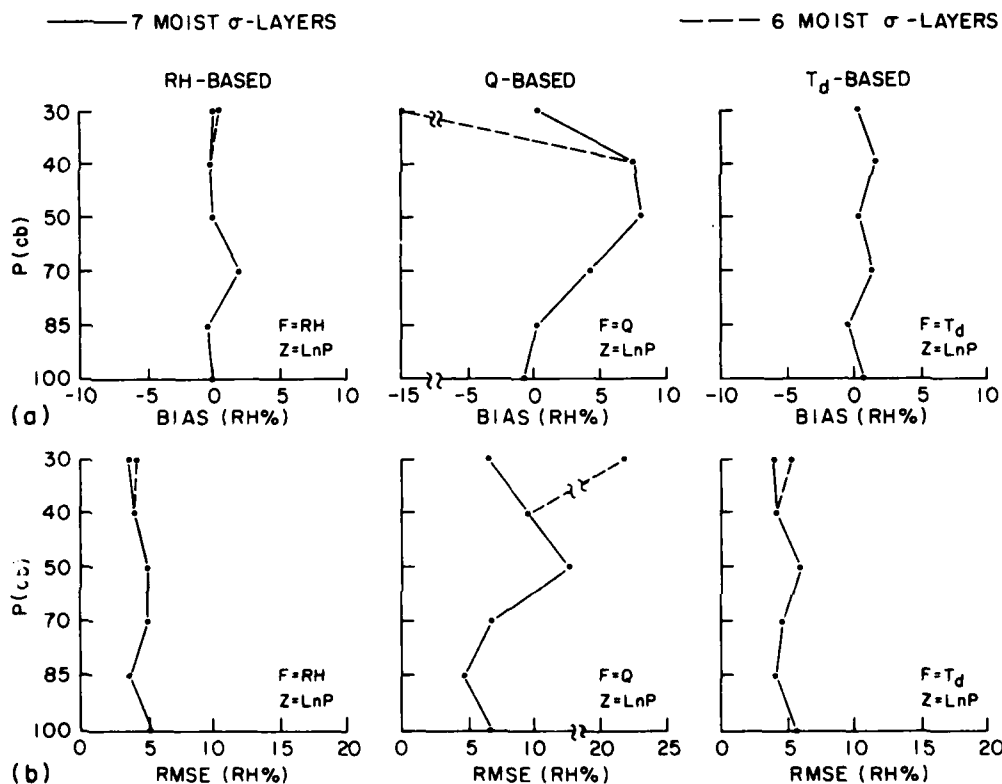


Figure 9. As in Figure 5 Except for Both Six (Dashed Curve) and Seven (Solid Curve) Moist σ -Layers and Using Linear Lower and Upper Extrapolation in Postprocessing. When not given, dashed curve is coincident with solid curve

the case of six moist layers, the BIAS and RMSE results are acceptably comparable to those of the case of seven moist layers, except in the Q-based vertical interpolations. In the latter case the nonlinearity of the sample mean Q-profile with respect to LnP in the upper troposphere in Figure 7 shows Q to be less amenable than RH or T_d to linear upper extrapolation in LnP. Figure 10 repeats the test of Figure 9, with similar results, for the 00Z FGGE III-A analysis of 18 July 1978.

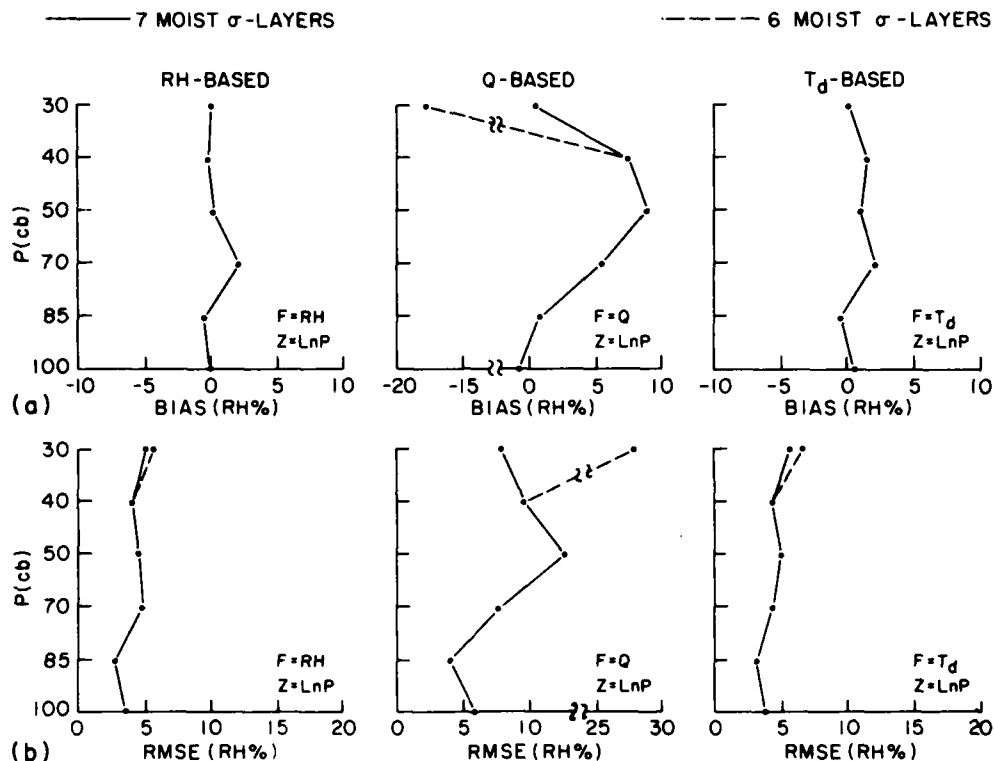


Figure 10. As in Figure 9 Except for the 00Z FGGE III-A Analysis of 18 July 1978

From the results of this section, it is clear that the upper and lower moisture extrapolation in the current NMC/AFGWC processors is acceptable (though not optimal) for $f = RH$, but is clearly unacceptable for $f = Q$ or $f = T_d$ (Figure 5). Admittedly, in the original design of the NMC processors the intent may have been to apply the moisture interpolation/extrapolation algorithms only to $f = RH$. Unfortunately, this likely intent was not followed in the later adaptation of the NMC processors for use by AFGWC.

In conclusion, for any choice of moisture variable $f = (RH, Q, \text{ or } T_d)$ in the NMC/AFGWC processors, it is recommended that (1) linear rather than constant upper and lower extrapolation be applied in postprocessing and (2) the highest

moist σ -layer be the lowest layer consistently above 30 cb. In Table 2 then the use of 5, 7, and 7 moist σ -layers is recommended in the 6-, 9-, and 12-layer resolutions, respectively. The second recommendation above is not crucial for $f = RH$ or T_d , but is imperative for logarithmic interpolations using $f = Q$. Lastly, results later in the next section suggest that six moist σ -layers is sufficient also when using $f = Q$ provided $F = Lnf = LnQ$ and $Z = LnP$ (power law interpolation), since LnQ will be shown to be nearly linear in LnP .

3.2 Interpolation Error

In the previous subsection, significant reductions in vertical extrapolation error were achieved. Yet, a further reduction in the processing error still present in the solid curves of Figures 9 and 10 is desirable. In particular, one would like to reduce the distressingly large positive BIAS and RMSE in the 40 to 70 cb domain of the Q -based error profiles. Toward this end, this section compares the performance of the standard logarithmic interpolation ($F = f$ and $Z = LnP$) with that of the other interpolation types in Table 3.

We recall from Eq. (3) that to achieve accuracy from the first-order interpolation of Eqs. (1) and (2), the dependent variable F must be fairly linear in Z (that is, $F'' \approx 0$). If $F(Z)$ is not linear but rather consistently convex (concave), as given by $F'' > 0$ ($F'' < 0$) throughout the domain, then a successive pair of first-order interpolations from $P \rightarrow \sigma$ and $\sigma \rightarrow P$ will yield a positive (negative) bias. This is demonstrated schematically in Figure 11. It is clear from Figure 7 that for $F = f = Q$ and $Z = LnP$ (logarithmic interpolation), the January mean function $F(Z)$ is consistently convex. It will be shown that the convex nature of Q in $Z = LnP$ is the direct cause of the positive bias at the interior pressure levels in the Q -based profile of Figures 9 and 10.

One can anticipate the preferable interpolation type for Q -based interpolations by examining Figure 12, which shows the N. H. 1978 FGGE III-A January and July sample mean vertical profiles of Q for all four specifications of F and Z in Table 3. Figure 13 shows the corresponding observed mean Q -profiles obtained from the 10-year (1963-1973) climatological RAOB statistics of Oort.¹⁶ In an absolute sense, the FGGE III-A profiles of Q are too moist compared to the RAOB climatology (except at 100 cb in January), but the shapes of the vertical profiles in Figures 12 and 13 are in good agreement. (In the case of LnQ , Figures 12 and 13 show $Ln\bar{Q}$; that is, Ln of the hemispheric average of Q . We would prefer to show \overline{LnQ} , the hemispheric average of LnQ , but this was not available in the Oort

16. Oort, A. (1983) Global Atmospheric Circulation Statistics, 1958-1973, NOAA Professional Paper No. 14, U.S. Government Printing Office, Washington, D. C. 180 pp.

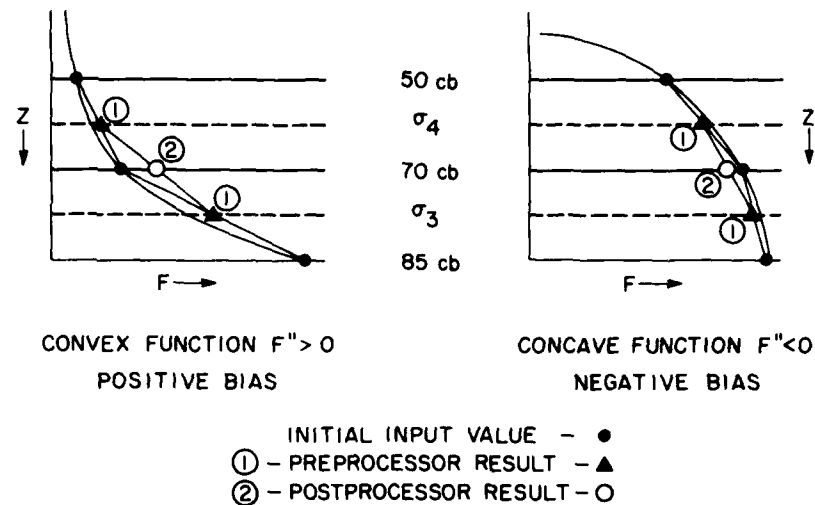
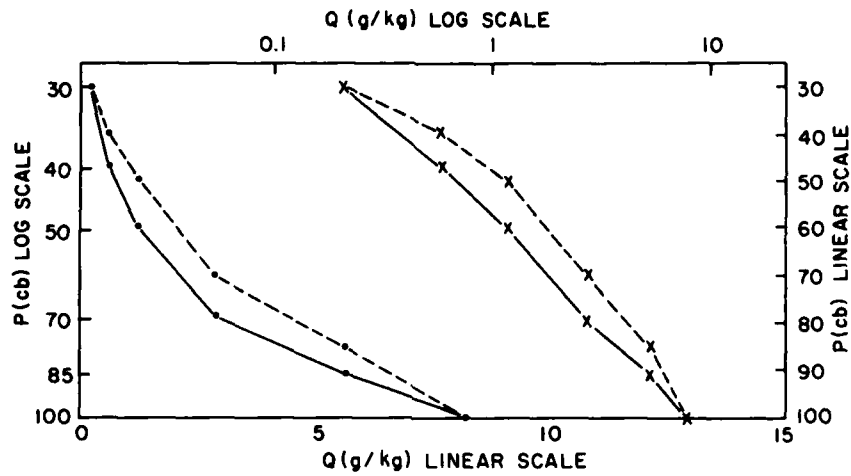


Figure 11. Illustration of Relation of Convex and Concave Curvature of a General Monotonic Increasing Function $F(Z)$ to Bias in First-Order Vertical Interpolation in Pre- and Postprocessing

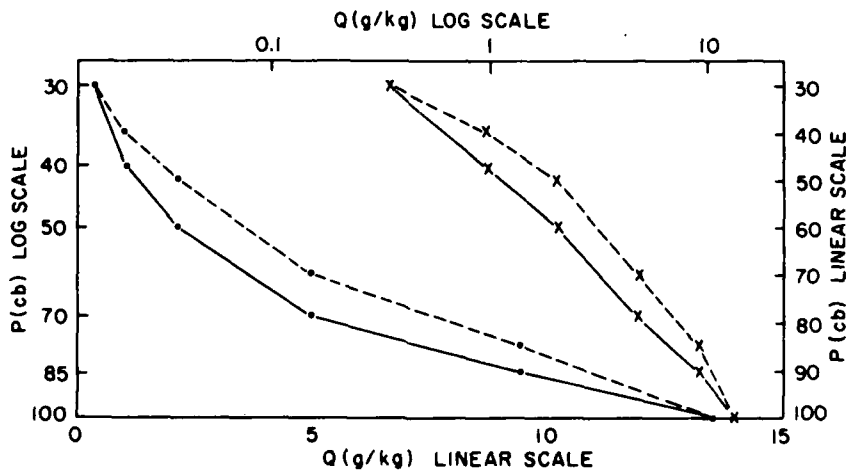
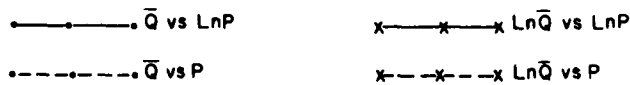
statistics. Strictly speaking $\overline{\text{Ln}\bar{Q}} \neq \overline{\text{Ln}\bar{Q}}$, but direct calculations of $\overline{\text{Ln}\bar{Q}}$ profiles from the FGGE III-A data showed a nearly uniform displacement of $\overline{\text{Ln}\bar{Q}}$ from the profile of $\text{Ln}\bar{Q}$ at all levels. Therefore, $\overline{\text{Ln}\bar{Q}}$ preserves the essential shape or curvature of $\text{Ln}\bar{Q}$.)

For either season, Figures 12 and 13 show that on the average \bar{Q} is sharply convex in $Z = \text{Ln}P$ and modestly convex in $Z = P$, while $\text{Ln}\bar{Q}$ is nearly linear in $Z = \text{Ln}P$ and modestly concave in $Z = P$. Thus, in vertical interpolations of Q using Eqs. (1) and (2), we expect from Figures 11 through 13 that the logarithmic, linear, power law, and exponential interpolations of Table 3, respectively, will yield biases that are positive, smaller positive, relatively zero, and negative. In conjunction with Figure 13, a least squares fit of the six discrete (Q, P) values in Figure 13(a) was performed against a logarithmic, linear, exponential, and power law function in turn. These curve fitting tests yielded, respectively, squared correlation coefficients of 0.735, 0.851, 0.978, and 0.998. Hence, the intrinsic mean vertical variation of Q in P is best described by a power law, which in the above exercise was given by $Q = aP^{3.5}$.

To quantify the expected response in bias error to variations in the curvature of $F(Z)$ for Q -based interpolations, an idealized test was performed that provided Table 6(a). In Table 6(a) are the results of applying Eqs. (1) and (2), including first-order extrapolation whenever necessary, for each case in Table 3 to a pair of $P \rightarrow \sigma$ and $\sigma \rightarrow P$ interpolations of the single January hemispheric mean profile

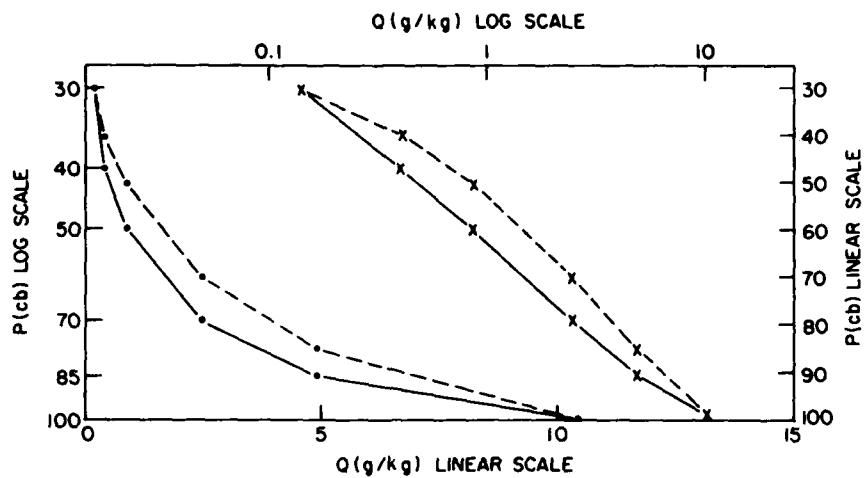


A.



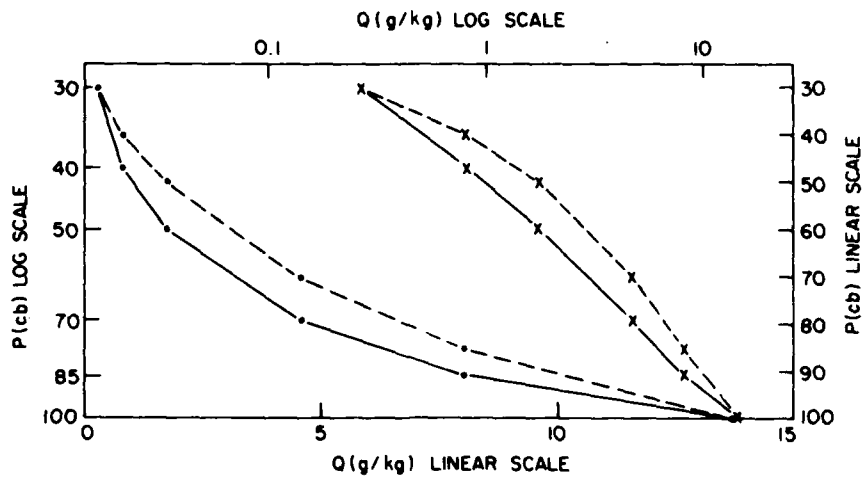
B.

Figure 12. Vertical Profiles of the Analyzed N. H. Mean Specific Humidity, \bar{Q} , and $\text{Ln}\bar{Q}$, Plotted Against P and $\text{Ln}P$ for an Averaged Sample of Six 1978 FGGE III-A Analyses in (a) January (Using 00Z on 15, 17, 19 January and 12Z on 15, 18, 20 January) and (b) July (Using 00Z on 16, 18, 20 July and 12Z on 17, 19, 22 July)



A.

\bar{Q} vs $\ln P$ $\ln \bar{Q}$ vs $\ln P$
 \bar{Q} vs P $\ln \bar{Q}$ vs P



B.

Figure 13. Vertical Profiles of the Observed January (a) and (b) July N. H. Mean Specific Humidity, \bar{Q} , and $\ln \bar{Q}$, Plotted Against P and $\ln P$ (From 1963-1973 RAOB Climatology of Oort¹⁶)

of Q in Figure 13(a). In these interpolations, the seven moist σ -layers of the 12-layer NMC GSM were still used, with $P_g = 101.3$ cb. Using the January hemispheric mean temperature profile (noninterpolated) corresponding to Figure 13(a), plus Eqs. (4) through (8) as necessary, one can express the interpolation error [$Q^r(P) - Q(P)$] equivalently as an RH error, as given in Table 6(a).

The RH errors in Table 6(a) show that for the given input Q -profile, the sign and relative magnitude of the interpolation error for each interpolation type is as expected from Figure 11. Most notably, the standard logarithmic interpolation indeed yields the largest error, while power law interpolation yields the smallest error. Furthermore, the sign of the error changes from positive to negative from left to right in Table 6(a) in agreement with the change from convex to concave curvature from left to right in Figure 13(a).

Even the cubic spline interpolation scheme does not eliminate the large positive bias arising from the linear interpolation of Q in $\text{Ln}P$. This is shown in Table 6(b), which repeats the test of Table 6(a) but using the cubic spline interpolation scheme described in Ahlberg et al.¹⁷ in place of the first-order scheme of Eqs. (1) and (2). Except for the large extrapolation errors at 30 cb, which we ignore for the moment, Table 6(b) shows that for each functional form $F(Z)$, the cubic spline scheme yields RH errors only negligibly smaller than the errors of the first-order scheme in Table 6(a). Of particular note, the first-order interpolation of $\text{Ln}Q$ in $\text{Ln}P$ is far superior to cubic spline interpolation of Q in $\text{Ln}P$. Thus, Table 6 shows that by choosing an appropriate transformation $(f, P) \rightarrow (F, Z)$ that minimizes F'' in Eq. (3), first-order interpolation can be substantially better than cubic spline interpolation applied to the original variables (f, P) . Tables 6(c) and 6(d) show similar results and correspond to Tables 6(a) and 6(b), respectively, but for the July mean Q -profiles in Figure 13(b). Finally, with the same implications, Table 7 repeats the tests of Table 6, but for the FGGE III-A January and July mean Q -profiles in Figure 12. Based on Tables 6 and 7, the use of cubic splines was not pursued further. If we had pursued cubic splines we presumably could have identified methods to reduce the large 30 cb errors of the cubic spline extrapolation, which in Tables 6 and 7 utilized "Type-3" of the three types of extrapolation or end-conditions that Ahlberg et al.¹⁷ present as choices with the cubic spline.

It is instructive to consider further the nature of first-order interpolation errors. It holds that for a given input profile $F(Z)$ of a given curvature (concave or convex), the application of n repetitions of a pair of $P \rightarrow \sigma$ and $\sigma \rightarrow P$ interpolations using Eqs. (1) and (2) will yield an interpolated profile that converges to a

17. Ahlberg, J., Nilson, E., and Walsh, J. (1967) The Theory of Splines and Their Applications, Academic Press, New York, 284 pp.

Table 6. Profiles of Interpolated Specific Humidity \tilde{Q} , After a Pair of $P \rightarrow \sigma$ and $\sigma \rightarrow P$ Interpolations Using the Functional Transformations $F(Z)$ in Table 2 Applied to the Observed N. H. Q-Profile for January in Figure 13(a) [Table 6(a) and (b)] and for July in Figure 13(b) [Table 6(c) and (d)]. Table 6(a) and (c) used the first-order interpolation in Eqs. (1) and (2). Table 6(b) and (d) used the cubic-spline interpolation after Ahlberg et al. 17. Seven moist σ -layers were taken from the last column in Table 2 (with $P_s = 101.3$ cb). Errors \tilde{Q} - Q are given as equivalent RH errors, derived using the corresponding temperature profile (uninterpolated)

Input		F = Q						F = LnQ						
		Z = LnP			Z = P			Z = LnP			Z = P			
		\tilde{Q}	ΔRH	\tilde{Q}	ΔRH	\tilde{Q}	ΔRH	\tilde{Q}	ΔRH	\tilde{Q}	ΔRH	\tilde{Q}	ΔRH	
(a) First-Order														
N. H. (Oort Climo) Jan														
P(cb)	T(K)	Q(g/kg)	\tilde{Q}	ΔRH	\tilde{Q}	ΔRH	\tilde{Q}	ΔRH	\tilde{Q}	ΔRH	\tilde{Q}	ΔRH	\tilde{Q}	ΔRH
100	287.03	10.43	10.43	0.00	10.43	0.00	10.43	0.00	10.43	0.00	10.43	0.00	10.43	0.00
85	276.77	4.91	5.40	8.38	5.31	6.84	5.04	2.17	4.96	0.77	4.96	0.77	4.96	0.77
70	269.99	2.48	2.77	6.70	2.69	4.94	2.52	0.88	2.44	-1.02	2.44	-1.02	2.44	-1.02
50	254.77	0.87	1.06	10.19	0.99	6.44	0.86	-0.83	0.81	-3.57	0.81	-3.57	0.81	-3.57
40	243.97	0.41	0.48	7.82	0.46	5.29	0.40	-1.03	0.38	-3.53	0.38	-3.53	0.38	-3.53
30	230.71	0.14	0.14	0.00	0.14	0.00	0.14	0.00	0.14	0.00	0.14	0.00	0.14	0.00
(b) Third-Order (cubic-spline)														
Input		F = Q						F = LnQ						
N. H. (Oort Climo) Jan		Z = LnP			Z = P			Z = LnP			Z = P			
P(cb)	T(K)	Q(g/kg)	\tilde{Q}	ΔRH	\tilde{Q}	ΔRH	\tilde{Q}	ΔRH	\tilde{Q}	ΔRH	\tilde{Q}	ΔRH	\tilde{Q}	ΔRH
100	287.03	10.43	10.43	0.01	10.43	0.01	10.43	0.01	10.43	0.03	10.43	0.03	10.43	0.03
85	276.77	4.91	5.39	8.24	5.30	6.74	5.02	1.98	4.95	0.63	4.95	0.63	4.95	0.63
70	269.99	2.48	2.76	6.51	2.69	4.85	2.51	0.71	2.43	-1.09	2.43	-1.09	2.43	-1.09
50	254.77	0.87	1.05	9.81	0.98	6.34	0.86	-0.82	0.80	-3.56	0.80	-3.56	0.80	-3.56
40	243.97	0.41	0.48	7.60	0.46	5.26	0.40	-0.78	0.38	-3.50	0.38	-3.50	0.38	-3.50
30	230.71	0.14	0.12	-7.67	0.11	-8.30	0.29	46.14	0.29	45.56	0.29	45.56	0.29	45.56

Table 6 (Contd)

(c) First-Order		F = LnQ											
		Input						F = Q					
		N. H. (Oort Climo) Jul		Z = LnP		Z = P		Z = LnP		Z = P		Z = P	
P(cb)	T(K)	Q(g/kg)	\tilde{Q}	ΔRH	\tilde{Q}	ΔRH	\tilde{Q}	ΔRH	\tilde{Q}	ΔRH	\tilde{Q}	ΔRH	
100	294.51	13.86	13.86	0.00	13.86	0.00	13.86	0.00	13.86	0.00	13.86	0.00	
85	288.02	8.06	8.47	3.23	8.36	2.40	8.14	0.65	8.04	-0.16	8.04	-0.16	
70	279.39	4.60	4.95	4.08	4.83	2.68	4.60	-0.04	4.46	-1.60	4.46	-1.60	
50	263.63	1.73	2.03	7.96	1.90	4.60	1.67	-1.70	1.57	-4.24	1.57	-4.24	
40	252.81	0.80	0.94	7.43	0.90	5.11	0.79	-0.81	0.74	-3.10	0.74	-3.10	
30	238.13	0.27	0.27	0.00	0.27	0.00	0.27	0.00	0.27	0.00	0.27	0.00	
(d) Third-Order (cubic-spline)		F = LnQ											
(d) Third-Order (cubic-spline)		F = Q											
		Input						F = P					
		N. H. (Oort Climo) Jul		Z = LnP		Z = P		Z = LnP		Z = P		Z = P	
P(cb)	T(K)	Q(g/kg)	\tilde{Q}	ΔRH	\tilde{Q}	ΔRH	\tilde{Q}	ΔRH	\tilde{Q}	ΔRH	\tilde{Q}	ΔRH	
100	294.51	13.86	13.86	0.01	13.86	0.01	13.86	0.01	13.86	0.02	13.86	0.02	
85	288.02	8.06	8.46	3.13	8.35	2.33	8.12	0.46	8.02	-0.29	8.02	-0.29	
70	279.39	4.60	4.93	3.90	4.82	2.60	4.58	-0.29	4.45	-1.72	4.45	-1.72	
50	263.63	1.73	2.01	7.60	1.90	4.50	1.66	-1.89	1.57	-4.29	1.57	-4.29	
40	252.81	0.80	0.94	7.22	0.90	5.07	0.79	-0.74	0.74	-3.09	0.74	-3.09	
30	238.13	0.27	0.22	-6.97	0.22	-7.58	0.45	26.79	0.45	26.30	0.45	26.30	

Table 7. As in Table 6 Except FGGE III-A Analyzed N. H. Mean Q-Profiles of Figure 12 Replace Those of Figure 13 as Inputs

(a) First-Order											
Input			F = Q				F = LnQ				
N. H. (78 FGGE III-A) Jan			Z = LnP		Z = P		Z = LnP		Z = P		
P(cb)	T(K)	Q(g/kg)	\bar{Q}	ΔRH	\bar{Q}	ΔRH	\bar{Q}	ΔRH	\bar{Q}	ΔRH	
100	281.51	8.20	8.20	0.00	8.20	0.00	8.20	0.00	8.20	0.00	
85	277.17	5.63	5.67	0.65	5.61	-0.36	5.49	-2.35	5.43	-3.44	
70	268.77	2.90	3.24	8.76	3.16	6.68	3.00	2.68	2.92	0.54	
50	254.98	1.26	1.39	7.06	1.32	2.97	1.20	-3.65	1.14	-6.94	
40	243.92	0.61	0.70	10.88	0.67	7.21	0.59	-1.69	0.56	-5.34	
30	231.05	0.21	0.21	0.00	0.21	0.00	0.21	0.00	0.21	0.00	

(b) Third-Order (cubic-spline)											
Input			F = Q				F = LnQ				
N. H. (78 FGGE III-A) Jan			Z = LnP		Z = P		Z = LnP		Z = P		
P(cb)	T(K)	Q(g/kg)	\bar{Q}	ΔRH	\bar{Q}	ΔRH	\bar{Q}	ΔRH	\bar{Q}	ΔRH	
100	281.51	8.20	8.20	0.01	8.20	0.01	8.20	0.02	8.20	0.02	
85	277.17	5.63	5.66	0.51	5.60	-0.46	5.48	-2.57	5.42	-3.59	
70	268.77	2.90	3.23	8.51	3.16	6.56	2.99	2.42	2.91	0.43	
50	254.98	1.26	1.38	6.56	1.32	2.84	1.19	-3.78	1.13	-6.97	
40	243.92	0.61	0.70	10.53	0.67	7.16	0.60	-1.47	0.56	-5.31	
30	231.05	0.21	0.17	-11.31	0.17	-12.28	0.38	50.69	0.38	49.92	

Table 7 (Contd)

(c) First-Order		Input		F = Q						F = LnQ								
				Z = LnP			Z = P			Z = LnP			Z = P					
				\tilde{Q}	ΔRH	\tilde{Q}	ΔRH	\tilde{Q}	ΔRH	\tilde{Q}	ΔRH	\tilde{Q}	ΔRH	\tilde{Q}	ΔRH			
N.H. (78 FGGE III-A) Jul		T(K)	Q(g/kg)	13.44	0.00	13.44	0.00	13.44	0.00	13.44	0.00	13.44	0.00	13.44	0.00	13.44	0.00	
100	295.37	13.44	13.44	0.00	13.44	0.00	13.44	0.00	13.44	0.00	13.44	0.00	13.44	0.00	13.44	0.00	13.44	
85	288.74	9.39	9.39	0.37	9.35	-0.37	9.35	-0.37	9.35	-0.37	9.35	-0.37	9.35	-0.37	9.06	-2.51	9.06	-2.51
70	279.24	4.97	4.97	6.34	5.37	4.71	5.37	4.71	5.37	4.71	5.37	4.71	5.37	4.96	4.96	-0.07	4.96	-0.07
50	264.56	2.11	2.11	6.21	2.23	2.96	2.23	2.96	2.23	2.96	2.23	2.96	2.23	1.91	1.91	-4.94	1.91	-4.94
40	253.04	1.03	1.03	7.77	1.13	5.02	1.13	5.02	1.13	5.02	1.13	5.02	1.13	0.94	0.94	-4.50	0.94	-4.50
30	238.34	0.35	0.35	0.00	0.35	0.00	0.35	0.00	0.35	0.00	0.35	0.00	0.35	0.00	0.35	0.00	0.35	0.00

(d) Third-Order (cubic-spline)		Input		F = Q						F = LnQ									
				Z = LnP			Z = P			Z = LnP			Z = P						
				\tilde{Q}	ΔRH	\tilde{Q}	ΔRH	\tilde{Q}	ΔRH	\tilde{Q}	ΔRH	\tilde{Q}	ΔRH	\tilde{Q}	ΔRH	\tilde{Q}	ΔRH		
N.H. (78 FGGE III-A) Jul		T(K)	Q(g/kg)	13.44	0.01	13.44	0.01	13.44	0.01	13.44	0.01	13.44	0.01	13.44	0.02	13.44	0.02	13.44	0.02
100	295.37	13.44	13.44	0.01	13.44	0.01	13.44	0.01	13.44	0.01	13.44	0.01	13.44	0.01	13.44	0.02	13.44	0.02	13.44
85	288.74	9.39	9.39	0.26	9.34	-0.44	9.34	-0.44	9.34	-0.44	9.34	-0.44	9.34	-0.44	9.04	-2.66	9.04	-2.66	9.04
70	279.24	4.97	4.97	6.14	5.36	4.62	5.36	4.62	5.36	4.62	5.36	4.62	5.36	4.95	4.95	-0.20	4.95	-0.20	4.95
50	264.56	2.11	2.11	5.82	2.22	2.86	2.22	2.86	2.22	2.86	2.22	2.86	2.22	1.91	1.91	-5.01	1.91	-5.01	1.91
40	253.04	1.03	1.03	7.50	1.12	4.98	1.12	4.98	1.12	4.98	1.12	4.98	1.12	0.94	0.94	-4.50	0.94	-4.50	0.94
30	238.34	0.35	0.35	-8.76	0.28	-9.56	0.28	-9.56	0.28	-9.56	0.28	-9.56	0.28	0.53	0.53	26.53	0.53	26.53	0.53

linear profile ($\tilde{F}'' \rightarrow 0$) for large n . Figure 11 showed the mechanics of this effect and Figure 14 provides an example. In Figure 14, the $F(Z)$ profile of $F = Q$, $Z = \text{Ln}P$ in Figure 13(a) was subject to $n = 8, 16,$ and 24 iterations of the $P \rightarrow \sigma$ and $\sigma \rightarrow P$ logarithmic interpolation (corresponding respectively to the number of pre- and postprocessor pairs executed in a 2-, 4-, and 6-day run of the assimilation system of Figure 1). In actual practice, the asymptotically linear profile in Figure 14 may not be reached owing to checks for supersaturation. Nevertheless, to inhibit climatic drift in humidity assimilations due to vertical interpolations, Figure 6 clearly demonstrates that one should choose a moisture function $F(Z)$ that on the average is intrinsically linear.

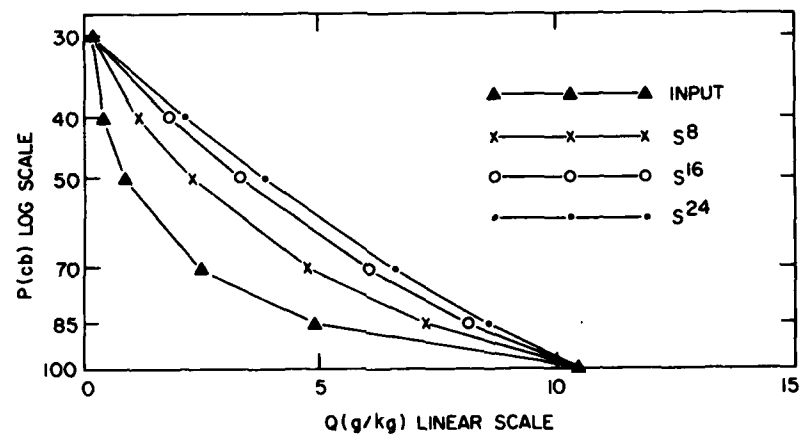


Figure 14. A Sample of Interpolated Q -Profiles for n Iterations ($n = 0, 8, 16, 24$) of the Pair of $P \rightarrow \sigma$ and $\sigma \rightarrow P$ Logarithmic Interpolations [Eqs. (1) and (2) With $F = Q$, $Z = \text{Ln}P$] Applied to the Input Q -Profile of Table 6(a) and Using the Seven Moist σ -Layers of the 12-Layer Column of Table 2 With $P_g = 101.3$ cb

The interpolation tests in Tables 6 and 7 were idealizations, since each was performed on a single hemispheric mean profile of Q . Certainly, local vertical profiles of Q within a global moisture analysis are less smooth, possessing more vertical variability and changes in curvature than their hemispheric mean counterparts. Therefore, to establish the representativeness of Tables 6 and 7 for practical applications, we extended the tests of the four interpolation types to actual executions of the pre- and postprocessor on a global data set and to all three moisture variables. Table 8 shows the (S_1, A_1) BIAS and RMSE obtained for each choice of $f = (\text{RH}, Q, \text{ or } T_d)$ and interpolation type in Table 3 used within the pre- and postprocessor executed on the same input FGGE analysis as in Figure 9. For

Table 8. Vertical Profiles of the Global Mean BIAS (a) and RMSE (b) for the Synthesized FGGE III-A Analysis (17 January 1978, 00Z) Obtained Using the Four Interpolation Types of Table 3 and the Moisture Variables $f = (RH, Q, T_d)$ in the Vertical Interpolations of the NMC/AFGWC Pre- and Postprocessor

(a) BIAS							(b) RMSE						
f	P	F = f			F = Lnf		f	P	F = f			F = Lnf	
		Z = LnP	Z = P	Z = P	Z = LnP	Z = P			Z = LnP	Z = P	Z = LnP	Z = P	
RH	100	-0.19	-0.11	0.28	0.39	0.39	100	5.22	5.72	5.66	6.13		
	85	-0.46	-0.61	-0.86	-1.04	-1.04	85	3.71	3.89	4.26	4.53		
	70	1.89	1.67	0.97	0.74	0.74	70	4.94	4.83	4.25	4.28		
	50	-0.03	-0.11	-0.80	-0.80	-0.80	50	4.91	4.44	5.12	4.62		
	40	-0.23	-0.33	-0.29	-0.39	-0.39	40	4.04	4.07	4.09	4.11		
	30	0.04	0.04	0.01	0.01	0.01	30	3.48	3.45	3.33	3.30		
Q	100	-0.73	-0.29	1.00	1.40	1.40	100	6.87	6.13	5.80	6.26		
	85	0.28	-0.06	-0.73	-1.13	-1.13	85	4.66	4.23	4.43	4.75		
	70	4.22	3.14	0.45	-0.78	-0.78	70	6.83	5.99	4.44	4.67		
	50	8.02	5.04	-1.48	-4.13	-4.13	50	12.64	9.98	5.83	6.91		
	40	7.43	5.54	0.06	-2.38	-2.38	40	9.57	7.64	4.05	5.03		
	30	0.34	0.25	-0.06	-0.24	-0.24	30	6.40	5.55	4.02	3.88		
T _d	100	0.72	1.34	0.86	1.46	1.46	100	5.55	5.93	5.63	6.12		
	85	-0.40	-0.96	-0.51	-1.08	-1.08	85	4.12	4.42	4.21	4.56		
	70	1.34	-0.32	1.00	-0.66	-0.66	70	4.45	4.49	4.38	4.61		
	50	0.32	-3.43	-0.41	-4.08	-4.08	50	5.84	6.64	5.70	6.98		
	40	1.69	-1.46	1.06	-2.10	-2.10	40	4.19	4.28	3.97	4.68		
	30	0.23	0.03	0.20	-0.03	-0.03	30	3.98	3.74	3.93	3.72		

reference, the leftmost error column in Table 8(a) and (b) corresponds to the solid curves in Figure 9.

Overall, Table 8 shows that the Q-based processing error is more sensitive to interpolation type than that of RH or T_d . Notably, the magnitude and sign of the Q-based errors follow closely those obtained earlier in the idealized tests of Tables 6 and 7 -- showing a minimum for power law interpolation and a maximum for logarithmic interpolation. The difference between the maximum and minimum Q-based errors in Table 8 are plotted in Figure 15. Based on Figure 15 and Table 8, we henceforth adopt power law interpolation (case 3, Table 3) as the preferred type for vertical interpolations of Q. Most significantly, Table 8 shows that power law interpolation of Q yields processing errors that are very competitive with the smallest errors obtained using $f = RH$ or $f = T_d$.

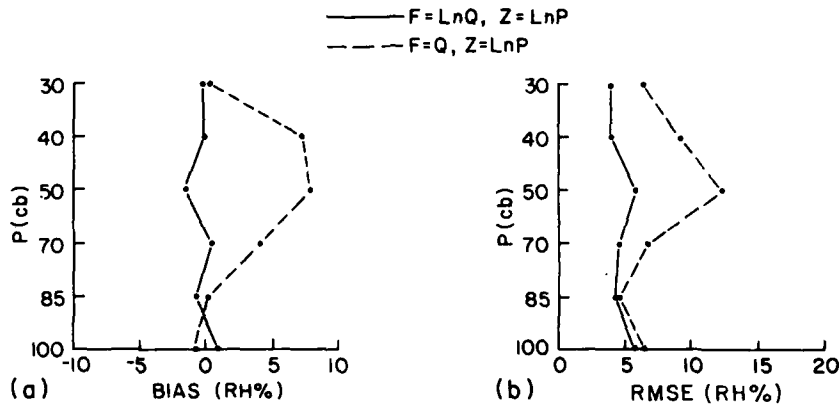
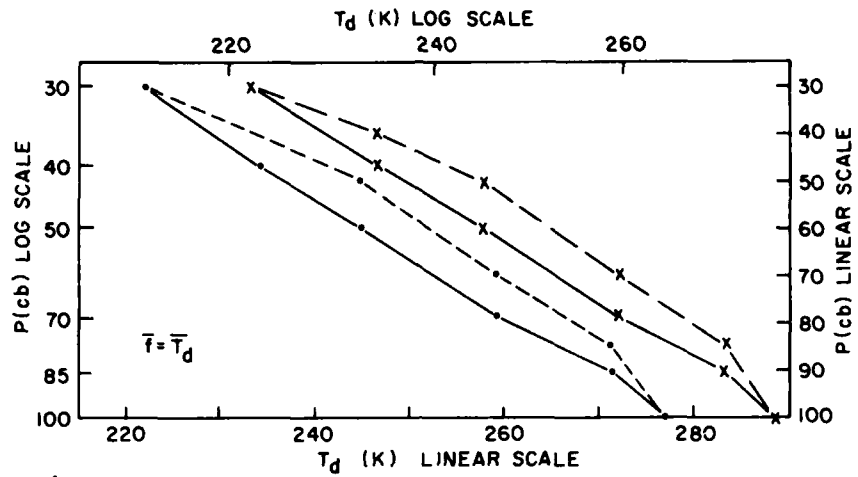
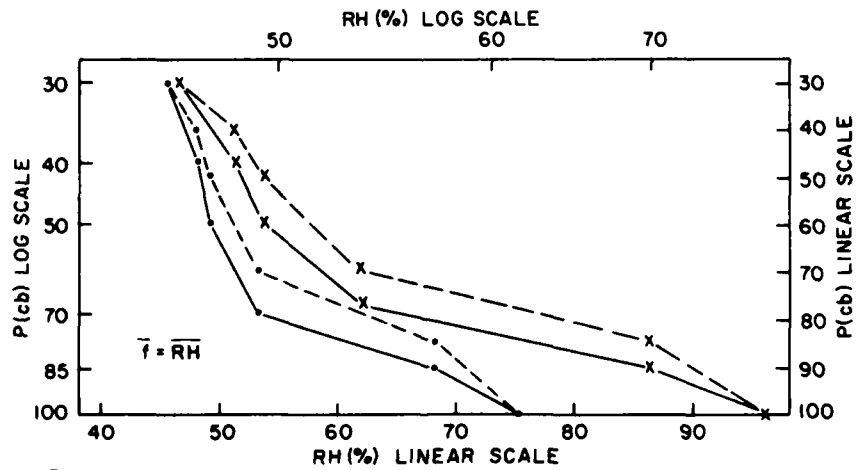


Figure 15. Vertical Profiles of the Global Mean BIAS and RMSE for the Synthesized FGGE III-A Analysis (17 January 1978, 00Z) Obtained Using Power Law Interpolation of Q (Solid Curve) and Logarithmic Interpolation of Q (Dashed Curve, Repeated From Q-Based Solid Curve in Figure 9) in the NMC/AFGWC Pre- and Postprocessor

The standard logarithmic interpolation ($F = f, Z = \text{Ln}P$) in general shows the smallest processing errors in Table 8 for the RH- and T_d -based interpolations and we shall retain this interpolation type henceforth in vertical interpolations of RH or T_d . However, this choice was less clear cut than that for Q since the RH-based and T_d -based errors in Table 8 show less sensitivity to interpolation type. To explain this we turn to Figure 16, which presents the T_d and RH profiles corresponding to those for Q in Figure 12(a). Unlike Q, which on the average changes by nearly two orders of magnitude between 30 to 100 cb, T_d and RH on the average change by less than 25 and 50 percent, respectively. Hence $f = RH$ or $f = T_d$ is less responsive than $f = Q$ to logarithmic transformation.



A.



B.

Figure 16. Vertical Profiles of the N.H. January Mean FGGE III-A Analyzed Relative Humidity, \overline{RH} , and Dewpoint, T_d , Plus $\text{Ln } \overline{RH}$ and $\text{Ln } T_d$, Plotted Against P and $\text{Ln } P$. From the same sample of analyses as Figure 12(a)

Figure 16 shows that all four functional choices of the T_d profile are quite similar in shape. The functions $F = T_d$, $Z = P$ and $F = \text{Ln}T_d$, $Z = P$ are both somewhat concave. Hence in Table 8, both yield larger bias errors (negative) and somewhat larger RMSE errors than the functions $F = T_d$, $Z = \text{Ln}P$ and $F = \text{Ln}T_d$, $Z = \text{Ln}P$, which are both nearly linear and which both yield comparatively small errors. The four RH profiles in Figure 16 are also similar in shape, being distinctly convex at 70 cb but slightly concave at 85 and 40 cb. Not surprisingly then in Table 8, the standard logarithmic interpolation for RH yields a fairly large positive bias at 70 cb and slight negative biases at the remaining interior levels. The other interpolation types for RH reduce the 70 cb positive bias, but increase the negative bias at the other interior levels. Ultimately, we retain logarithmic interpolation for RH, because when averaged over the six mandatory levels, it yields the smallest absolute BIAS and RMSE.

We conclude from Table 8 that logarithmic interpolation of RH or T_d and power law interpolation of Q all yield comparably small processing errors. We will adopt these three interpolation schemes as our nominal methods henceforth. Table 9 shows the sample mean processing errors and their sample standard deviation over three January and three July 1978 FGGE III-A analyses for the nominal interpolation schemes. In Table 9, the results shown for the single FGGE III-A analysis of 00Z, 17 January 1978 (used exclusively thus far) represent well the results of the other sample dates. The differences in error between the three interpolation schemes is sufficiently small that the final decision to pursue one particular approach may depend on secondary factors such as programming convenience, geographical distribution of the error, horizontal truncation error, or sensitivity to spacing of σ -layers. We shall address the latter three factors further.

Regarding sensitivity to σ -structure, we suspected that the close proximity of the σ_3 layer to the 70-cb mandatory level in the 12-layer structure of Table 2 may be suppressing potentially large bias errors in vertical interpolations using RH. We recall that the hemispheric mean profile of RH in LnP in Figure 7 is sharply convex at 70 cb. Therefore, the alternative σ -spacing in Table 10 was tested. The only changes in Table 10 from Table 2 occur for layers σ_2 , σ_3 , and σ_4 , which in Table 10 are further separated from the mandatory levels of 85, 70, and 50 cb, respectively (assuming $P_g = 101.3$ cb). Figure 17 shows the sensitivity of the processing error to the new σ -spacing for the three nominal interpolation schemes.

In Figure 17, the logarithmic interpolation of RH indeed yielded the largest increase in processing error for the new σ -structure, with T_d following as second. However, the Q-based profile was notably insensitive to the change in σ -spacing, especially in the BIAS error. One recognizes from Figure 11 that the more linear is a given function $F(Z)$, such as $F = \text{Ln}Q$, $Z = \text{Ln}P$ in Figure 12, the less sensitive the vertical interpolation error will be to the location of the σ -layers. We

Table 9. Vertical Profiles of the Global Mean BIAS and RMSE for Three Winter and Three Summer Synthesized FGGE III-A Analyses Obtained Using Logarithmic Interpolation of RH and Td and Power Law Interpolation of Q in the Vertical Interpolations of the NMC/AFGWC Pre- and Postprocessor. Also given are the sample mean and sample standard deviation BIAS and RMSE

F	Z	P	BIAS (RH%)						RMSE (RH%)									
			Date (1978)						Date (1978)									
			1/15	1/17	1/19	7/16	7/18	7/20	1/15	1/17	1/19	7/16	7/18	7/20	Mean \bar{X}_n	STD σ_{n-1}		
F=RH	Z=LnP	100	-0.10	-0.19	-0.13	-0.17	-0.11	-0.09	-0.13	0.04	6.27	5.22	5.36	3.71	3.51	3.58	4.61	1.16
		85	-0.52	-0.46	-0.48	-0.56	-0.61	-0.57	-0.53	0.06	4.16	3.71	3.60	2.76	2.71	2.85	3.30	0.61
		70	1.98	1.89	2.04	2.00	2.15	2.07	2.02	0.09	4.98	4.94	4.80	4.68	4.74	4.82	4.83	0.12
		50	0.05	-0.03	-0.04	0.46	0.18	0.42	0.17	0.22	4.78	4.91	4.58	4.51	4.42	4.65	4.64	0.18
		40	-0.23	-0.23	-0.22	-0.13	-0.26	-0.13	-0.20	0.06	3.61	4.04	3.84	4.41	4.10	4.25	4.04	0.29
		30	0.01	0.04	0.03	0.08	-0.01	0.16	0.05	0.06	2.89	3.48	3.64	4.23	5.08	5.15	4.08	0.91
F=LnQ	Z=LnP	100	0.96	1.00	0.94	0.23	0.88	0.68	0.78	0.29	6.37	5.80	5.85	4.24	4.17	4.21	5.11	1.01
		85	-0.79	-0.73	-0.74	-0.25	-0.86	-0.75	-0.69	0.22	4.54	4.43	4.19	3.61	3.35	3.54	3.94	0.51
		70	0.60	0.45	1.02	1.21	1.04	1.05	0.90	0.30	4.40	4.44	4.17	4.35	3.97	4.10	4.24	0.19
		50	-1.48	-1.48	-1.25	-1.77	-0.99	-0.90	-1.31	0.33	5.28	5.83	5.07	5.81	4.75	4.99	5.29	0.45
		40	0.09	0.06	-0.17	0.34	-0.32	-0.33	-0.06	0.26	3.73	4.05	3.98	4.36	4.13	4.31	4.09	0.23
		30	0.01	-0.06	-0.25	0.26	-0.03	0.14	0.01	0.18	3.49	4.02	4.29	4.61	5.60	5.35	4.56	0.80
F=T _d	Z=LnP	100	0.66	0.72	0.67	-0.12	0.50	0.37	0.47	0.32	6.32	5.55	5.49	3.64	3.82	3.82	4.77	1.15
		85	-0.44	-0.40	-0.35	0.26	-0.47	-0.32	-0.29	0.27	4.44	4.12	3.91	3.28	3.04	3.08	3.65	0.59
		70	1.48	1.34	1.92	2.19	2.03	2.03	1.83	0.34	4.55	4.45	4.42	4.71	4.30	4.36	4.47	0.15
		50	0.28	0.32	0.48	0.05	0.85	0.90	0.48	0.34	5.19	5.84	5.07	5.64	4.85	5.22	5.30	0.37
		40	1.71	1.69	1.50	1.95	1.37	1.30	1.59	0.24	4.01	4.19	4.13	5.11	4.28	4.47	4.37	0.40
		30	0.29	0.23	0.02	0.40	0.09	0.13	0.19	0.14	3.57	3.98	4.22	4.86	5.73	5.66	4.67	0.90

Table 10. The 12-Layer σ -Structure Used in the Pre- and Postprocessor Runs for Figure 17 (Compare With Table 2)

k	$\Delta\sigma_k$	σ_k
1	0.075	0.962
2	0.075	0.887
3	0.150	0.774
4	0.200	0.598
5	0.125	0.436
6	0.075	0.337
7	0.050	0.275
8	0.050	0.225
9	0.050	0.175
10	0.050	0.124
11	0.050	0.074
12	0.050	0.021

expect from these results that Q-based power law interpolations would be rather suitable also for lower vertical resolutions with fewer σ -layers.

All (S_1 , A_1) processing errors shown thus far have been vertical profiles of the global mean BIAS and RMSE. To assess the geographical distribution of processing error, we show in Figure 19 the latitude-height contour analyses of the zonal mean BIAS and RMSE resulting from logarithmic interpolation of RH, Q, and T_d and power law interpolation of Q. The zonal averages in Figure 19 are based on the input winter FGGE III-A analysis of 00Z on 17 January 1978 and thus are counterparts to the global mean profiles given by the solid curves in Figures 9 and 15. Also, Figure 20 is a repeat of Figure 19, but for the input summer FGGE III-A analysis of 00Z on 18 July 1978. The bottom of each part of Figures 19 and 20 shows the zonal average of the final synthesized analysis for the respective interpolation.

For reference purposes, Figures 18(a) and (b) show the zonal average of the original input analyses for Figures 19 and 20, respectively. In Figure 18, the dry tongues of the descending branches of the Hadley circulation are clearly discernible. Moreover the Hadley circulation shows a reasonable northward shift from January to July. In addition, the relative humidity decreases with height at most latitudes. In general, then, the features of the input RH analyses appear reasonable. We caution, however, that the RH in the upper-half of the southern

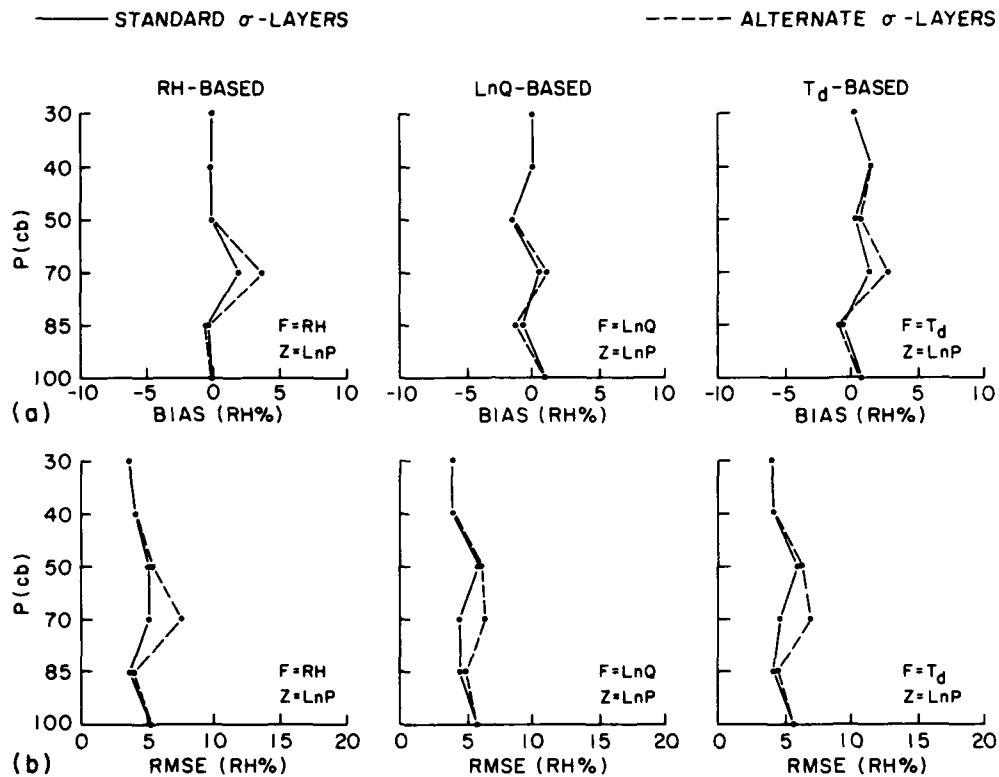
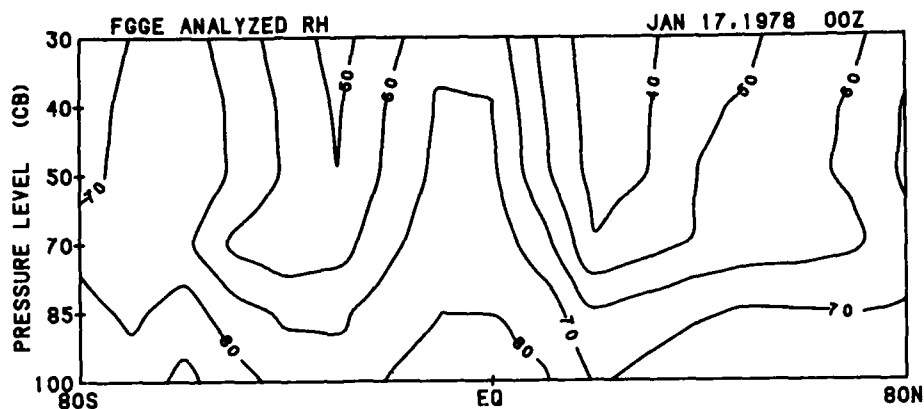


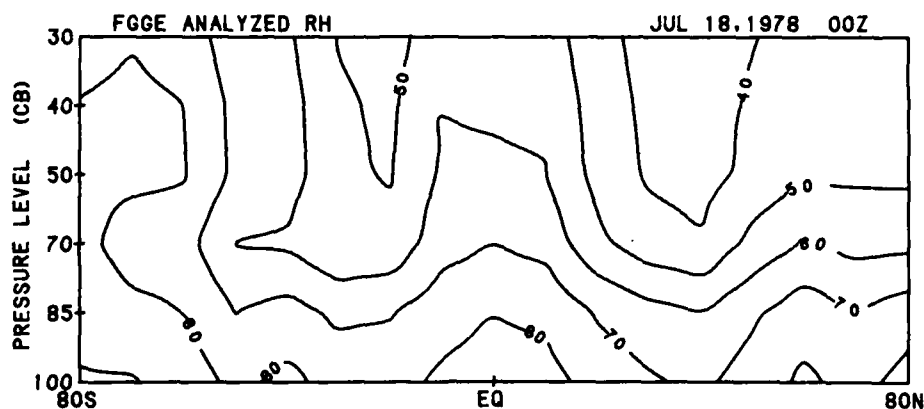
Figure 17. Vertical Profiles of the Global Mean BIAS and RMSE for the Synthesized FGGE III-A Analysis (17 January 1978, 00Z) Obtained by Executing the NMC/AFGWC Pre- and Postprocessor for the 12-Layer σ -Structures of Table 2 (Solid Curve) and Table 10 (Dashed Curve) Using Vertical Interpolations of $F = (RH, LnQ, T_d)$ in $Z = LnP$

hemisphere troposphere is significantly higher than that in the corresponding season of the northern hemisphere. Although this may depict true inter-hemispheric variability, it also is very likely an erroneous artifact of the forecast model in the assimilation system, since the southern hemisphere is persistently data sparse (especially regarding moisture observations, which at this time were not augmented by satellite soundings or imagery in the southern hemisphere).

In the processing errors in Figure 19, the most dramatic result is the latitudinal pervasiveness and magnitude of the large errors arising from logarithmic interpolation of Q in Figure 19(d). Compared to the other plots of Figure 19, this is by far the worst choice of vertical interpolation. The RH-based logarithmic interpolation in Figure 19(a) appears to give the most satisfactory processing error over all latitudes and heights. The processing errors for logarithmic interpolation of T_d in Figure 19(c) and power law interpolation of Q in Figure 19(b) are also



A.



B.

Figure 18. Latitude-Height Contour Analysis of the Zonal Mean of the 1978 FGGE III-A Analysis of RH for the Winter Case (a) and the Summer Case (b) Representing the Inputs for Figure 19 and 20, Respectively. Contour interval is RH = 10 percent

small and competitive with those in Figure 19(a), except in the middle troposphere at high latitudes in the southern hemisphere, where Figure 19(b) and 19(c) show larger errors.

The above discussion of Figure 19 also holds for Figure 20. We further note only the consistent increase in RMSE toward both poles evident in parts (a), (b), and (c) of both Figures 19 and 20. In Figure 20, this poleward increase in RMSE is much more dominant in the winter hemisphere than in Figure 19. Further inspection shows this poleward increase in RMSE is not the result of a closely

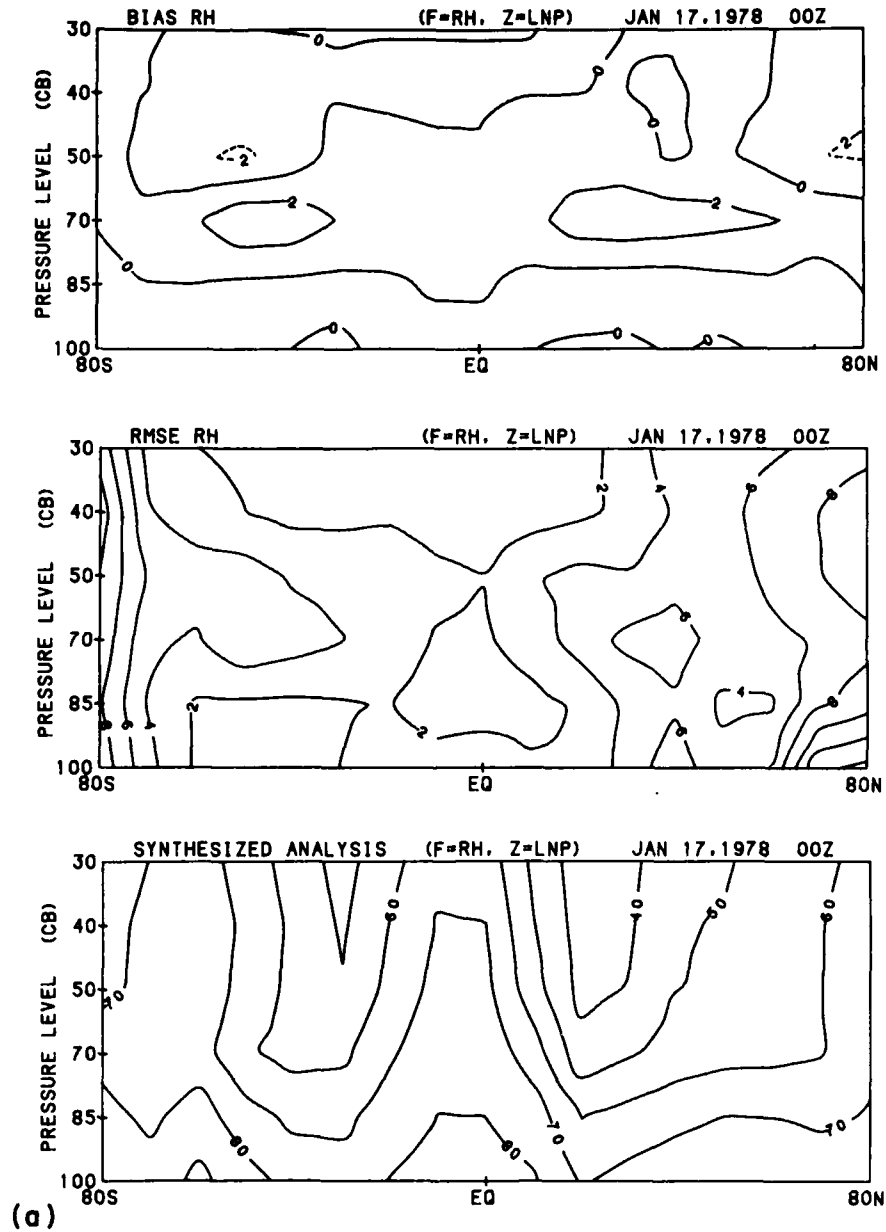


Figure 19. Latitude-Height Contour Analysis of the Zonal Mean BIAS (Top), RMSE (Middle), and Analyzed RH (Bottom) for the Synthesized FGGE III-A Analysis (17 January 1978, 00Z) Obtained Using Logarithmic Interpolation of RH (a), T_d (c), and Q (d), and Power Law Interpolation of Q (b). Contour interval is RH = 2 percent (except RH = 10 percent in bottom plot). Dashed contours denote negative values (BIAS only)

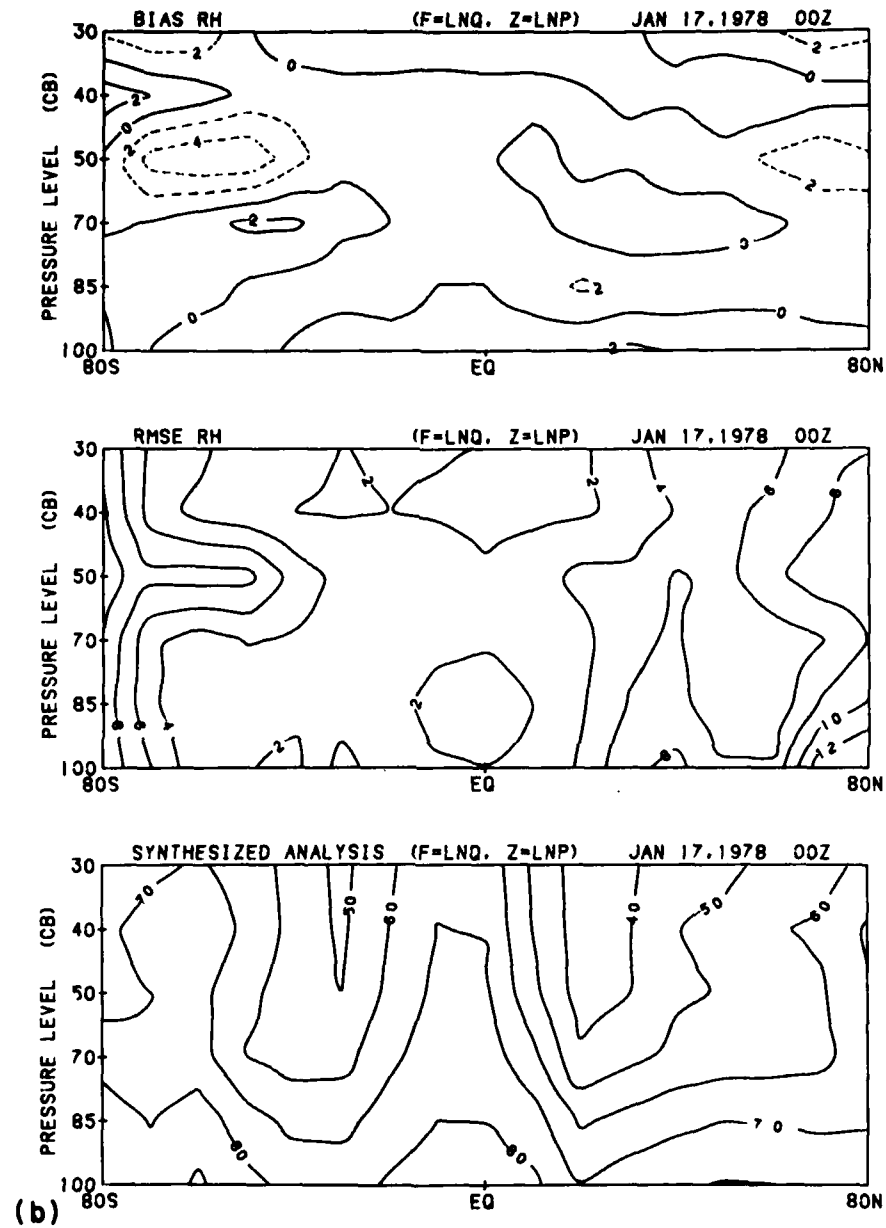


Figure 19 (Contd)

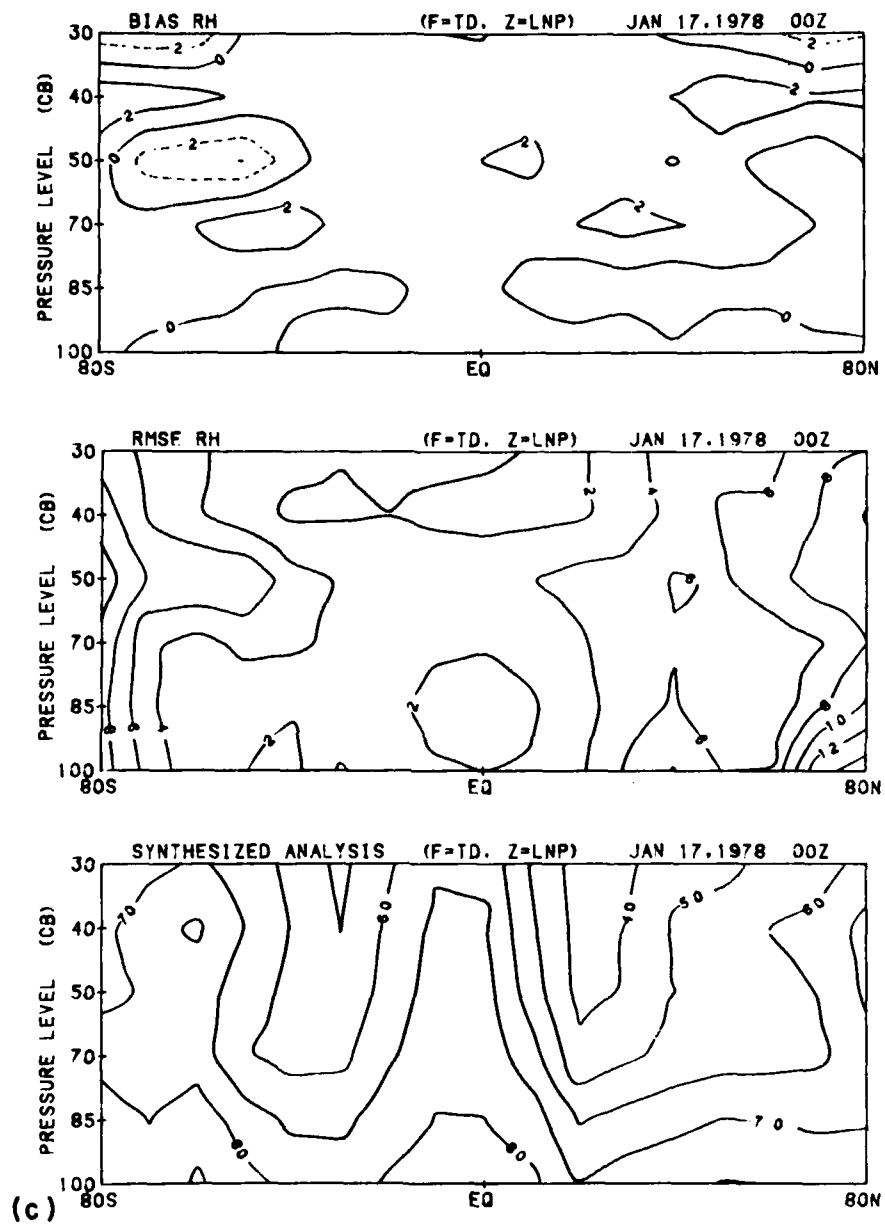


Figure 19 (Contd)

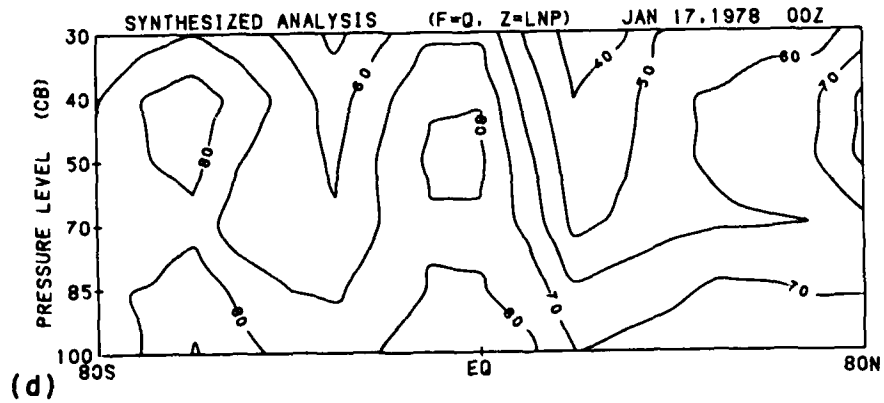
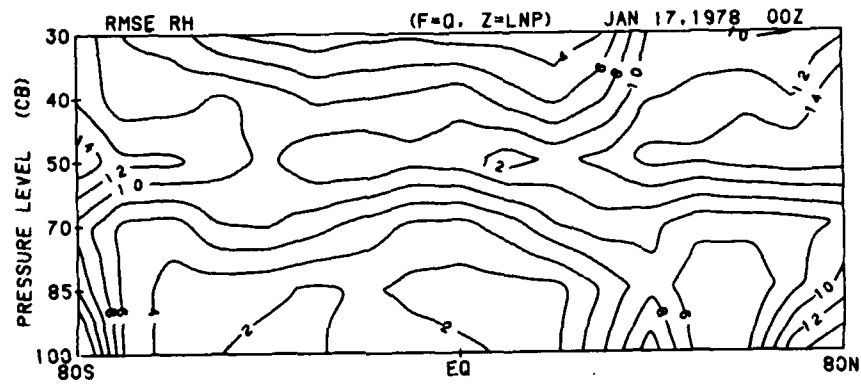
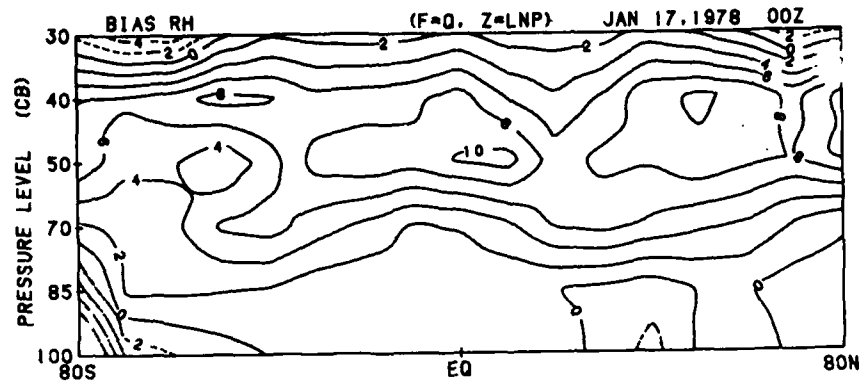


Figure 19 (Contd)

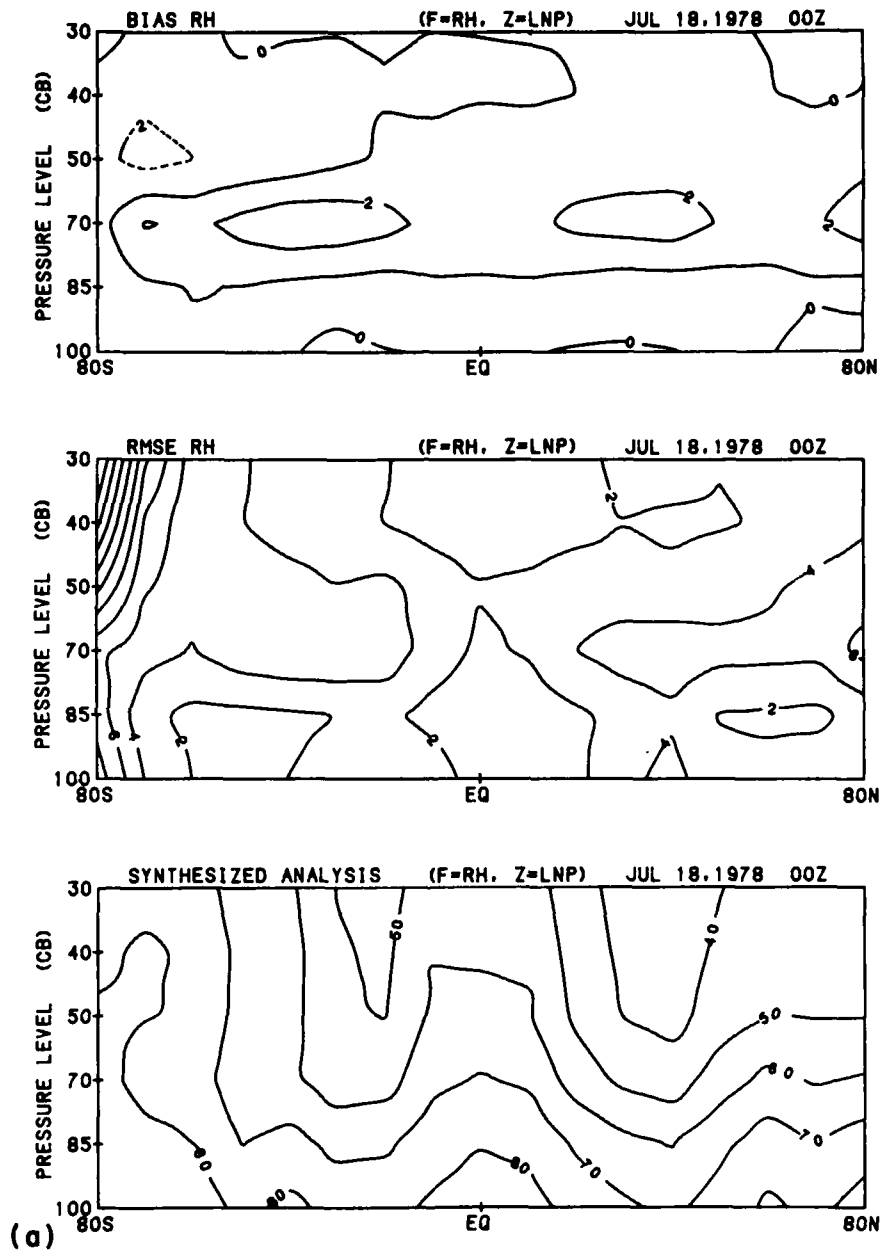


Figure 20. As in Figure 19 Except for the FGGE III-A Analysis of 18 July 1978, 00Z

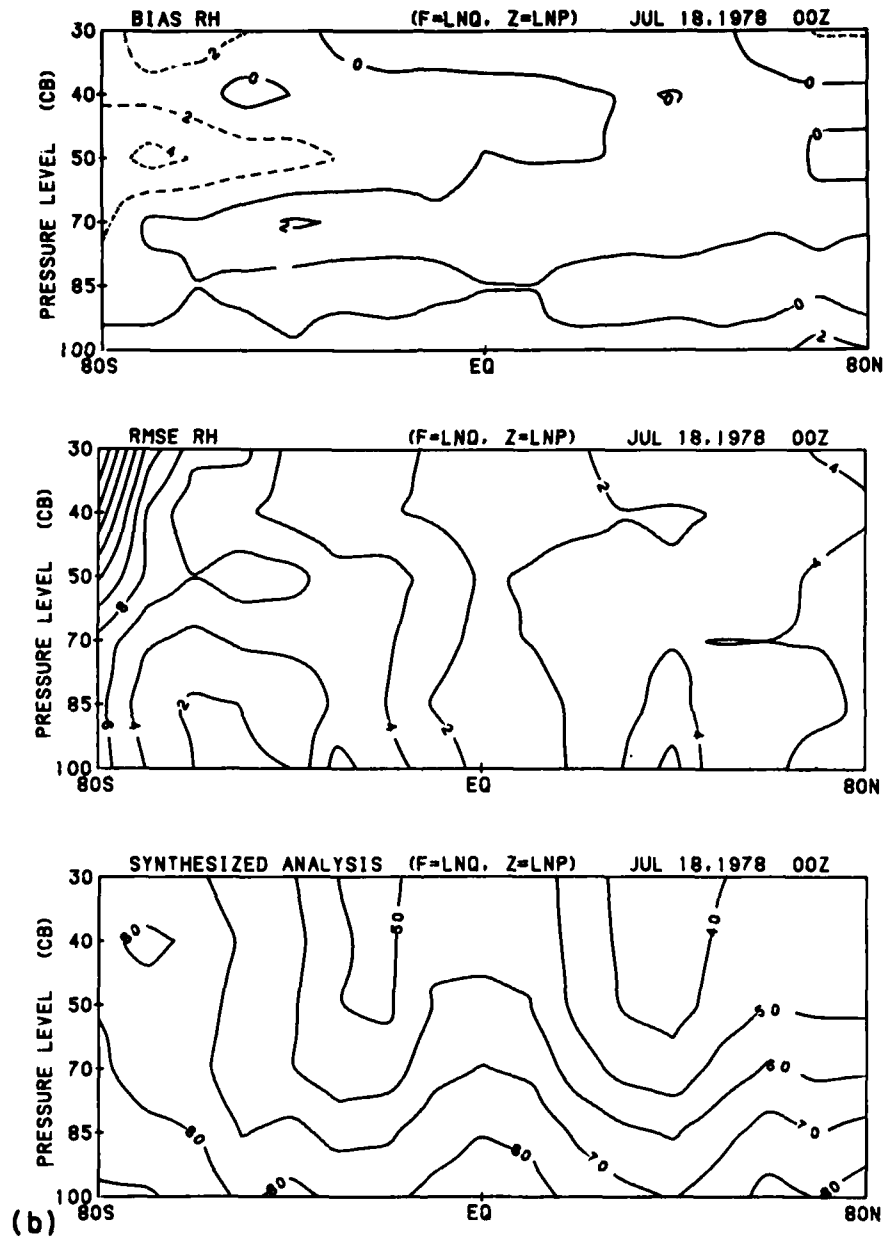


Figure 20 (Contd)

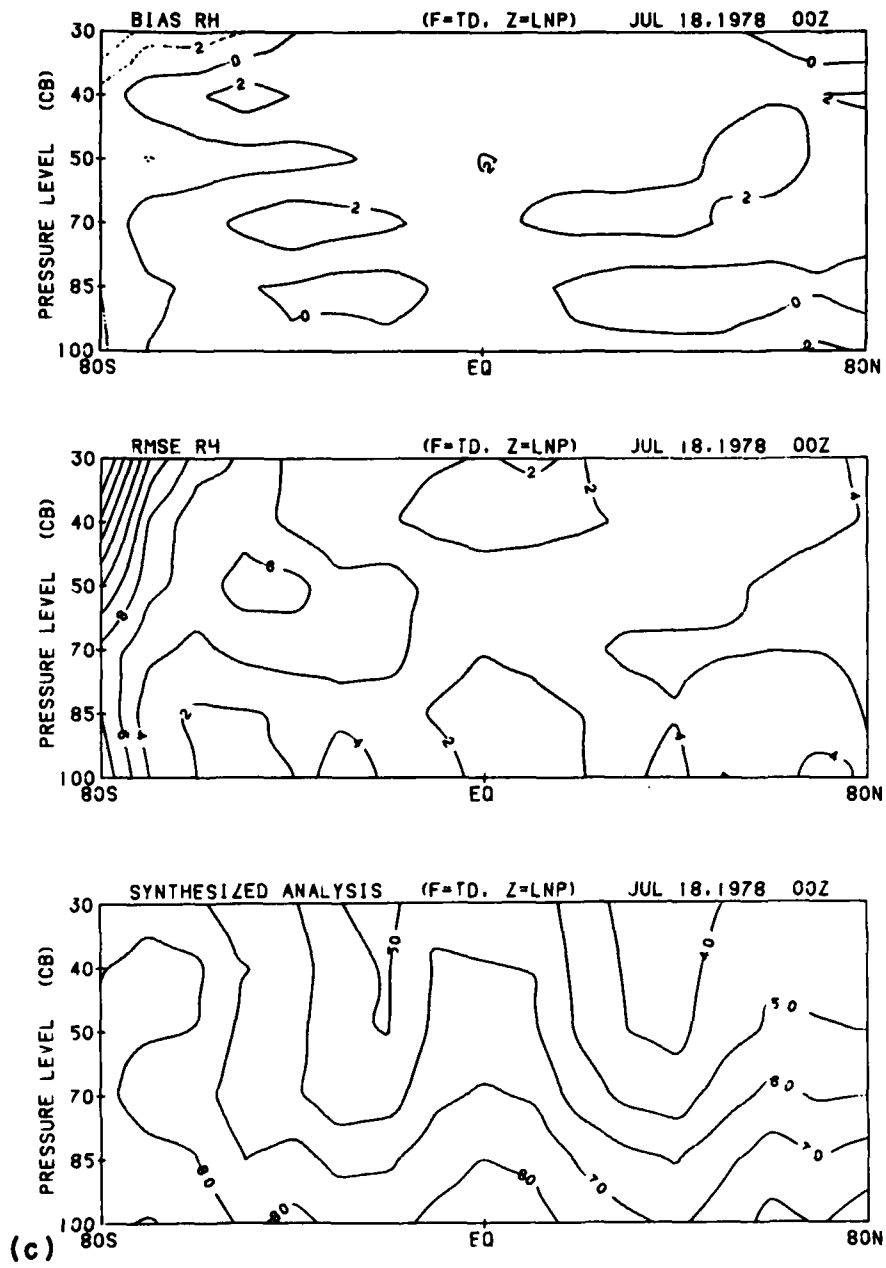


Figure 20 (Contd)

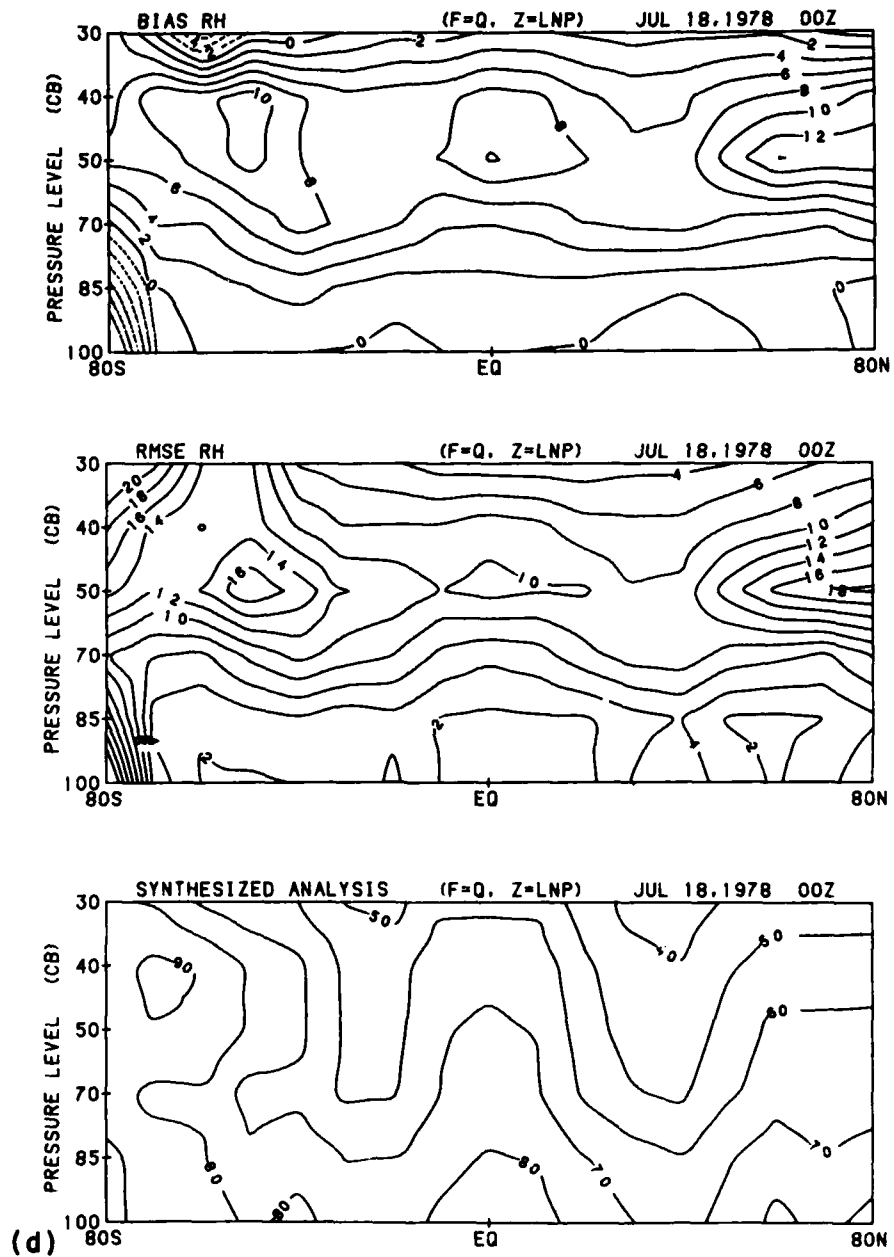


Figure 20 (Contd)

parallel increase in the BIAS (see RH-based plots in particular). However, the next section on spectral truncation error will provide crucial insight into the cause of the maximum of RMSE in polar regions.

3.3 Horizontal Truncation Error

In Sections 3.1 and 3.2 we have identified and eliminated the larger sources of bias error that dominated the earlier (S_1 , A_1) error statistics. In the remainder of Section 3, we shift the focus primarily to RMSE and to identifying some key sources of RMSE. In particular, we seek to determine why the RMSE consistently increases toward both poles in Figures 19 and 20. This poleward increase of RMSE occurs at all levels and for all the given vertical interpolation approaches. Thus we speculate that its cause lies with horizontal spectral truncation errors.

Figure 21 from top to bottom, respectively, shows the RMSE plots corresponding to parts (a) through (c) of Figure 19, but wherein all the spectral transforms in the pre- and postprocessor [that is, steps 6 and 7 in Table 5(a) and steps 1 and 2 in Table 5(b)] have been skipped. Clearly the poleward increase in RMSE has been greatly reduced by eliminating the spectral transforms. However, much of the source of the spectral transform error lies not with the spectral transform operation itself, but rather with the truncation error associated with the particular moisture field being transformed -- namely Q . As an illustration, in Figure 22 the spectral transforms have been reinstated, but the moisture field chosen for spectral transformation in each plot corresponds to that used for vertical interpolation (RH, $\ln Q$, or T_d). The resemblance between Figure 22, which includes spectral transforms, and Figure 21 is dramatic. Most significantly, neither Figure 22 nor Figure 21 show the systematic increase of RMSE toward the poles that was present in the RMSE plots of Figure 19.

The moisture variable Q is substantially more prone to horizontal spectral truncation error than the moisture variables of RH, $\ln Q$, and T_d when the error is measured in terms of equivalent RH error. This conclusion is highlighted in Figure 23(a), which depicts the vertical profiles of the global mean RMSE for the three spectral transform cases just discussed. The solid curves in Figure 23(a) represent the standard case, repeated from the bottom of Figure 17 and corresponding to the zonal mean RMSE in parts (a) through (c) of Figure 19. The dotted and dashed curves in Figure 23(a) correspond to Figures 21 and 22 respectively. The results in Figure 23(a) agree with the results of Simmonds,¹⁸ who compared the horizontal spectral truncation errors for moisture fields of RH, Q (or mixing

18. Simmonds, I. (1975) The spectral representation of moisture, J. Appl. Meteorol. 14:175-179.

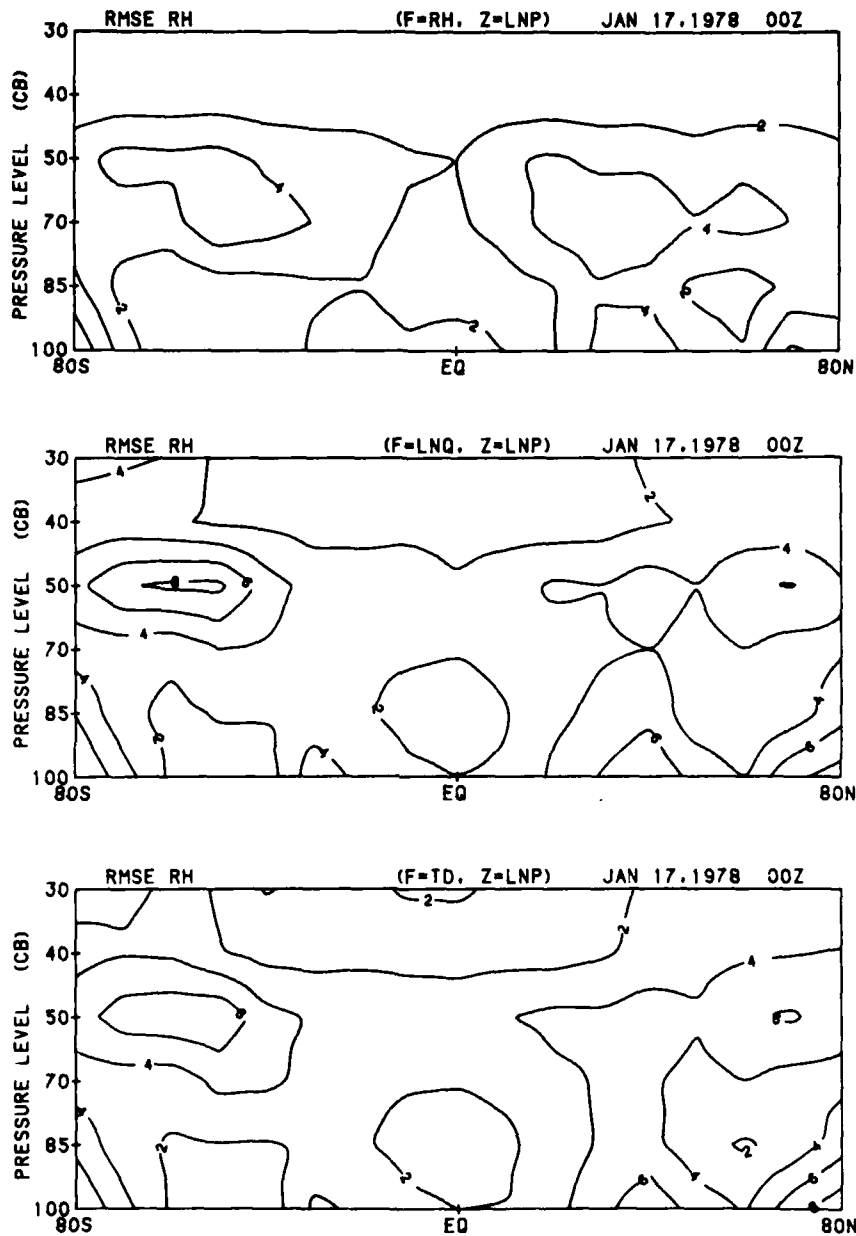


Figure 21. Latitude-Height Contour Analysis of the Zonal Mean RMSE for the Synthesized FGGE III-A Analysis (17 January 1978, 00Z) Obtained by Skipping All Spectral Transforms in Pre- and Postprocessing While Using Logarithmic Interpolation of RH (Top), and T_d (Bottom), and Power Law Interpolation of Q (Middle). Contour interval is RH = 2 percent

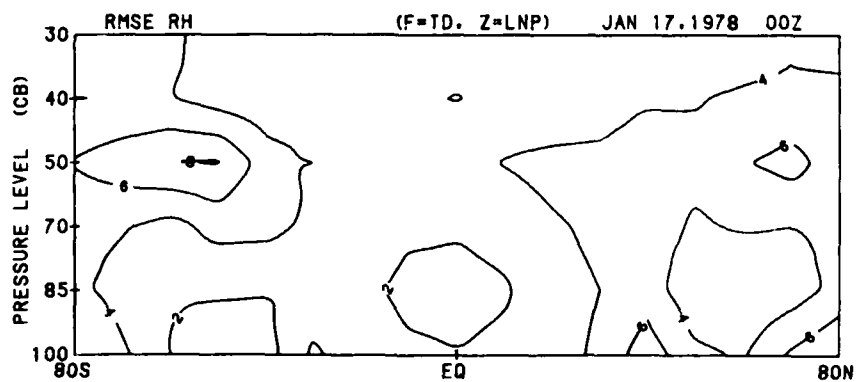
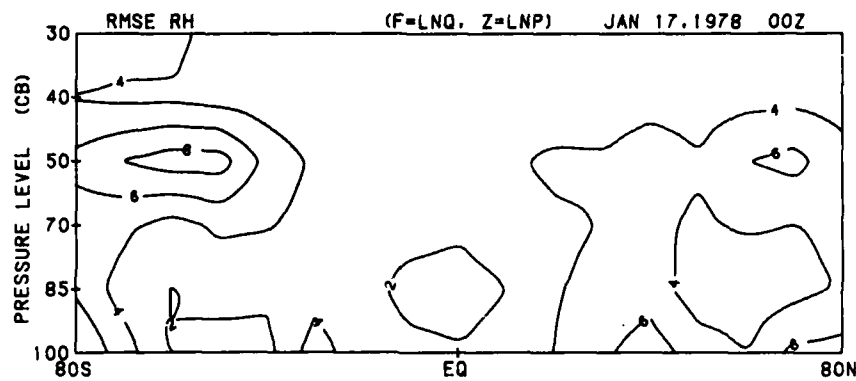
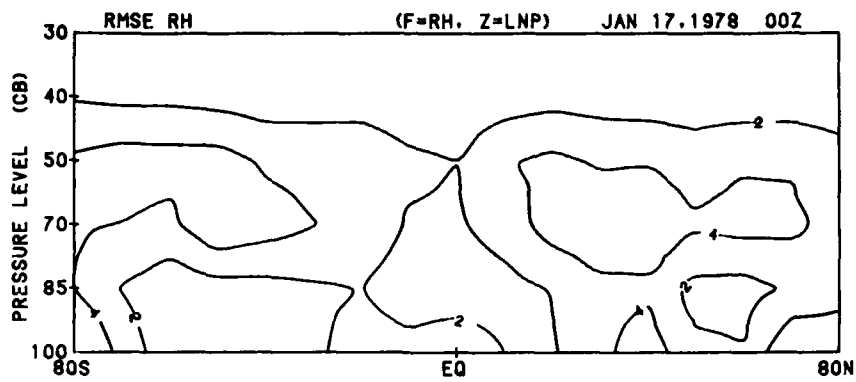


Figure 22. As in Figure 21 Except Spectral Transforms Reinstated in Pre- and Postprocessing, Where Transformed Moisture Variable was RH (Top), $\ln Q$ (Middle), and T_d (Bottom)

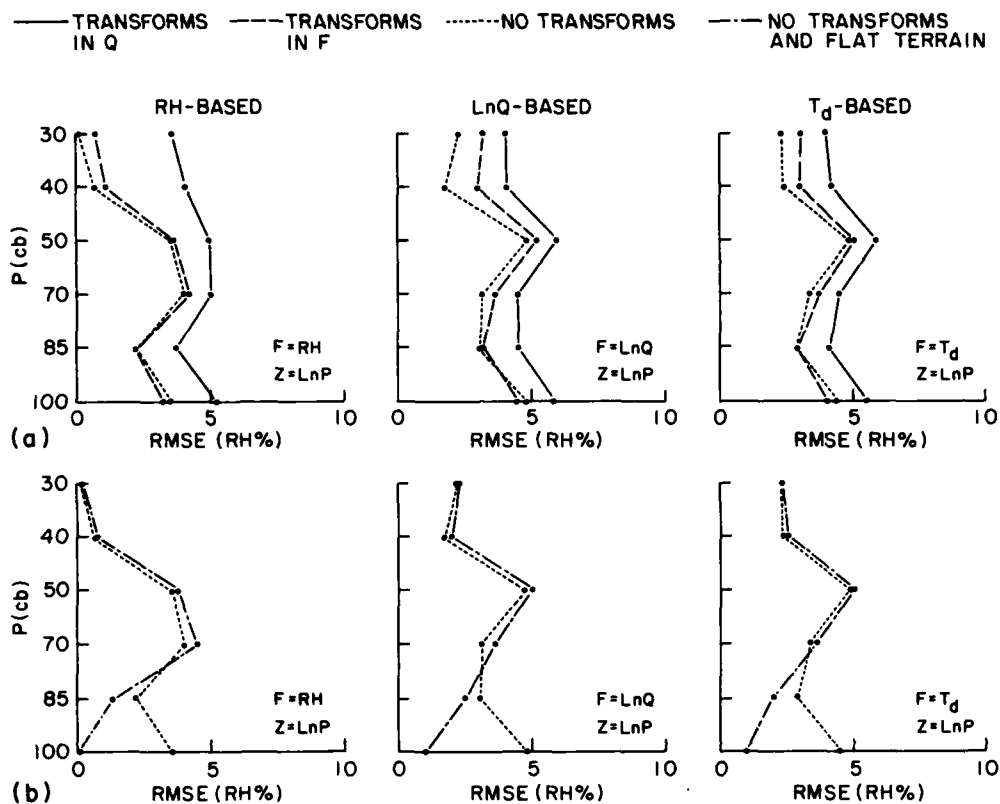


Figure 23. Vertical Profiles of the Global Mean BIAS and RMSE for the Synthesized FGGE III-A Analysis (17 January 1978, 00Z) Obtained by Executing the NMC/AFGWC Pre- and Postprocessor Using Vertical Interpolation of $F = (RH, LnQ, \text{ or } T_d)$ in LnP With the Indicated Choices of Horizontal Spectral Transforms (a) and With no Transforms for Either the Original or Zero Terrain (b)

ratio), and dewpoint depression $T - T_d$. He concluded that the truncation errors of RH and $T - T_d$ were substantially less than those of Q. He speculated, as actually found here, that T_d also would yield less truncation error than Q.

The large truncation errors found here near the poles with transforms of Q owes to the fact that the zonal mean value of Q falls off rapidly from the tropics to the poles following the decrease in temperature. Thus, locally small spatial deviations of Q in the tropics may lead to locally large deviations in Q in the polar regions following spectral reconstitution of the grid point values from spectral coefficients. Spectral transform theory guarantees only minimization of the global RMSE between input field and spectrally reconstructed field. This global minimization implicitly forces a closer fit of the larger Q values in the tropics and relatively poorer fit of the smaller Q values in polar regions. In the cases of RH,

$\ln Q$, and T_d , the decrease in zonal mean value toward the poles is relatively much less (or nonexistent in the case of RH -- see Figure 18) and hence the standard deviation of these fields in the tropics is not as large relative to the respective zonal mean values in the polar regions -- a characteristic that yields significantly smaller spectral truncation error in polar regions.

The standard use of Q as the moisture variable for spectral transformation in the pre- and postprocessor here is of course dictated by the use of Q as the prognostic moisture variable in the companion GSM. The popularity of Q as the prognostic moisture variable in many global forecast models stems from the fact that it is a conservative quantity in adiabatic flow. However, the cited spectral truncation errors in Q in spectral forecast models make it difficult to maintain the physical constraint that Q be non-negative and casts doubt on the suitability of using Q as the prognostic moisture variable in a spectral model. Indeed, based on Simmonds' work,¹⁸ Daley et al¹⁹ adopted $T-T_d$ as the prognostic moisture variable in the operational GSM of the Canadian Meteorological Center. As a companion argument against using Q for the GSM prognostic moisture variable, we propose that the vertical power law variation of Q as $\approx P^3$ (that is, σ^3) cited in Section 3.2 makes it particularly vulnerable to vertical truncation errors. Hansen et al²⁰ briefly discussed the vertical differencing of Q in their GCM as the source of a systematic positive prognostic moisture bias. As an apparent solution they used a harmonic mean in place of the arithmetic mean to compute values of Q at the σ -layer interfaces from values of Q at the σ -layers. In a planned follow-on study to the present one, we hope to compare the suitability of various moisture variables including Q , $\ln Q$, T_d , and $T-T_d$ as the prognostic moisture variable in a GSM.

3.4 Terrain Effects

It is instructive to consider the consistent increase in RMSE at 100 cb over that at 85 cb in all the vertical profiles of Figure 23(a). This increase occurs not only for all the given types of vertical interpolation, but also irrespective of the presence or absence of spectral transforms. Tracing the cause is aided, nonetheless, by first eliminating the spectral transform error as was accomplished in Figure 21. Inspection of Figure 21 reveals that low-level RMSE is a maximum

-
19. Daley, R., Girard, C., Henderson, J., and Simmonds, I. (1976) Short-term forecasting with a multi-level spectral primitive equation model: Part I -- model formulation, Atmosphere 14:98-116.
 20. Hansen, J., Russell, G., Rind, D., Stone, P., Lacis, A., Lebedeff, S., Ruedy, R., and Travis, L. (1983) Efficient three-dimensional global models for climate studies: Models I and II, Mon. Wea. Rev. 111:609-662.

at middle and high latitudes in the N.H. and at high latitudes in the S.H. This pattern suggests a relationship with latitudes having higher zonal mean terrain heights.

As a test for terrain effects, the experiments for the dotted curves in Figure 23(a) were repeated wherein a globally constant terrain height of 1 m was imposed. The resulting global mean and zonal mean RMSE are given in Figure 23(b) and Figure 24 respectively. These figures, by their absence of low-level RMSE, verify by counterexample that the presence of realistic terrain increases low-level RMSE.

The terrain-induced increase in 100-cb RMSE stems from increased low-level extrapolation errors in postprocessing. We recall that the representative position of the σ -layers given in Figure 7 assumes a surface pressure of $P_s = 101.3$ cb. Over higher terrain, surface pressures will be substantially less and the σ -layers will be displaced substantially upward with respect to the standard pressure surfaces. Recalling that $\sigma_2 = 0.862$ from Table 2, we find that $P_s < 98.6$ cb (that is, a terrain height above approximately 250 m) implies $P(\sigma_2) < 85$ cb and thus only one σ -layer will exist within 85 to 100 cb. One thereby loses the exactness of the low-level linear extrapolation afforded by two σ -layers occurring within 85 to 100 cb, as depicted in the right of Figure 8. For surface pressures increasingly less than 98.6 cb, the lower extrapolation error will increase as the extrapolation interval from σ_1 to 100 cb increases. Indeed the larger RMSE at 100 cb likely is dominated by the higher terrain cases where $P_s < 88.4$ cb (that is, terrain height above about 1.1 km), when the lowest σ -layer ($\sigma_1 = 0.962$) is above the 85-cb mandatory level. The larger 100-cb RMSE in this case, however, should not be particularly detrimental to the continuous 4-D data assimilation process as the $P \rightarrow \sigma$ vertical interpolation in the preprocessing that begins each GSM first-guess forecast will not utilize 100-cb values when σ_1 is above 85 cb.

It is noteworthy in Figure 23(b) that although the presence of terrain increases the RMSE at 100 and 85 cb, it slightly decreases the RMSE at 70, 50, 40, and 30 cb. This appears consistent with the fact that the presence of terrain raises the mean elevation of all σ -layers. This likely displaces layers σ_3 , σ_4 , σ_5 , and σ_6 closer on average to their nearest standard pressure surfaces (thus decreasing the interpolation intervals) than that shown in Figure 7. The latter figure assumed $P_s = 101.3$ cb, which is representative of sea level (zero terrain) and yields σ_3 , σ_4 , σ_5 , and σ_6 layers below the closest mandatory levels.

An earlier portion of Section 3 discussed how verification against RH analyses could implicitly favor RH-based vertical interpolations. Prior to the no-transform cases of Figure 23, this favoritism in RH-based interpolations was largely negated by the spectral transform steps, which required conversion from RH to Q

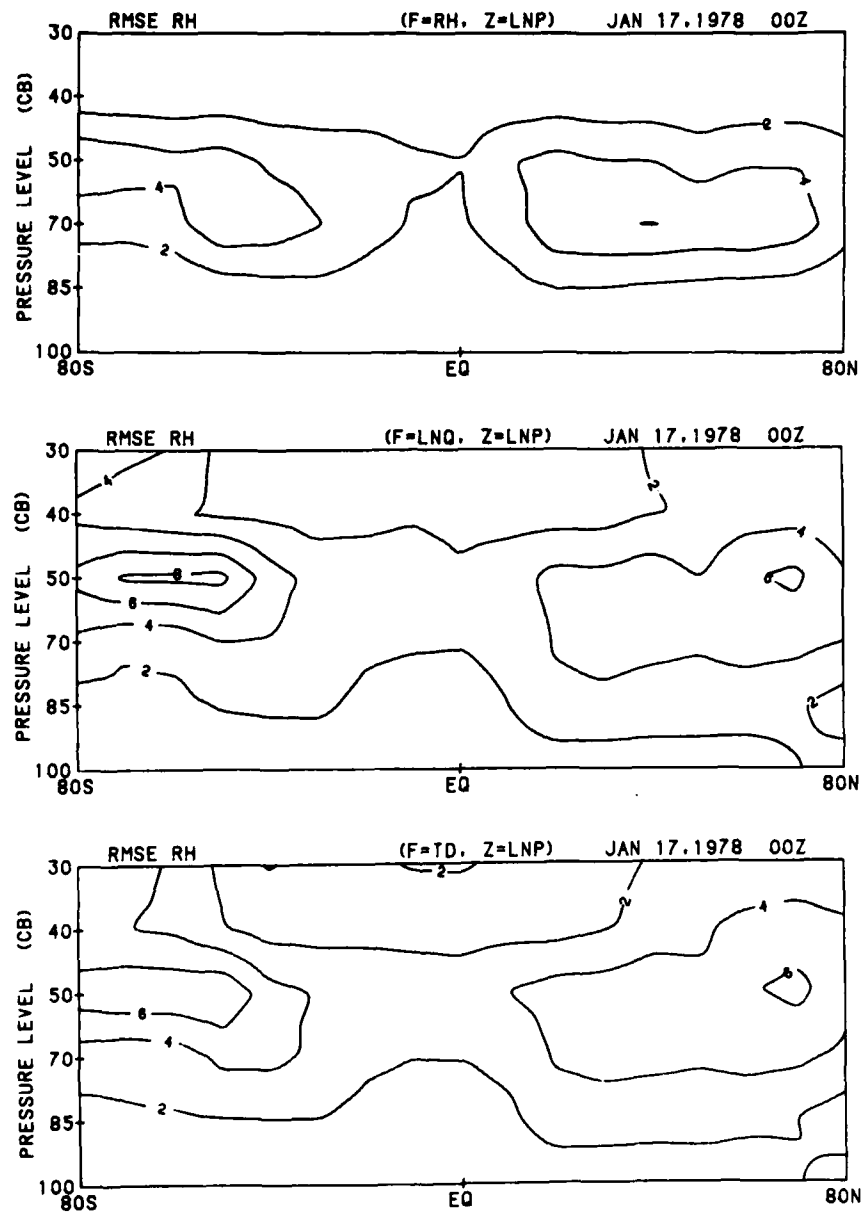


Figure 24. As in Figure 21 Except Zero Terrain Imposed Globally

and from Q to RH utilizing the processed temperature field before and after the transforms. Now, however, in the no-transform, zero-terrain RMSE profiles and plots of Figures 23 and 24, the RH favoritism in the verification appears to be appreciable at 100 and 30 cb. We proceed to examine this further in Figures 25 and 26 by verifying an adjusted RH field. This adjusted field includes errors

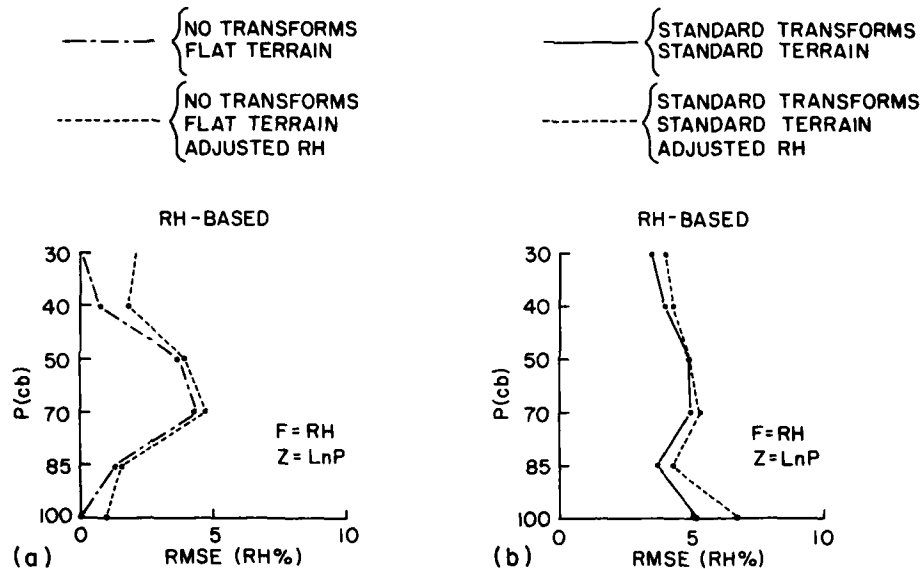
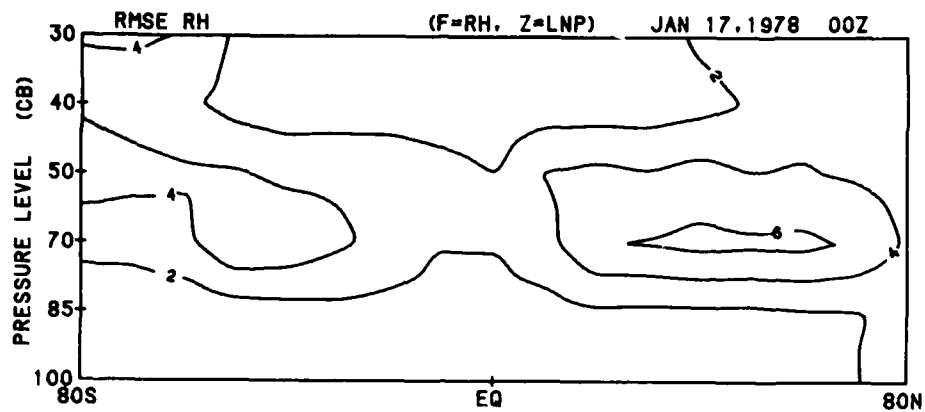


Figure 25. Repeat of the Dot-Dashed Curve (a) and the Solid Curve (b) of Global Mean RMSE in the RH-Based Interpolations of Figure 23(b) and (a) Respectively, Alongside the Parallel Cases (Dotted Curves) Where Post-processed RH Values are the Adjusted Values of RH^* in Eq. (B1)

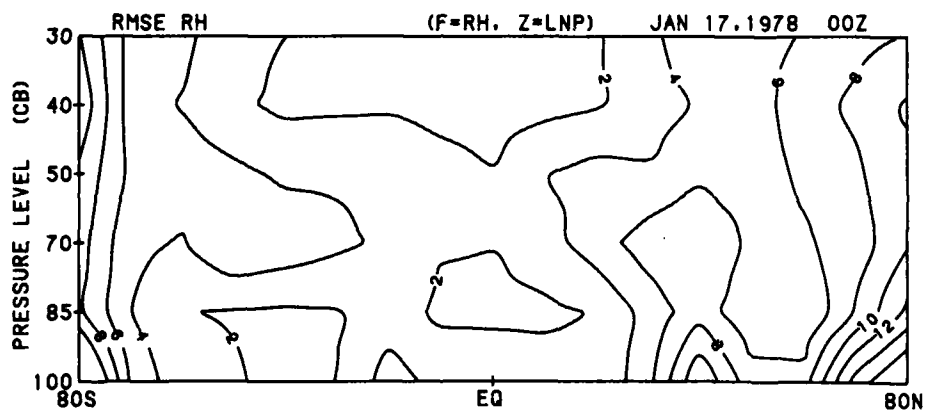
from the synthesized temperature field in a manner consistent with the influence of temperature errors in the Q-based and T_d -based interpolations. The development and discussion of Figures 25 and 26 are not crucial to the conclusions reached in this study and are therefore presented in Appendix B. The reader may choose to proceed immediately to Section 4, which will resume discussion of the figures with Figure 27.

4. A PSEUDO 4-D DATA ASSIMILATION

A major concern with pre- and postprocessing errors lies with their cumulative impact over time on the accuracy of an intermittent 4-D data assimilation system. As discussed in the introduction, these errors are among many sources of error that can contribute substantially to undesirable climatic drift and error growth in the assimilation system. As a means of measuring the error impact of moisture pre- and postprocessing, a 48-hr "pseudo" 4-D assimilation was executed. That is, all components of the 4-D assimilation in Figure 1 were run for eight cycles, but skipping the objective analysis stage while still interrupting the forecast every 6 hrs to run the pre- and postprocessor. The resulting pseudo assimilated moisture fields were verified at 24-hr intervals and compared with



A.



B.

Figure 26. Latitude-Height Contour Analysis of the Zonal Mean of RH^* in Eq. (B1) Corresponding to the Global Mean of RH^* in Figure 25(a) and Figure 25(b)

the verifications of a parallel standard forecast initialized from the same data (bottom, Figure 1). If the pre- and postprocessing steps in the pseudo 4-D assimilation do not significantly alter the moisture fields of the global forecast model, then their contribution to the overall error growth in moisture assimilation can be disregarded.

To measure the degree to which this is the case for this pseudo assimilation we shall extend the (F_1, A_1) and (S_1, A_1) verifications defined at the start of Section 3. The verification nomenclature (F_1^{nT}, A_1) and (S_1^n, A_1) is introduced where the former denotes the verification of the RH fields from n successive executions

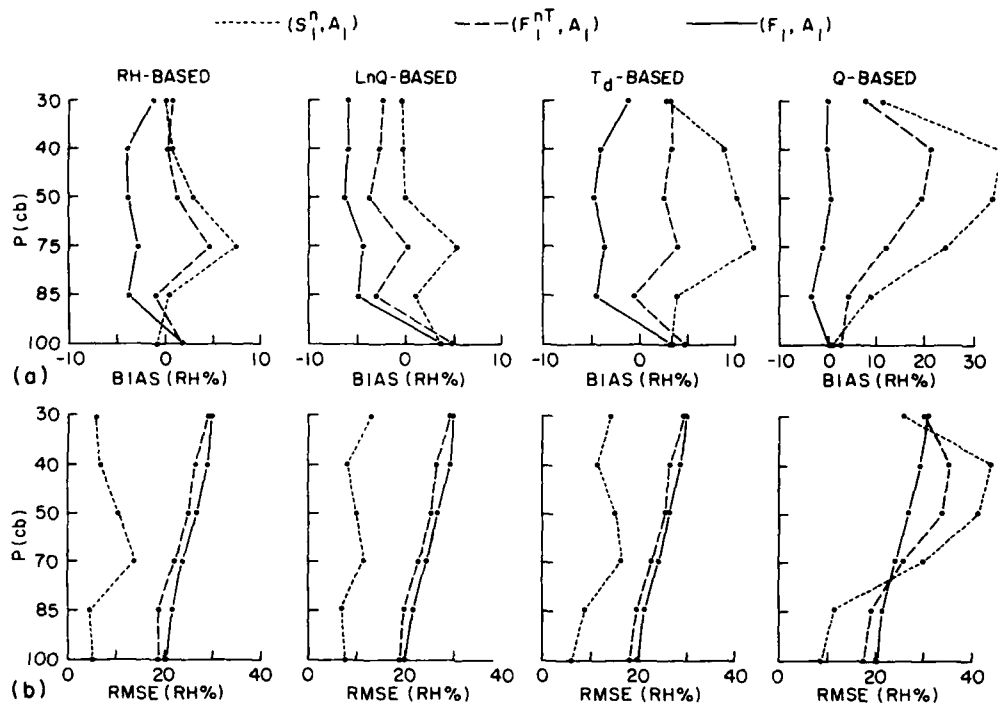


Figure 27. Vertical Profiles of the Global Mean BIAS and RMSE for the (S_1^n, A_1) , (F_1^{nT}, A_1) , and (F_1, A_1) Verifications (Defined in Text) Associated With the 48-hr Pseudo 4-D Assimilation ($n=8$, $T=6$ hr) Starting From the 00Z 1978 FGGE III-A Analysis of 17 January [19 January for (S_1^n, A_1)]. Results given for the four vertical interpolations of $F = (RH, LnQ, T_d, \text{ or } Q)$ in $Z = LnP$

of the "update" cycle without the objective analyses. The initial FGGE III-A objective analysis at time t_0 is designated A_0 while the verifying analysis at time t_1 is designated A_1 . Since each cycle in (F_1^{nT}, A_1) is $T = 6$ hr and since we choose $n = 8$, the overall pseudo assimilation period is $nT = 48$ hr. The quantity (S_1^n, A_1) denotes the verification of the RH fields from n successive executions of only the pre- and postprocessor pair applied to the final analysis A_1 . Thus, (F_1^{nT}, A_1) is a dynamic, temporally evolving forecast from the initial state A_0 , whereas (S_1^n, A_1) is again a static transformation or synthesis of the final verifying analysis A_1 . Hopefully, (S_1^n, A_1) is sufficiently small that its implied effect upon (F_1^{nT}, A_1) is minimal, thereby yielding $(F_1^{nT}, A_1) \approx (F_1, A_1)$, where F_1 denotes a standard 48-hr forecast execution.

Figure 27 presents results of a pseudo assimilation starting from the 00Z FGGE III-A analysis of 17 January 1978. The global mean BIAS and RMSE given for the (S_1^n, A_1) , (F_1^{nT}, A_1) , and the (F_1, A_1) verifications are valid at 48 hr. Four vertical interpolation alternatives are presented from left to right in Figure 27 as follows: (1) logarithmic interpolation of RH, (2) power law interpolation of

Q, (3) logarithmic interpolation of T_d , and (4) logarithmic interpolation of Q. It should be emphasized that only the processing steps involve the alternative moisture variables, while all forecast steps employ Q as the prognostic moisture variable. The forecast model used in these experiments is the AFGL global spectral model (Brenner et al.²¹) with the same R30 truncation and 12-layer structure as the pre- and postprocessor. Figure 28 shows the corresponding temporal trends of the global mean BIAS and RMSE at the 40-cb level. This level is highlighted because the logarithmic interpolations of Q yield the largest and most unacceptable errors at this level. Lastly, Figure 29 and Figure 30 show the zonal mean BIAS and RMSE, respectively, corresponding to the global mean plots in Figure 27 and in the same order.

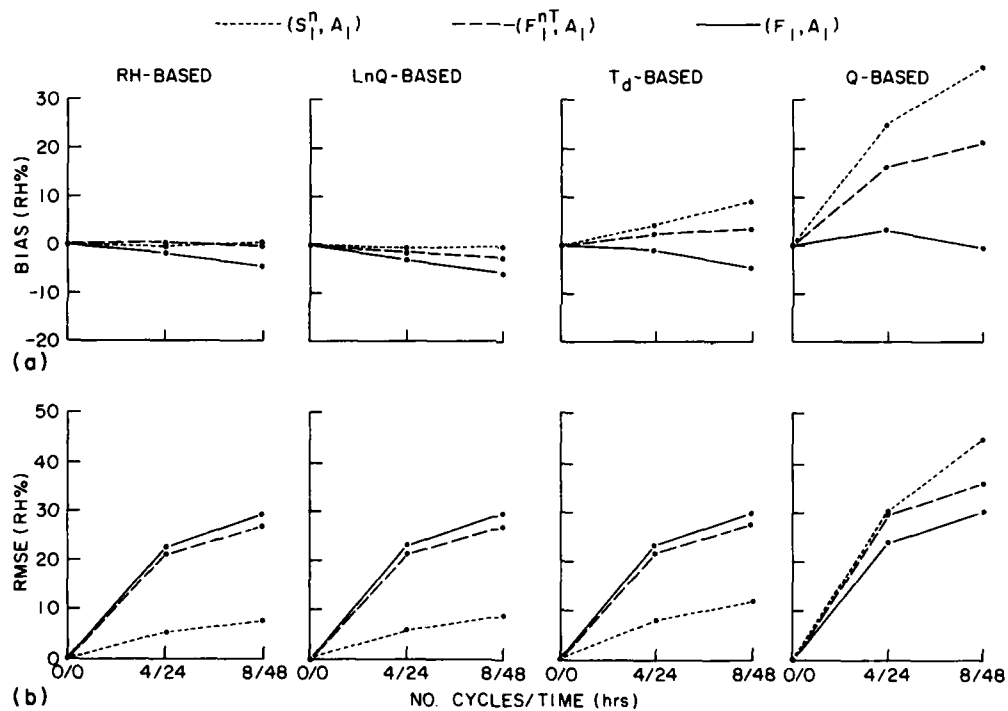


Figure 28. Temporal Trend at P = 40 cb Level for the Global Mean BIAS and RMSE of the (S_1^n, A_1) , (F_1^T, A_1) , and (F_1, A_1) Verifications in Figure 27. The (S_1^n, A_1) trend is shown for a given number of cycles, n, as it is not strictly defined over time intervals

21. Brenner, S., Yang, C., and Mitchell, K. (1984) The AFGL Global Spectral Model: Expanded Resolution Baseline Version, AFGL-TR-84-0308.

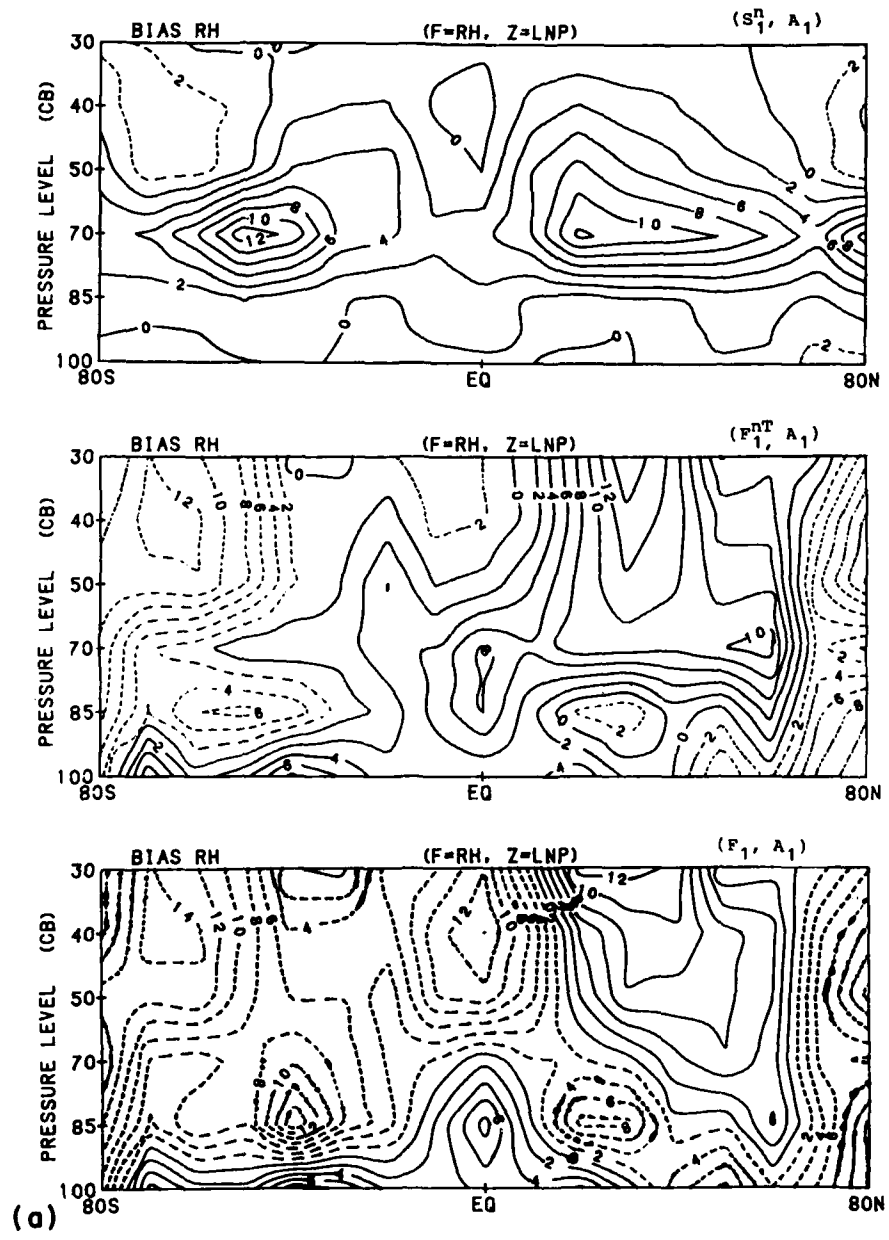


Figure 29. Latitude-Height Contour Analysis of the Zonal Mean BIAS Valid at 48 hr ($n = 8, T = 6$ hr) and Given From Top to Bottom for the (S_1^N, A_1), (F_1^N, A_1), and (F_1, A_1) Verifications, Respectively, in Figure 27. Parts (a) through (d), respectively, represent the interpolation types depicted from left to right in Figure 27

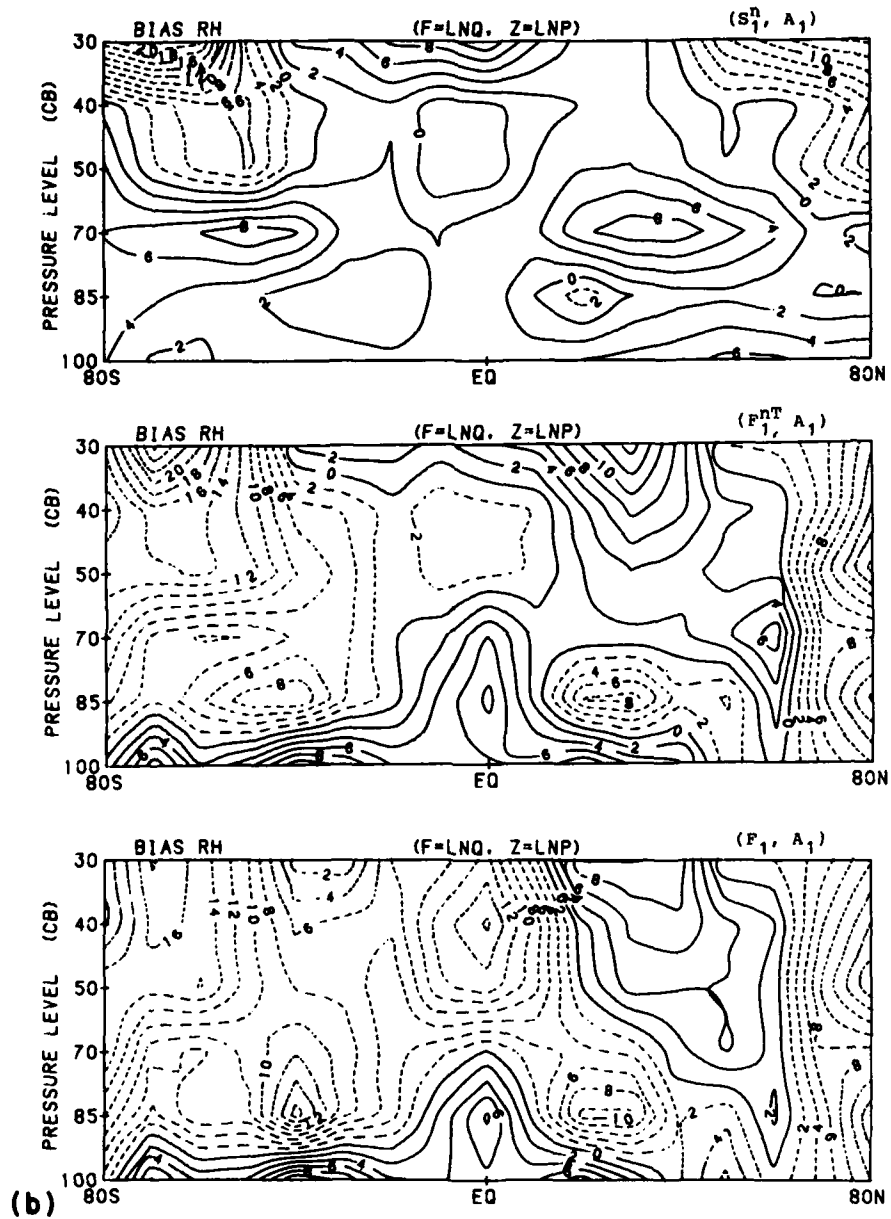
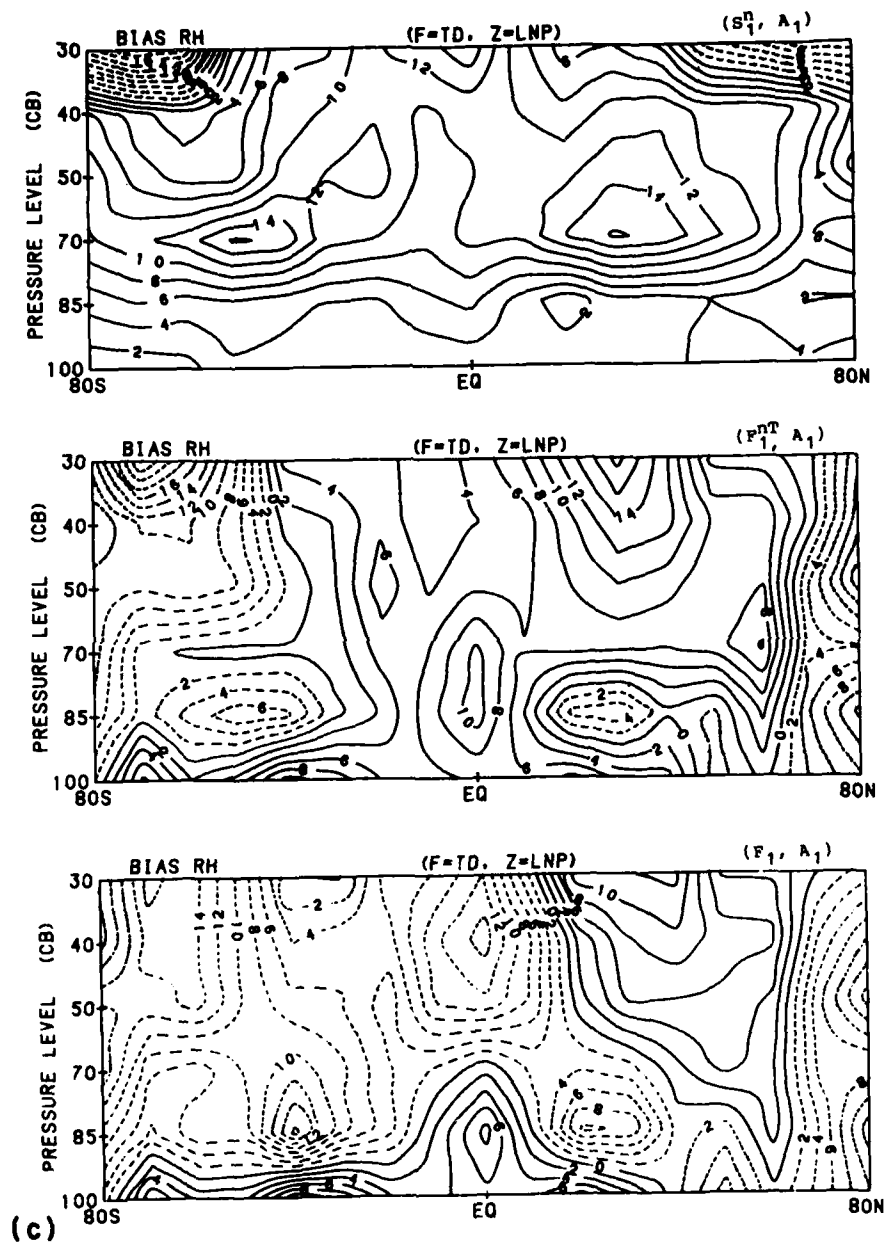


Figure 29 (Contd)



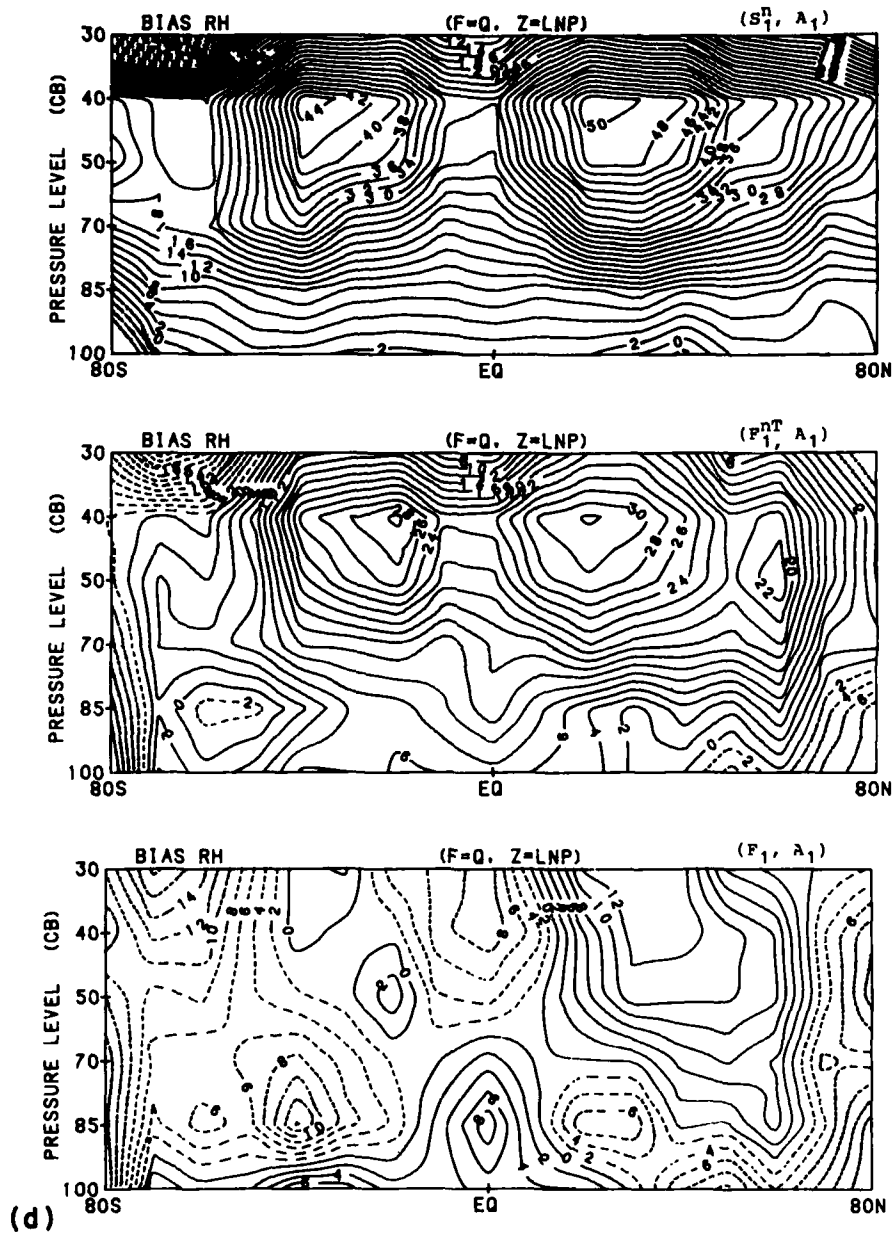


Figure 29 (Contd)

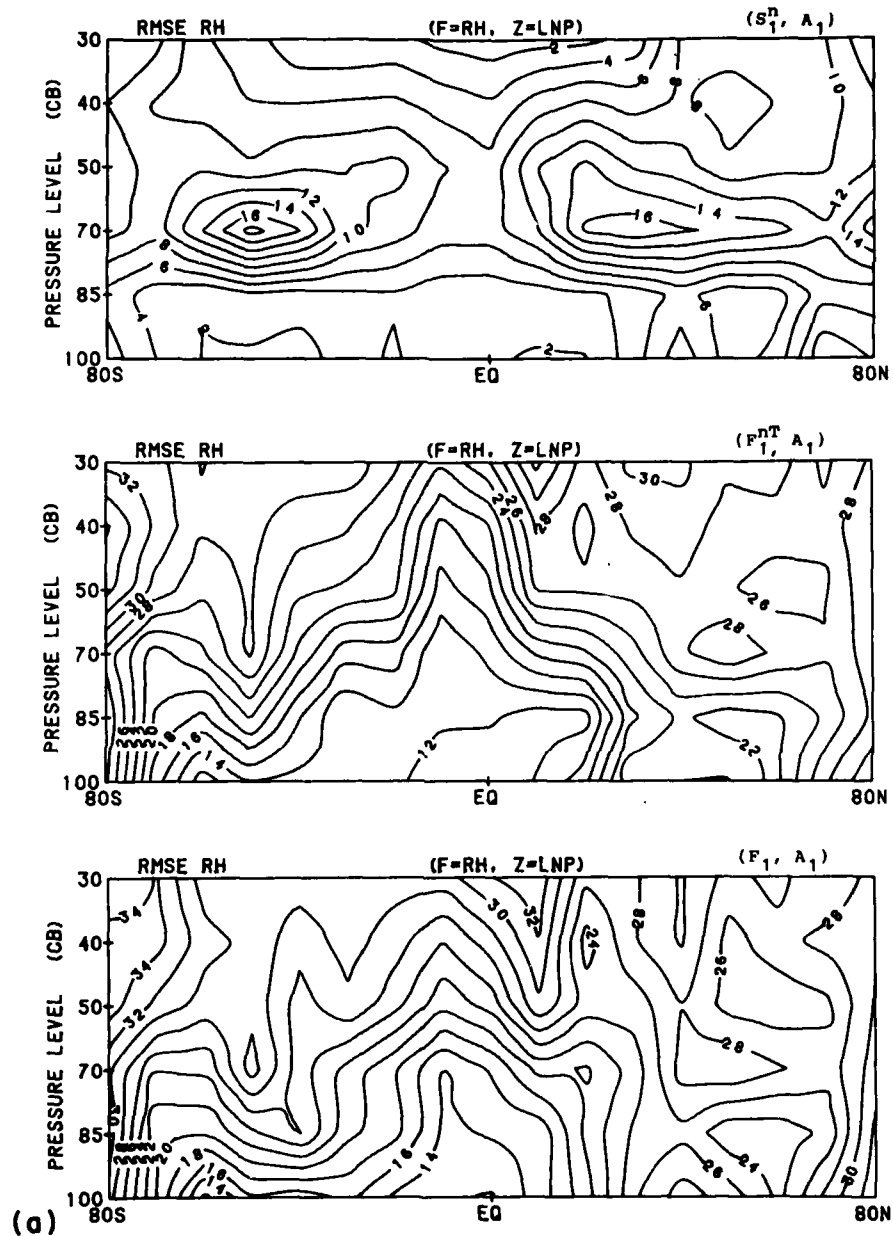


Figure 30. As in Figure 29 but for Zonal Mean RMSE

Looking first at the solid BIAS curves in Figure 27, the standard 48-hr forecast shows a modest negative bias for all interpolation types except at 100 cb. This forecast bias is significant here not so much in an absolute sense but rather in defining the trend of the forecast when devoid of processing interruptions. Consistent with the BIAS plots in Figure 19, the dotted BIAS curves in Figure 27

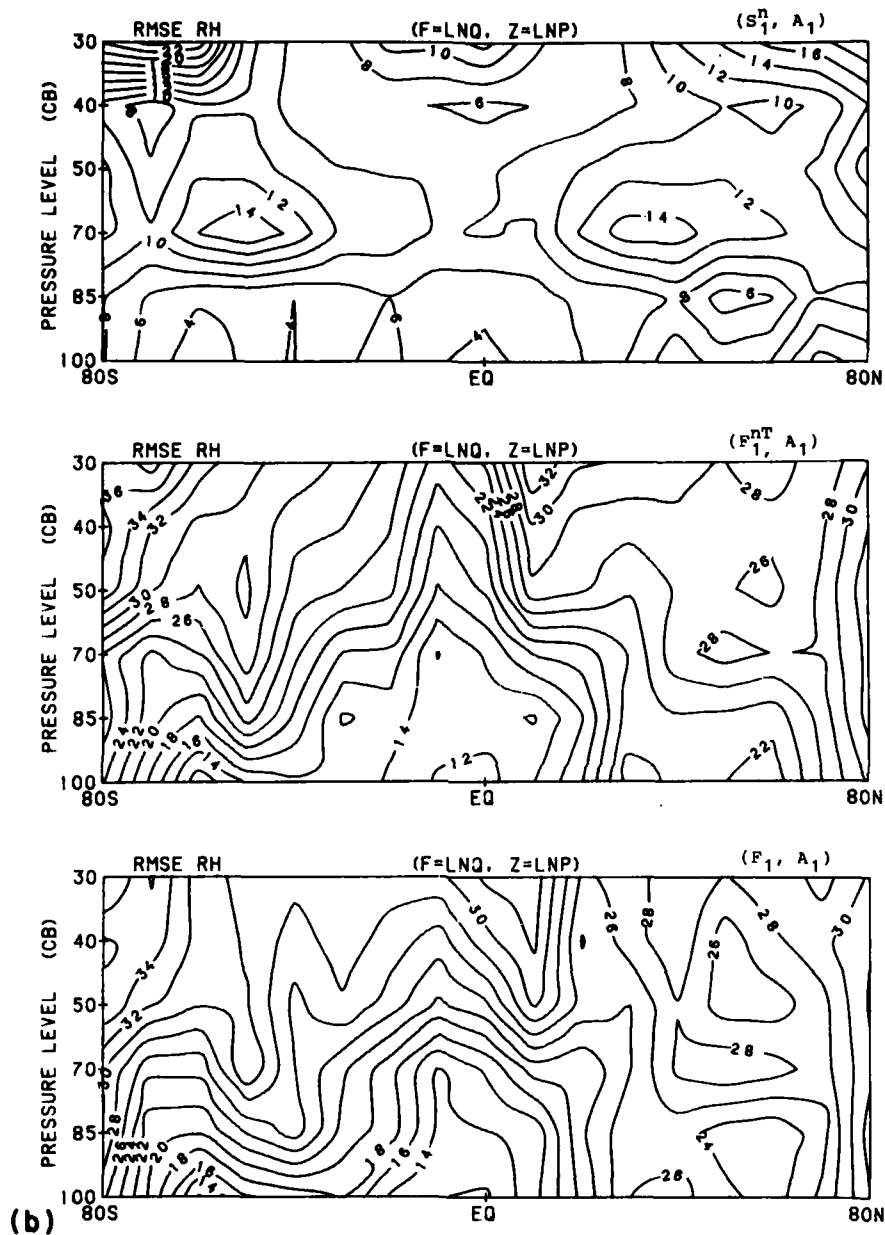


Figure 30 (Contd)

show that the synthesized analyses have a decidedly positive BIAS for all interpolation types (drastically so for logarithmic interpolation of Q). Not surprisingly then, the dashed BIAS curves for the pseudo assimilations (F_1^{nT}, A_1) lie between those for (S_1^n, A_1) and (F_1, A_1). The preferred choice of vertical interpolation is that which yields both BIAS and RMSE curves for (F_1^{nT}, A_1) closest to those for

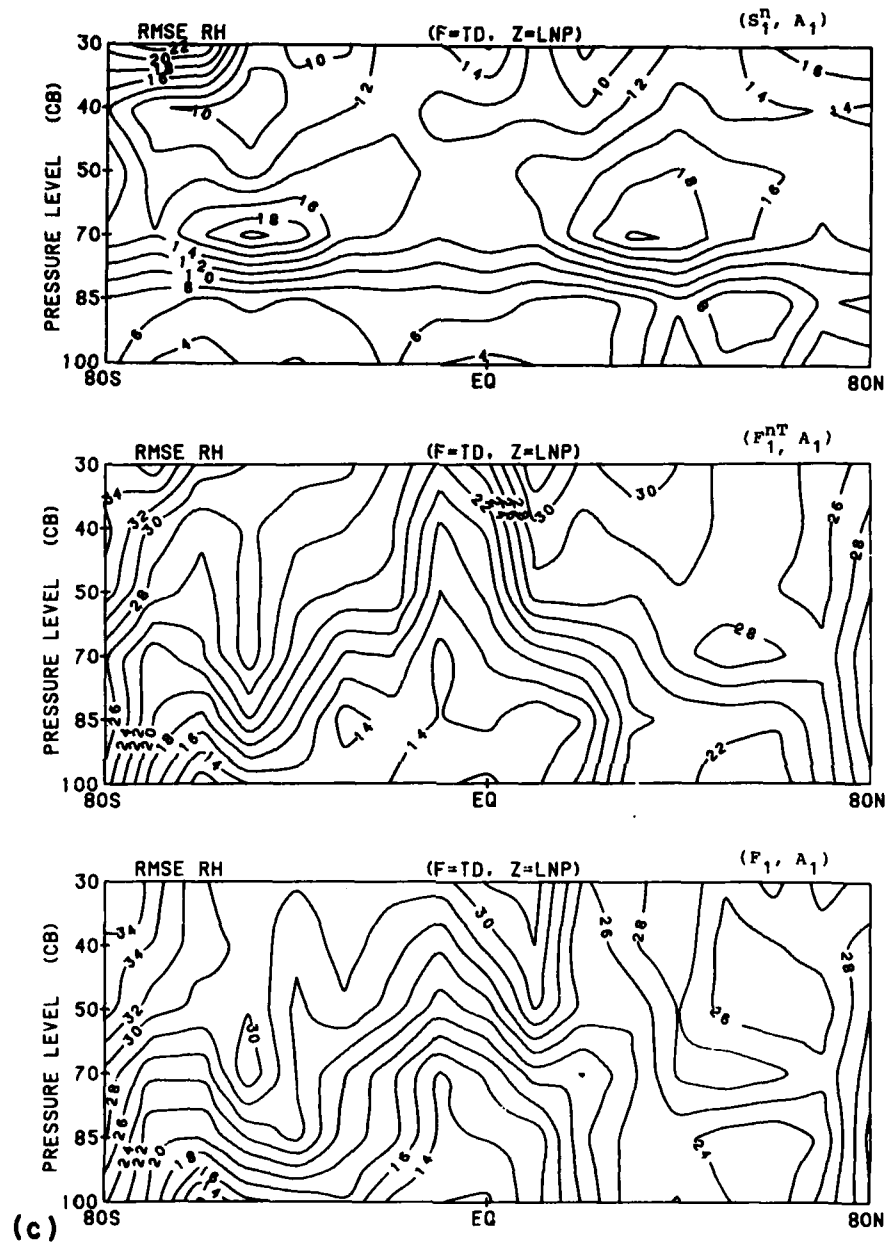


Figure 30 (Contd)

(F₁, A₁). Given this criterion, the power law interpolation of Q is superior, but only slightly more so than logarithmic interpolation of RH.

It is clear from Figure 27 that the substantial middle level positive biases in synthesized analyses using logarithmic interpolations of Q are severe enough to spoil the associated pseudo 4-D assimilations [compare middle and bottom plots

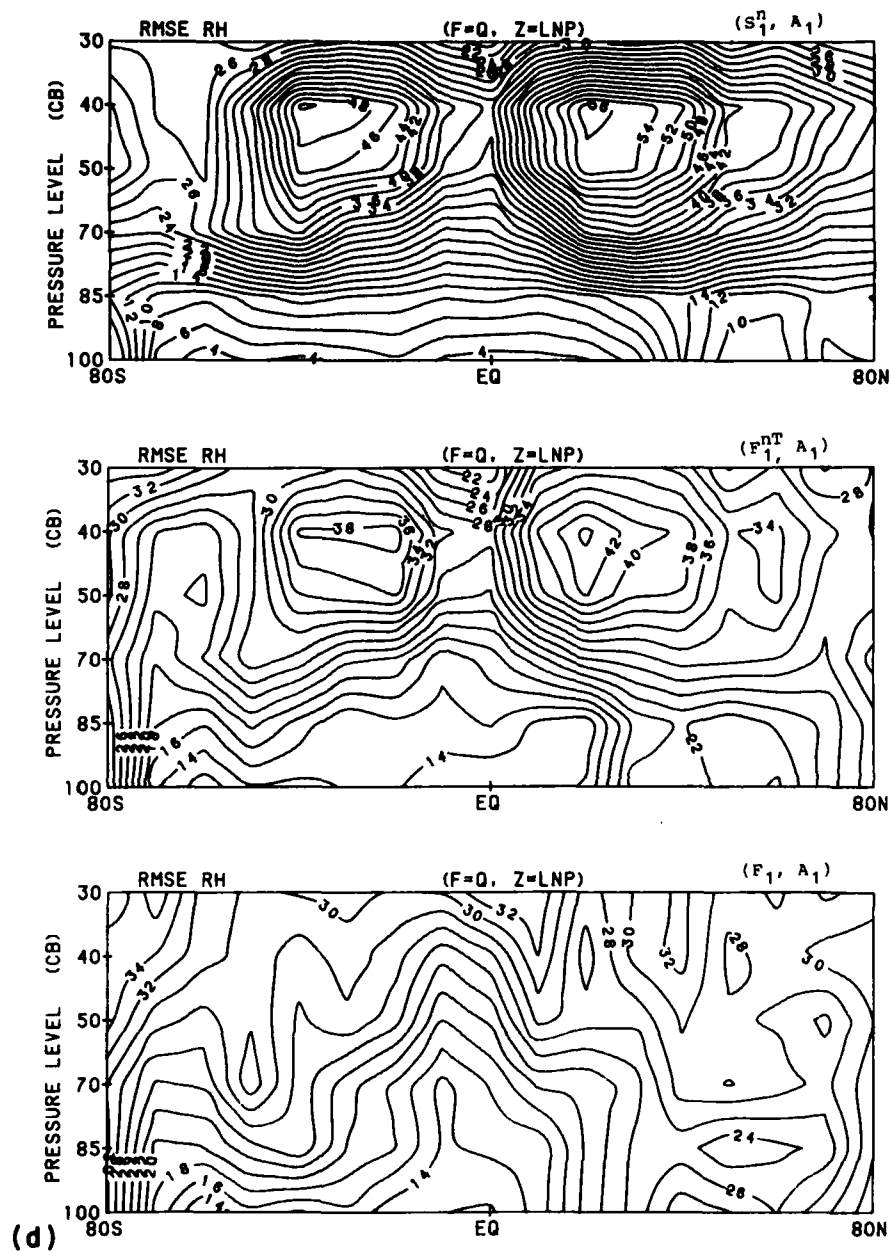


Figure 30 (Contd)

of Figures 29(d) and 30(d)]. The magnitude of the middle level positive BIAS in the second plot of Figure 29(d) is so large that it clearly dominates the middle level RMSE in the second plot of Figure 30(d). Similarly, in the bottom of Figure 27, the pseudo assimilation using the logarithmic interpolation of Q is the only one showing greater RMSE than that of the standard forecast. Even the RMSE of

the associated synthesized analysis is greater than that of the standard forecast, a result not even closely approached by the other interpolation types.

Recall from the simple, one-cycle (S_1, A_1) error statistics of Section 3.2 that T_d -based interpolations yielded competitively small processing errors. Contrary to these earlier simple tests, the present T_d -based interpolations over several cycles exhibit an appreciable (though not overwhelming) inferiority to the two leftmost interpolations in Figure 27. Aside from the logarithmic interpolations of Q , the T_d -based interpolation shows the largest (S_1^n, A_1) BIAS at all levels except 100 cb and consequently the greatest spread between the BIAS curves of the (F_1, A_1) and (F_1^{nT}, A_1) verifications. Among the three nominal interpolations, we conclude that the BIAS processing error of T_d -based interpolations is more subject to continuous accumulation in numerous repetitions of pre- and postprocessing. This conclusion is supported by Figure 28, which shows that of the three nominal interpolations, the spread between the (F_1^{nT}, A_1) and (F_1, A_1) BIAS curves at 40 cb is growing most rapidly for the T_d -based interpolations.

Thus, logarithmic interpolation of RH and power law interpolation of Q remain as the most likely choices. To identify a preference between these two interpolations, the zonal mean BIAS plots in parts (a) and (b) of Figure 29 are considered. At 70 cb, both interpolation types exhibit a disappointing accumulation of positive BIAS errors in their (S_1^n, A_1) verifications. The RH-based interpolation, though, yields a somewhat larger BIAS at 70 cb. Further evidence of this disadvantage in RH-based interpolations is apparent in a somewhat poorer preservation in part (a) over part (b) of the (F_1, A_1) midtropospheric BIAS by the (F_1^{nT}, A_1) BIAS.

On the other hand, the power law interpolation of Q yields a much larger accumulation of BIAS errors at 30 cb in the top of part (b) than in the top of part (a) of Figure 29. The influence of this BIAS error is clearly present in the (F_1^{nT}, A_1) BIAS in the middle of part (b). Recalling Figure 6, the underlying vertical extrapolation error in the moisture field in these tests is virtually zero at 30 cb for any choice of moisture variable. Rather, the 30 cb BIAS in the uppermost plots of parts (b) and (c) of Figure 29 were traced to small BIAS errors in the (S_1^n, A_1) temperature verifications. Thus, rather small temperature biases (that is, biases in saturation Q or T_d) at the cold temperatures typical of 30 cb can cause nontrivial biases in derived RH values computed from bias-free values of Q or T_d . This effect was evidently not large enough to make RH biases at 30 cb a dominant feature in the single cycle (S_1, A_1) BIAS plots at the top of Figure 19(b) and (c) (although the initial hints of the problem are discernible).

In conclusion, there appears to be no clear superiority between selecting logarithmic interpolation of RH or power law interpolation of Q . Either of these two vertical interpolations is suitable, provided in all cases some attention is

given to the chosen σ -structure (to minimize the interpolation interval to 70 cb) and to the magnitude and impact of temperature biases at high altitudes (or cold temperatures).

5. CONCLUSIONS

This study examined and sought methods to reduce the vertical interpolation/extrapolation errors of moisture in the pre- and postprocessor of an intermittent 4-D data assimilation system, such as that used at AFGWC. The tests of vertical interpolation utilized the three moisture variables of relative humidity (RH), specific humidity (Q), and dewpoint (T_d). The input fields for the pre- and postprocessor executions were chosen from a sample of January and July 1978 FGGE III-A objective analyses.

The sample mean FGGE III-A vertical profiles of RH, Q, and T_d all decreased with height at all moist analyzed standard pressure levels. This property dictated that the constant extrapolation of moisture in the NMC/AFGWC postprocessor be replaced with linear extrapolation. This is particularly true when Q or T_d were extrapolated. When the prognostic moisture variable is carried only at model σ -layers in the troposphere, one can further reduce upper extrapolation error by selectively choosing the topmost σ -layer. Since 30 cb is the highest standard pressure surface for which moisture is analyzed, the topmost prognostic layer carrying moisture should be the lowest σ -layer consistently above 30 cb. Lastly regarding extrapolation, one should try to include at least two σ -layers between 85 through 100 cb to further minimize lower extrapolation errors.

Of more significance are the results obtained for vertical interpolations interior to the modeled moist domain. It was found that the fairly popular use of logarithmic interpolation (that is, linear interpolation in $\ln P$) is a good approach for the variables RH and T_d , but a singularly poor approach for the variable Q. Logarithmic interpolation of Q leads to substantial positive moist biases in the middle and upper troposphere because, on average, Q is not a linear function in $\ln P$. Rather it varies in P approximately as a power law (that is, $\approx P^3$). Hence power law interpolation of Q (that is, linear interpolation of $\ln Q$ in $\ln P$) yields excellent interpolation accuracy. In arriving at the above result, it has been demonstrated that it is good practice to seek an elementary functional transformation $F = F(f)$ and $Z = Z(P)$ of the moisture variable f and pressure P such that on the average the function $F(Z)$ is closely linear. Straightforward linear interpolation of F in Z can thus yield interpolation accuracy greatly surpassing higher-order interpolations (for example, cubic spline) of the original variable f. Also,

vertical interpolations of a linear function $F(Z)$ are less sensitive to changes in σ -structure or resolution and submit better to linear extrapolation when necessary.

The vertical interpolations discussed above were first tested in a static fashion by executing just the NMC/AFGWC pre- and postprocessor pair. The tests were then extended to running 48-hr pseudo 4-D intermittent data assimilations wherein the objective analysis steps in Figure 1 (top) were eliminated while still interrupting the forecast every 6 hr to execute the pre- and postprocessor. The pseudo assimilations using logarithmic interpolation of Q were severely contaminated by the positive bias discussed above. A similar exceptional positive bias, also attributed to vertical interpolations of Q , was previously noted by Lorenc and Tibaldi¹ in actual ECMWF 4-D data assimilations of moisture.

The pseudo assimilations in this study showed that logarithmic interpolation of RH or power law interpolation of Q yield comparably good results in minimizing the accumulative effects of vertical interpolation error on the global forecast model's first-guess fields. Logarithmic interpolation of T_d , though performing well in the static tests, showed a greater tendency toward error accumulation in the pseudo assimilations. Therefore, it is not to be recommended.

It was noted that even the satisfactory logarithmic interpolation of RH and power law interpolation of Q both yielded nontrivial positive bias tendencies at 70 cb in the 48-hr pseudo assimilations [note top of parts (a) and (b) in Figure 29]. This result points to the desirability in the preprocessor, even when using fairly accurate vertical interpolations, to interpolate the analyzed residuals. This increasingly popular approach (for example, NMC, ECMWF, GLAS) will leave the forecast first-guess fields unmodified \downarrow the update cycle in data-void regions. Nevertheless, the postprocessing step to provide forecast first-guess values on pressure surfaces must still necessarily interpolate full-value fields from σ to P.

There are other alternative 4-D data assimilation approaches besides use of residuals that can minimize the effects of vertical interpolation error. For example, in the OI objective analysis model being developed at AFGL by Norquist et al,²² following the approach of Bergman,²³ the analysis is performed on model σ -surfaces, eliminating the need for pre- and postprocessing. It does, however, contain a one-way interpolation from P to σ within the analysis model to represent the observations on σ -surfaces. In the continuous GFDL 4-D assimilation system

22. Norquist, D., Halberstam, I., Tung, S. -L., and Johnson, C. (1984) Two Methods of Global Data Assimilation, AFGL-TR-84-0260.

23. Bergman, K. (1979) Multivariate analysis of temperature and winds using optimum interpolation, Mon. Wea. Rev. 107:1423-1444.

described by Stern and Ploshay,⁹ the model forecast is not intermittently interrupted. Rather OI-analyzed observations (full values) are continuously and asynchronously inserted into the model forecast, thereby leaving the forecast unaltered in data-void regions as well. In the GFDL assimilation, however, the OI analysis is again performed on pressure surfaces so there are $\sigma \rightarrow P$ and $P \rightarrow \sigma$ interpolations before and after the analysis.

All three methods cited above (residuals, σ -based OI, continuous insertion), reduce the effects of vertical interpolation errors. However, they still include vertical moisture interpolations at key points in the assimilation. Consequently, the basic sources of interpolation error demonstrated in this study will still impact the assimilations. Therefore, the ease with which the moisture interpolations recommended in this study can be implemented suggest their application in all data assimilation schemes.

A test of the robustness of these results when using the 1979 FGGE III-A analyses of NMC is presently underway. In 1979, the NMC analyses were performed using optimal interpolation methods rather than using Hough functions. Finally, follow-on investigations are underway to test the implications of the power law dependence of Q in the truncation errors of the vertical finite differencing of Q -based prognostic moisture equations in global forecast models.

References

1. Lorenc, A., and Tibaldi, S. (1979) The Treatment of Humidity in ECMWF's Data Assimilation Scheme, ECMWF Research Department, Technical Memorandum No. 7, Reading, Berkshire, U.K., 103 pp.
2. Morone, L., and Dey, C. (1983) The NMC Global Data Assimilation System. Preprints, Sixth Conf. on Numerical Weather Prediction, 6-9 June, 1983, Amer. Meteor. Soc., Omaha, Nebr., pp. 115-119.
3. Koermer, J. (1983) The Advanced Weather Analysis and Prediction System. Preprints, Sixth Conf. on Numerical Weather Prediction, 6-9 June, 1983, Amer. Meteor. Soc., Omaha, Nebr., pp. 82-84.
4. Tibaldi, S. (1982) The ECMWF humidity analysis and its general impact on global forecasts and on the forecast in the Mediterranean area in particular, Riv. Meteorol. Aeronaut. 42:311-328.
5. Smagorinsky, J., Miyakoda, K., and Strickler, R. (1970) The relative importance of variables in initial conditions for dynamical weather prediction, Tellus 22:141-157.
6. Rosmond, T. (1981) NOGAPS: Navy Operational Global Atmospheric Prediction System. Preprints, Fifth Conf. on Numerical Weather Prediction, 2-6 November, 1981, Amer. Meteor. Soc., Monterey, Calif., pp. 74-79.
7. Sirutis, J., Miyakoda, K., and Ploshay, J. (1979) Moisture distribution derived in mathematical models and four-dimensional analysis. Proceedings, International Workshop on Atmospheric Water Vapor, 11-13 September, 1979, Vail, Colo., pp. 489-496.
8. Wilfong, T., Stobie, J., Renninger, L., Lewis, M., Lewis, F., Carr, E., Weiner, A., and Tuell, J. (1984) The Air Force Global Weather Central's high resolution analysis system. Preprints, Sixth Conf. on Numerical Weather Prediction, 6-9 June, 1983, Amer. Meteor. Soc., Omaha, Nebr. pp. 266-268.

9. Stern, W. , and Ploshay, J. (1983) An assessment of GFDL's continuous data assimilation system used for processing FGGE data. Preprints, Sixth Conf. on Numerical Weather Prediction, Amer. Meteor. Soc., 6-9 June, 1983, Omaha, Nebr., pp. 90-95.
10. Baker, W. (1983) Objective analysis and assimilation of observational data from FGGE, Mon. Wea. Rev. 111:328-342.
11. Brenner, S., Yang, C., and Yee, S. (1982) The AFGL Spectral Model of the Moist Global Atmosphere: Documentation of the Baseline Version, AFGL-TR-82-0393, AD A129283.
12. Lönnerberg, P., and Shaw, D., Eds. (1983) ECMWF Data Assimilation: Scientific Documentation, ECMWF Research Dept., Research Manual 1, Reading, Berkshire, U.K., 103 pp.
13. Warburton, J., Ed. (1983) NMC/AWS Global Spectral Model Maintenance Manual, NMC Development Division, National Meteorological Center, NOAA, Washington, D. C.
14. Sela, J. (1980) Spectral modeling at the National Meteorological Center, Mon. Wea. Rev. 108:1279-1292.
15. Lowe, P. (1977) Approximating polynomial for the computation of saturation vapor pressure, J. Appl. Meteorol. 16:100-105.
16. Oort, A. (1983) Global Atmospheric Circulation Statistics, 1958-1973, NOAA Professional Paper No. 14, U.S. Government Printing Office, Washington, D. C. 180 pp.
17. Ahlberg, J., Nilson, E., and Walsh, J. (1967) The Theory of Splines and Their Applications, Academic Press, New York, 284 pp.
18. Simmonds, I. (1975) The spectral representation of moisture, J. Appl. Meteorol. 14:175-179.
19. Daley, R., Girard, C., Henderson, J., and Simmonds, I. (1976) Short-term forecasting with a multi-level spectral primitive equation model: Part I -- model formulation, Atmosphere 14:98-116.
20. Hansen, J., Russell, G., Rind, D., Stone, P., Lacis, A., Lebedeff, S., Ruedy, R., and Travis, L. (1983) Efficient three-dimensional global models for climate studies: Models I and II, Mon. Wea. Rev. 111:609-662.
21. Brenner, S., Yang, C., and Mitchell, K. (1984) The AFGL Global Spectral Model: Expanded Resolution Baseline Version, AFGL-TR-84-0308.
22. Norquist, D., Halberstam, I., Tung, S. -L., and Johnson, C. (1984) Two Methods of Global Data Assimilation, AFGL-TR-84-0260.
23. Bergman, K. (1979) Multivariate analysis of temperature and winds using optimum interpolation, Mon. Wea. Rev. 107:1423-1444.

Appendix A

Power Law Interpolation

Suppose given quantity f satisfies a power law in P according to

$$f = aP^b \quad , \quad (A1)$$

where (a, b) are constants. Given known values of f_1 and f_2 at P_1 and P_2 , Eq. (A1) can be applied twice to obtain the two simultaneous equations $f_1 = aP_1^b$ and $f_2 = aP_2^b$. Solving these equations for the constants (a, b) yields

$$b = \frac{\text{Ln}f_2 - \text{Ln}f_1}{\text{Ln}P_2 - \text{Ln}P_1} \quad , \quad a = f_1/P_1^b \quad . \quad (A2)$$

Now the interpolated value of \tilde{f} at \tilde{P} between P_1 and P_2 is given by

$$\tilde{f} = a\tilde{P}^b \quad , \quad (A3)$$

in which (a, b) are given by Eq. (A2). Finally to express Eq. (A3) in the form of Eq. (1) in the text, the logarithm of both sides of Eq. (A3) is taken and then Eq. (A2) is substituted for (a) , which after some algebra gives

$$\text{Ln}\tilde{f} = \text{Ln}f_1 + b(\text{Ln}\tilde{P} - \text{Ln}P_1) \quad . \quad (A4)$$

With (b) defined in Eq. (A2), the above result is equivalent to Eqs. (1) and (2) in the text for the case of $F = \text{Ln}f$ and $Z = \text{Ln}P$, in agreement with Table 3. By similar analysis, the equivalence of Eqs. (1) and (2) to the remaining interpolation types in Table 3 for the given forms of F and Z can be validated.

Appendix B

An Alternative Verification

In the no-transform cases of Figures 21, 23, and 24, which eliminated steps 6 and 7 of Table 5(a) and steps 1 and 2 of Table 5(b), the pre- and postprocessing of the input moisture field (RH, $\text{Ln}Q$, or T_d) proceeded fully independent of the temperature field until the final conversion to RH before verification [step 4 in Table 5(b)]. In RH-based interpolations, even this last step was unnecessary. Thus, in the no-transform RH-based interpolations, the processed moisture field was completely uncontaminated by temperature processing errors. For example, the accuracy of the upper and lower extrapolation of the moisture field in the no-transform, zero-terrain RH-based interpolations is particularly good at 100 and 30 cb (virtually zero RMSE) at the left of Figure 23(b) and top of Figure 24. This follows because as the right of Figures 6 and 8 showed, over zero terrain the present extrapolation procedures exactly reproduce the input moisture value f at 100 and 30 cb. In the no-transform, zero-terrain, $\text{Ln}Q$ - and T_d -based interpolations of Figures 23(b) and 24, the lower and upper extrapolation of the moisture variable ($\text{Ln}Q$ or T_d) is still exact but now obscured by the verification step, which as stated earlier requires postprocessed temperature fields to convert postprocessed $\text{Ln}Q$ or T_d to RH. In all three no-terrain profiles of Figure 23(b), the corresponding global mean RMSE of temperature was 0.17, 0.19, 0.21, 0.34, 0.28, and 0.33 K at 100, 85, 70, 50, 40, and 30 cb respectively.

To impose a representative effect from processed temperature error on the verification of the no-transform, zero-terrain, RH-based interpolation of Figure 23(b), we modified the postprocessed RH field with the adjustment given by

$$\tilde{RH}^* = \frac{[\tilde{RH} \times e_s(T)]}{e_s(\tilde{T})} \quad (B1)$$

where (\sim) denotes a postprocessed value and T denotes the original input temperature value. To motivate the chosen adjustment in Eq. (B1), we note that in the $\ln Q$ - or T_d -based interpolations, step 4 of Table 5(b) involves first obtaining \tilde{e} directly from \tilde{Q} or \tilde{T}_d (as yet unaffected in no-transform cases by processing errors in temperature) and finally dividing by $e_s(\tilde{T})$ to obtain \tilde{RH} according to Eq. (6). Likewise, $\tilde{RH} \times e_s(T)$ in Eq. (B1) represents an expression for \tilde{e} that is unaffected by temperature processing errors, which are lastly imposed by the division by $e_s(\tilde{T})$.

The comparison of the RMSE verifications of \tilde{RH} and \tilde{RH}^* in the no-transform, zero-terrain, RH-based interpolation is given in Figure 25(a). The corresponding zonal mean cross-section of RMSE for \tilde{RH}^* is given in Figure 26(a) (compare with top plot in Figure 24). As expected, the RMSE at 100 and 30 cb in these figures is noticeably larger for \tilde{RH}^* than for \tilde{RH} . Clearly, the RMSE of \tilde{RH}^* in Figures 25(a) and 26(a) is a fairer measure than that of \tilde{RH} for comparison with the zero-transform, no-terrain, $\ln Q$ - and T_d -based RMSE results of Figures 23(b) and 24 respectively. The close resemblance between Figure 26(a) and the lower two plots of Figure 24 is particularly noteworthy (especially in the N. H.) and serves to highlight once again the nearly equal performance among the choices of RH, $\ln Q$, or T_d as the moisture F variable in vertical interpolations in $Z = \ln P$.

With the above as background, we next examine the impact of the favoritism toward RH-based interpolations in the verification of the standard case that includes full transforms in Q and realistic terrain. Figure 25(b) compares the \tilde{RH} -derived and \tilde{RH}^* -derived profile of global mean RMSE and Figure 26(b) shows the \tilde{RH}^* -derived cross section of zonal mean RMSE [compare with \tilde{RH} -derived RMSE plot of Figure 19(a)]. As anticipated, the optimism toward RH-based interpolations in verifying the standard cases with full transforms in Q and realistic terrain is negligible at all levels, except at 100 cb. Even for the latter, the cross section of zonal mean RMSE in Figure 26(b) vs that in Figure 19(a) shows the bulk of the increased RMSE for adjusted \tilde{RH}^* to be present at the highest latitudes. Lastly and most significantly, comparison of Figure 26(b) with the RMSE plots of Figures 19(b) through (d) upholds the conclusion of Section 3.2 that the (S_1, A_1) error characteristics for vertical interpolations in $\ln P$ using RH, $\ln Q$, or T_d are very competitive with one another (and all vastly superior to vertical interpolations of $F = Q$ in $Z = \ln P$).

LIST OF ACRONYMS

AFGL	Air Force Geophysics Laboratory
AFGWC	Air Force Global Weather Central
AWAPS	Advanced Weather Analysis and Prediction System
ECMWF	European Center for Medium Range Weather Forecasts
FGGE	First GARP Global Experiment
FNOC	Fleet Numerical Oceanography Center
GARP	Global Atmospheric Research Program
GFDL	Geophysical Fluid Dynamics Laboratory
GLAS	Goddard Laboratory for Atmospheric Sciences
GSM	global spectral model
HIRAS	High Resolution Analysis System
NMC	National Meteorological Center
NMI	normal mode initialization
NWP	numerical weather prediction
OI	optimal interpolation

END

FILMED

12-85

DTIC